Physics of Showers induced by Accelerator Beams

Alfredo Ferrari, and Paola R. Sala
INFN, Sezione di Milano, Via Celoria 16, 20133 Milano, Italy

Abstract

The basic aspects of particle interactions and showers in the energy range from a few tens of MeV up to several hundreds GeV, are presented, with particular emphasis on the intermediate energy range (from 20 MeV to $\approx$ 1-2 GeV). All topics are discussed mainly on a phenomenological basis, focussing on the general aspects, rather than going into detail. A particular effort will be made to illustrate the general features of the processes through the discussion of models of common use in practical calculations.

1 Introduction

The importance of shower simulations in many fields of present day particle physics has grown considerably during the last years, in parallel with the rapid increase in available CPU power. However there has been no corresponding development concerning the physical models used for such simulations, despite the strong impact that simulation studies have on the analysis of running experiments and on the design of future detectors.

A great importance has been attached instead to the development of sophisticated informatics packages to describe and visualize complex detectors and to provide the generic user with powerful interactive tools for detector modelling and data analysis. Perhaps the best example of such philosophy is the GEANT code [1], developed at CERN and widely used in the high energy physics community.

Besides physics experiment, there is an increasing interest for applications of accelerator beams. A new generation of intermediate energy proton and electron accelerators is under construction or planned in the near future, spanning a variety of applications, ranging from energy production, waste transmutation, synchrotron radiation to radiotherapy. Such applications call for more and more refined simulations tools, to be able to design and properly operate these facilities.

A good knowledge of radiation transport is critical also for other activities which apparently have very little in common with the new medical and industrial accelerators. Radiation background in the large experiments which are currently planned to be installed at the future LHC proton-proton collider will be dominated by particle fluxes which can only be estimated by simulation of the whole hadronic cascade from several TeV down to thermal energies. Most of the particle production will take place at energies below 1 GeV. A similar situation arises in the assessment of the radiation dose affecting the crew of commercial airplanes or of space stations. In general all aspects connected with the dosimetry of medium and high energy particles are still waiting for a fresh and more systematic treatment.

Detailed physical models are also required when designing and operating experiments based on calorimetry. Missing p_t measurements and CP violation experiments are very sensitive to the response of calorimeters to relatively low energy hadrons. A detailed comprehension of active device responses to subGeV hadrons will be a key issue for many of the future experiments, both at accelerator beams, or in underground laboratories. The recent question about the reality of the Kamiokande result about the deficit of atmospheric μ-neutrinos is a typical example. According to some calculations [2], the "signal" could be explained as due to π^0s produced by energetic neutrons generated in the surrounding rock by high energy muons. A precise knowledge of the full chain of muon photonuclear interactions, hadron showers, and finally pion production in the intermediate energy range is required to settle the question. It must be stressed that the GEANT code cannot be used for this purpose, because its physics is inadequate in the energy range of interest.

Despite they heavily rely on MonteCarlo modelling when designing and understanding their devices, and when analyzing experimental data for backgrounds and kinematical cuts, high energy physicists tend to consider all the complex phenomena of hadronic and electromagnetic showers occurring in their experimental apparatus as well understood physics, without recognizing the still large uncertainties connected with the physical description of showers. While QCD inspired models are very powerful in predicting and describing the rare interesting phenomena searched for by high energy experiments, efforts in describing the bulk of high energy interactions, which cannot be understood in terms of perturbative QCD, are relatively rare, despite their striking importance in understanding the complex experimental setups required by modern experiments.

Nuclear physicists are often working on a small subset of "interesting" phenomena related to nuclear interactions, and usually do not like to spend time on more general models which can be used for whichever application, particularly for technological ones. Very interesting physics researches are going on in the description of nucleon induced interactions below the pion threshold (see the reviews [4, 3]), however little or no work is done in the understanding of interactions at higher energies, with possibly the exception of some interesting developments in the pion sector [6, 5, 7]. Anyway, new or updated models are seldom formulated in such a way as to allow a general application. As a consequence, most applications must rely on models, like the glorious Bertini INC model, which are 20 to 30 years old, and which are no longer up-to-date with the present knowledge.

As soon as the energy of a primary hadron beam exceeds few tens of MeV, inelastic interactions start to play a major role and secondaries have enough energies to trigger further interactions, giving rise to a hadronic shower. Whenever the beam energy is such that significant pion production can occur (the pion production threshold for nucleons interacting with stationary nucleons is around 290 MeV), an increasing fraction of the energy is transferred from the hadronic (HAD) to the electromagnetic (EM) sector due to production of mesons (mainly π^0 and η) which quickly decay into EM particles (e^+, e^-, and γ). Hadron and electromagnetic showers are very complex phenomena, whose description in terms of basic physical interactions requires a lot of knowledge. There are two basic differences between hadronic and EM showers. The first is that, while energetic hadronic showers are always giving rise to significant EM ones (and we shall see in section 9 how such EM component is more and more important with increasing primary energy), EM showers develop independently without further hadronic particle production, forgetting for a while the (small) probability of electro and photonuclear interactions. The second difference is that, while EM interactions are in principle well understood (see however [8]) and described by QED, the same does not apply to hadronic nuclear interactions, where such a complete theory does not exist and one has to resort to suitable models to have some insight into the physics of the processes.

The development of hadron initiated showers is determined both by atomic processes (dE/dx, multiple Coulomb Scattering etc), which take place very frequently, and by the relatively rare nuclear interactions (both elastic and nonelastic). EM showers are determined by the same atomic processes (dE/dx, multiple Coulomb Scattering etc), plus other atomic processes (Bremsstrahlung, pair production, Compton scattering etc), which are specific of $e^\pm$ and photons, while nuclear interactions play a minor role, and whenever the interest is not in the small amount of hadrons produced by EM particles, they can be safely neglected.

A simple and schematic description of shower development is presented in section 2. The atomic processes common to HAD and EM showers are briefly described in section 3, while the description of hadron-nucleus interactions is presented in sections 6,7. In particular section 6 describes hadronic inelastic interactions in the framework of the IntraNuclear Cascade approach, whose basis are presented in section 4. A discussion of practical implementations of INC models, and examples of performances are given in section 8. Finally a short introduction to EM showers is presented in section 9.

Before going on with the proposed scheme, it is important to make the reader aware of a few important warnings and comments. The present lecture is based on the experience and feelings of the authors, who work since several years in the field of shower modelling, mainly for applications connected with high energy accelerators and experiments. Their opinions are not necessarily those of the majority of people working in the field.

Whenever presented, plots of cross sections etc are to be intended as indicative. Usually the data used for such plots are taken from the tabulations used by the author code (FLUKA). Whenever experimental data are plotted, the source is always indicated. Most of the examples have been computed again with FLUKA, just for convenience: indications whether they can be considered or not as typical examples are given every time.

No discussion is given about hadron interactions below, say, 20 MeV, both because they are outside the aim of this lecture, and because they are essentially restricted to neutron interactions, for which a huge and accurate body of experimental informations, sometimes supplemented by sophisticated modelling does exist in official compilations like ENDF-B, JEF, JENDL etc. It is always assumed that (neutron) interactions below 20 MeV can be accurately simulated with the codes developed for this energy range [13, 12, 14], which make use of such informations.

Furthermore, only single hadrons (and in practice only nucleons and pions, due to the energy range of interest), will be considered as possible projectiles. The extension to very light nuclei (deuterons and alphas), is relatively straightforward, at least for projectile energies much in excess of the binding of these nuclei, but will not be explicitly described. Models for complex nucleus-nucleus interactions will not be considered at all. Such interactions have indeed little or no interest for technological applications (with the possible exception of cancer therapy with ion beams), and for high energy experiment analysis (unless a primary ion beam is used).

The description of hadron interactions above few GeV is forcibly limited to few remarks, because of space reasons and of the relative scarce interest of this energy range for accelerator technological applications.

2 Shower Development

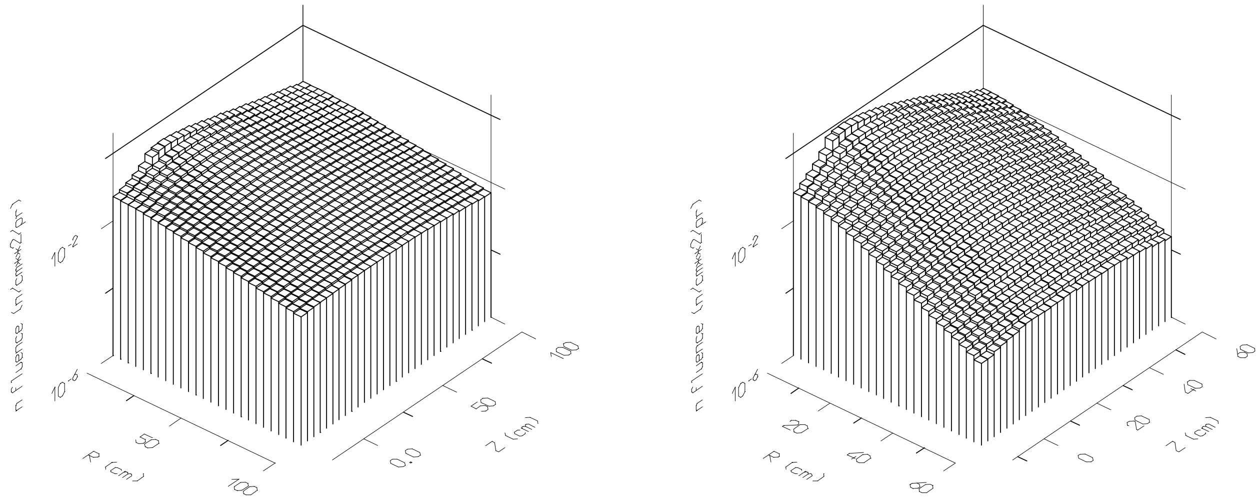

Figure 1: Spatial distribution of neutron fluence in an infinite natural Pb (left) and depleted U (right) target, for a 1.5 GeV incident proton beam

Before discussing specific aspects of hadronic and EM showers, there are a few comments which help in focusing the problem. Assuming one is dealing with some technological application of an accelerator beam (energy production, waste transmutation, cancer therapy etc), which kind of informations does he need? Without claiming that these are all the possible informations required, a reasonable list could be the following:

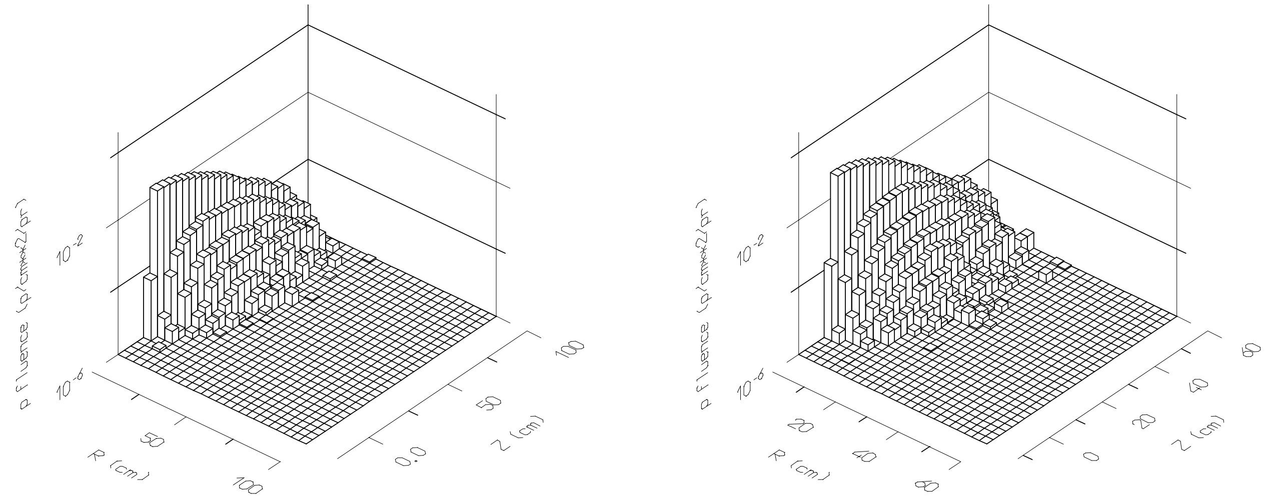

Figure 2: Spatial distribution of proton fluence in an infinite natural Pb (left) and depleted U (right) target, for a 1.5 GeV incident proton beam

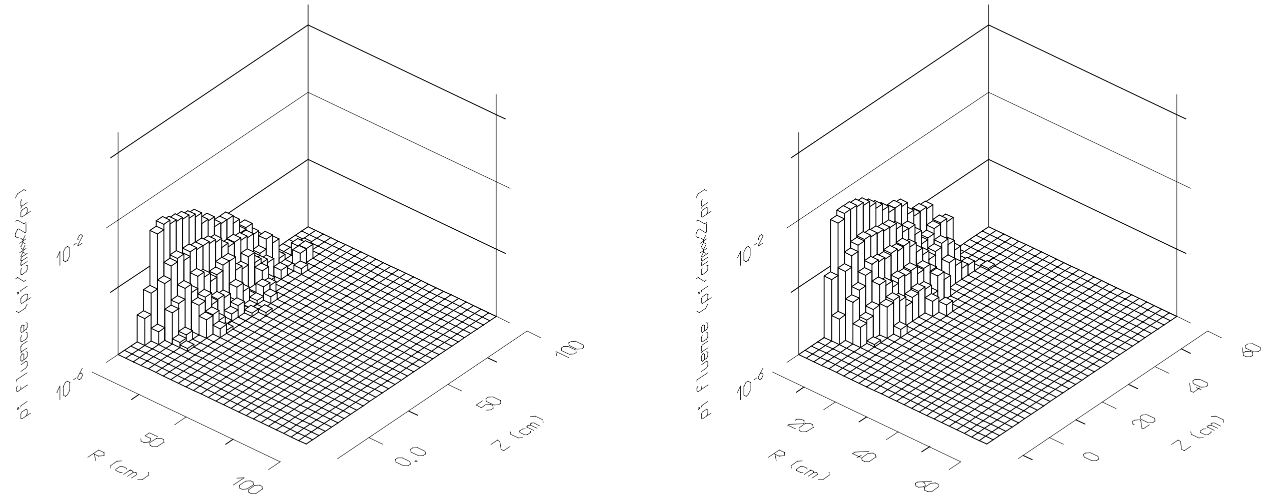

Figure 3: Spatial distribution of charged pion fluence in an infinite natural Pb (left) and depleted U (right) target, for a 1.5 GeV incident proton beam

- Energy deposition (with possibly the chance to weight energy deposition according to the "depositing" particle/process, as required for example for biological effectiveness evaluation and for radioprotection)
- Particle fluences as a function of energy, angle and position

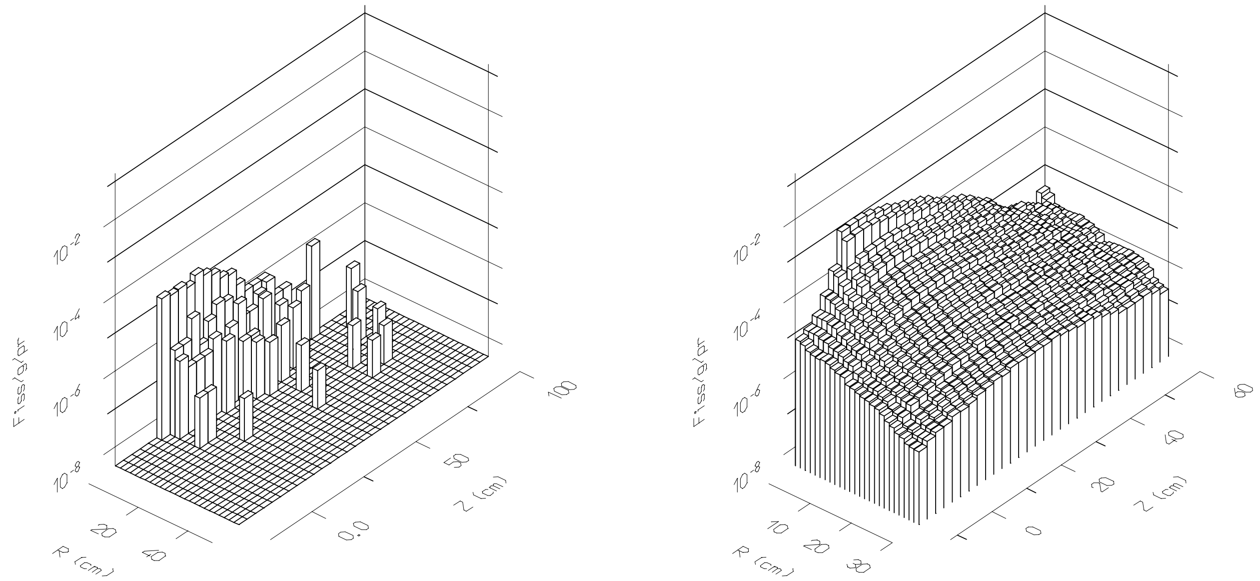

Figure 4: Spatial distribution of fission density in an infinite natural Pb (left) and depleted U (right) target, for a 1.5 GeV incident proton beam

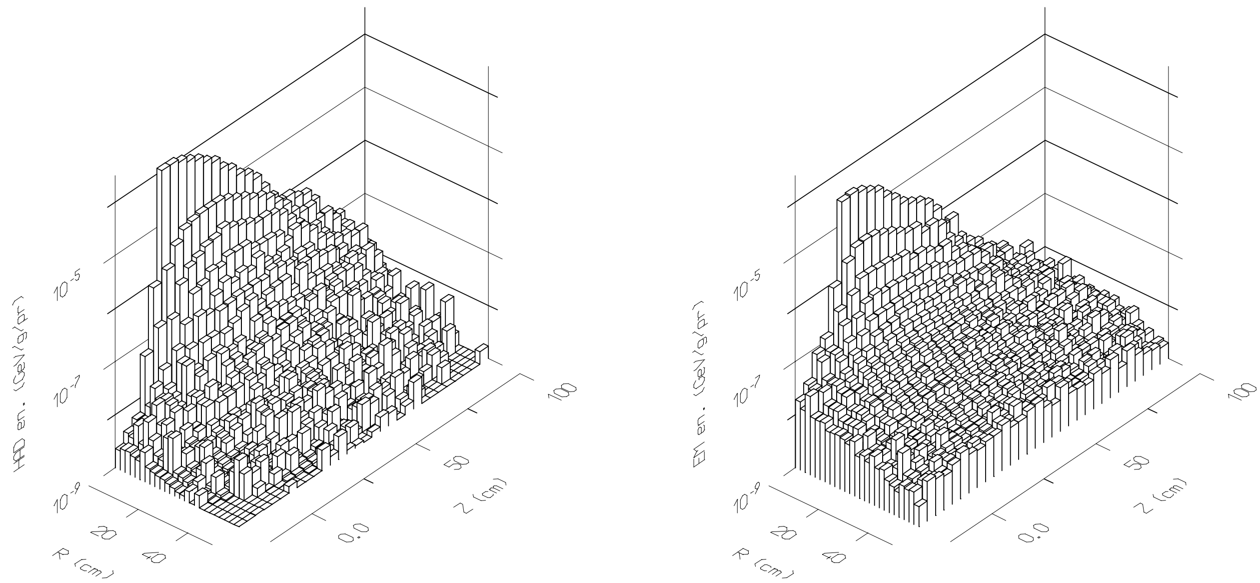

Figure 5: Hadronic (left) and EM (right) energy density distribution in an infinite natural Pb target, for a 1.5 GeV incident proton beam

- Interaction distributions (inelastic interaction density, fission density etc)
- Residual nuclei, that is the (possibly radioactive) isotopes generated by beam interactions in the target

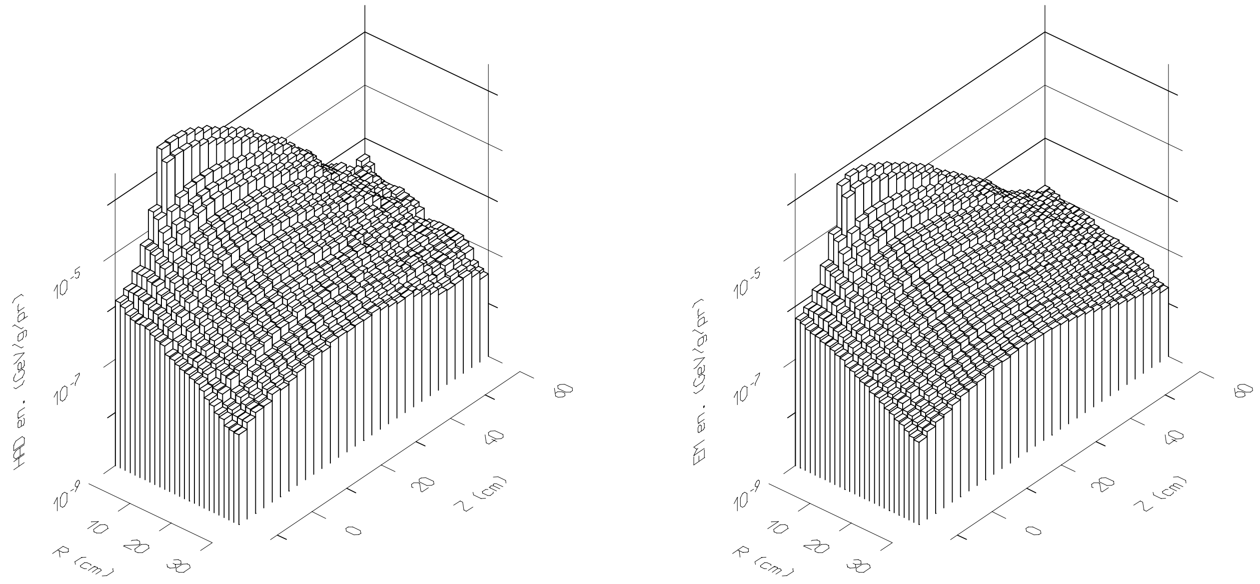

Figure 6: Hadronic (left) and EM (right) energy density distribution in an infinite natural U target, for a 1.5 GeV incident proton beam

Ideally, our tool, from now identified with some MonteCarlo program, should be able to give us accurate predictions about all the above points, for any desired spatial mesh. Usually the degree of accuracy required for the different kind of informations is not the same. For example, residual nuclei are seldom required to an accuracy better than one order of magnitude, while neutron fluence can well be requested to be within a factor 10% or better.

2.1 HAD shower examples

As an example of the development of hadronic showers, and at the same time of the kind of informations which can be obtained by modern MonteCarlo codes, let us consider a 1.5 GeV proton beam impinging at the coordinate origin on infinite natural lead and depleted uranium (0.2% ^{235}U) targets. These targets have been selected because most of the proposed technological applications of accelerator beams will make use of heavy (and possibly fissionable) targets. In fig. 1,2,3, the spatial distribution of neutron, protons, and charged pion fluences in both targets are presented, while the fission distributions are shown in fig. 4. The Z and R axis have been rescaled in such a way as to cover the same "length" for the two targets when expressed in g/cm^2, in order to mask every difference due to the different densities. The hadronic and EM energy densities (the last due to π^0's, capture photons etc) are plotted in fig. 5 and 6 for the Pb and U target respectively.

There are similarities and striking differences between the two targets, which need a bit of discussion. Proton and pion fluence distributions look very similar both in shape and in absolute value. They are both concentrated close to the primary beam axis, as expected since

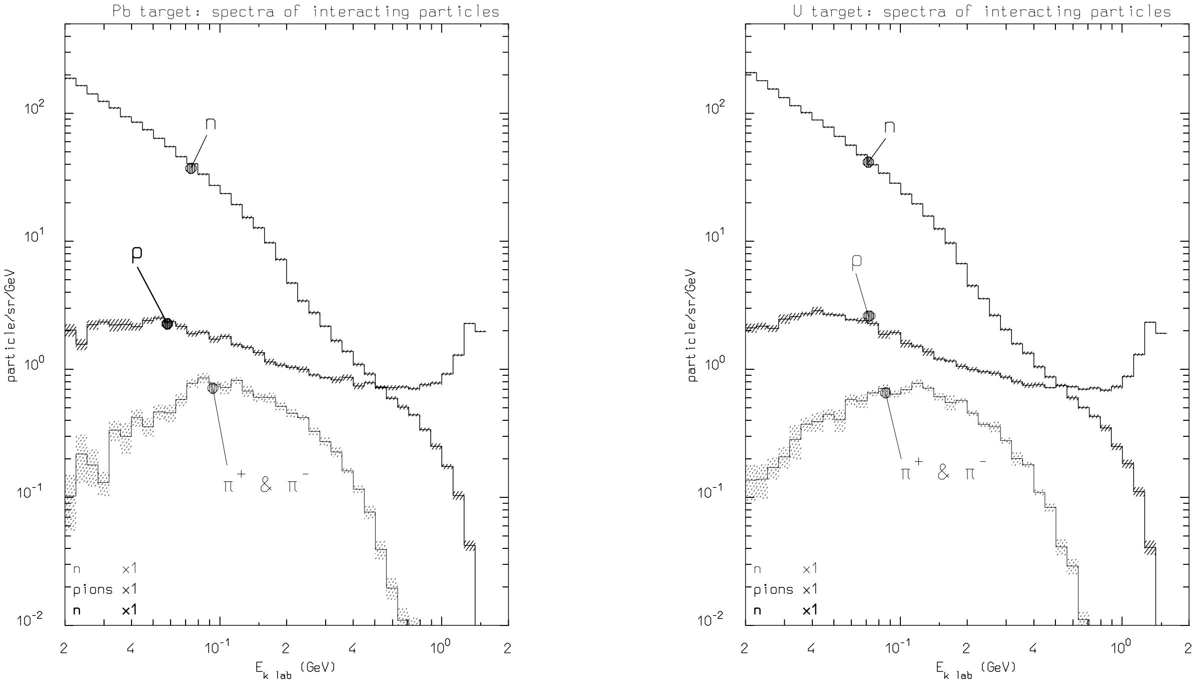

Figure 7: Spectra of p,n, and pions undergoing nuclear interactions in an infinite natural U (right) and Pb (left) target, for a 1.5 GeV incident proton beam

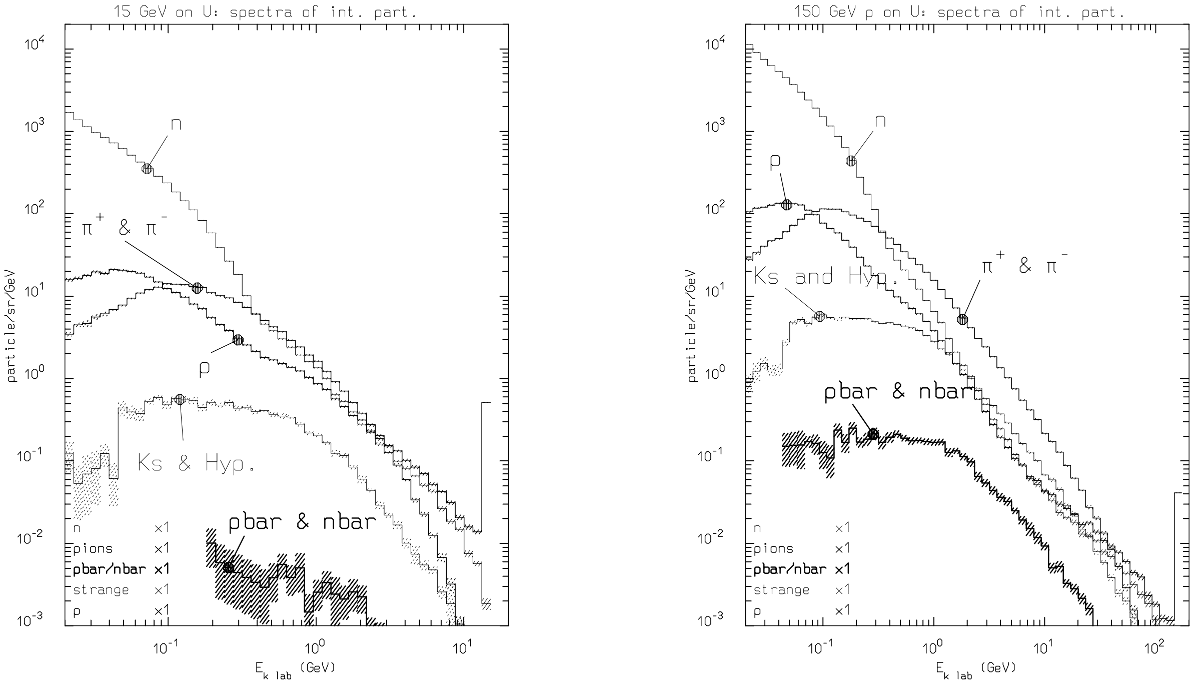

Figure 8: Spectra of particles undergoing nuclear interactions in an infinite natural U for 15 GeV (left) and 150 (right) incident proton beam. Note the different scale with respect to the previous figures

they originate mainly from energetic particles which, by virtue of momentum conservation and of the forward asymmetry in most c.m. interaction angular distributions, are strongly peaked in the original direction. The proton distribution is higher and wider than the pion one, because protons can be produced also during the final evaporation stage and by particles of relatively low energy (see section 6), while the threshold for pion production is much higher. The number of neutrons is much bigger, and spread over a much larger volume. The faster decrease of neutron fluence with radius in the U target is just due to the larger absorption than in the Pb target. To better understand the role of different particles/energies in determining the shower evolution, it is interesting to look at the spectra of particle undergoing nuclear inelastic interactions. These spectra are shown in fig. 7 for both targets. The peak due to interactions of primary protons is clearly visible. The most striking feature is the large number of interacting neutrons at low energy. This feature can be easily explained, observing that charged particles start to be rapidly absorbed without further reinteractions, as soon as their range becomes comparable to the inelastic interaction length. This condition is fulfilled around 450 MeV for protons (range $\approx \lambda_{in} \approx 200$ g cm^{-2}), and 200 MeV for pions in heavy materials. The importance of pions is quickly rising with the energy of the primary beam, since in high energy interactions pions are the most likely particles to be produced. The increasing importance of pions can be appreciated in fig. 8, where the same information of fig. 7 is presented for 15 and 150 GeV protons on uranium. It is also interesting to note the onset of kaon (and hyperon) production as well as of antinucleons.

Let's turn our attention to the energy deposition profiles: the large differences between Pb and U are mainly due to very different fission probabilities (see fig. 4). Indeed only a fraction of high energy particles can induce fissions in lead, ≈ 0.1 fissions per primary proton in this example, while ≈ 28 fissions occur in the uranium target, out of which ≈ 7 are due to energetic particles and ≈ 21 to neutrons below 20 MeV. As a result the uranium target is strongly exoenergetic: please note that also the EM energy deposition is strongly boosted due to the large number of neutrons, and hence of capture photons, produced because of these fissions. However such large differences are only apparent. The same physical mechanisms are at work in both cases, and will be explained in the next sections. The ridge in the hadronic energy deposition around the beam axis is just due to the primary beam ionization plus heavy recoils ($\rightarrow$ short ranges) due to primary interactions, and to the most energetic particles emerging from inelastic interactions which are still strongly forward peaked. The higher values for U also in this region are due again to fissions occurring during primary interactions. The EM component can better be commented looking at the lead data, which are not masked by fissions. Two components can be identified: the first is due to π^0 decays and is concentrated again around the beam axis. This is due to the spatial scale of EM cascades, which is given by the radiation length (see paragraph 9.1) in the longitudinal direction, and by the Molière radius in the radial one. In medium and heavy materials both are much shorter than the "natural" hadronic length scale, given by the nonelastic interaction length. The second component is less intense but much more spread out, and it is given by photons locally produced by neutron reactions (capture, (n,n') etc). Of course this component is following the neutron pattern: the reason why it appears to be more extended in lead than the hadronic energy density, despite we claim it is due to neutron produced photons, is just that pure lead is a very bad moderator, but does not absorb too much neutrons. Therefore low energy neutrons are slowly moderated and diffuse much further away from the beam axis, depositing a small amount of hadronic energy through recoils, but a substantial amount of EM energy when captured.

Summarizing, what can be learned from these simple examples?

a) Energetic particles (often called *shower* particles) are concentrated mainly around the primary beam axis, regardless of their identity. Their dE/dx and the EM cascades associated with π^0 constitute the "core" of the energy profiles.

b) Neutral particles ($\rightarrow$ neutrons, since these are the only neutral hadrons with enough long lifetime) dominate at energies such that charged particle ranges become shorter than the interaction length. The energy deposition associated with "low" energy neutron interactions, both recoils and photons, constitute the long tails in the energy deposition profiles.

c) Most of the interactions are due to particles (mainly neutrons) of moderate energy, $\rightarrow$ a good description of this energy range is mandatory.

d) On the contrary the longitudinal shower development is ruled by *shower* particles, which carry a good fraction of the energy and have a longer interaction length. Taking also into account that any approximation or inaccuracy in the first interactions cannot be recovered with a better physics in the following ones, this means that a good description of energetic particle interactions is also mandatory.

e) Pions can be only produced by *shower* particle interactions, so they are the real "tracer" of the high energy cascade. Neutrons and to less extent protons are copiously produced also in the final (evaporation) stages of nuclear interactions down to projectile energies comparable with their nuclear binding energy (see paragraph 6.7).

The term *shower* particles comes from the early experiments of high energy physics, where nuclear emulsions were often used as recording media. Charged particle tracks are therefore customarily classified in weakly ionizing, or *shower* tracks, medium ionizing, or *grey* tracks, and heavily ionizing, or *black* tracks, just according to their ionization rate (see the next section for a description of charged particles ionization). In practice, *shower* tracks correspond to (charged) particles with $\beta = \frac{v}{c} \geq 0.7$, *grey* tracks to $0.25 \leq \beta < 0.7$, and *black* tracks to $\beta < 0.25$. Forgetting the original meaning, but just retaining their velocity interval interpretation, such definitions are sometimes used also for neutral particles. $\beta = 0.7, 0.25$ corresponds to $\approx$ 400 MeV and 30 MeV for nucleons, and to $\approx$ 50 and 5 MeV for pions. Therefore black tracks are a good indicator of evaporation products.

2.2 The Shower Tree

In this paragraph a schematic description of the main phenomena occurring in hadron and electromagnetic showers is outlined. Such a description is organized in a way which strictly follows what is done in practice in simulation codes.

In most simulation models, and in almost all of practical use for accelerator beam applications, there is a basic distinction between "continuous" and "discrete" or "explicit" processes. This distinction follows a real physical distinction among processes which occur very frequently ($\rightarrow$ with mean free paths much shorter than particle ranges) along particle paths, and less frequent interactions, which however are often the dominating ones in determining the shower development. dE/dx, Coulomb scattering, and bremsstrahlung below some suitable cut-off energy are usually included in the former group. The latter one includes all other processes of interest, briefly listed below. Codes which adopt such a division are usually referred to as "condensed" history MonteCarlo. For condensed history MonteCarlo, possible explicit interactions for hadronic particles are:

- δ ray production
- elastic nuclear interaction
- nonelastic nuclear interaction
- decay

and for EM particles:

- δ ray production (Møller scattering for electrons, Bhabha scattering for positrons)
- Bremsstrahlung (for electrons and positrons)
- Annihilation (for positrons)
- Photoelectric effect (for photons)
- Compton scattering (for photons)
- Pair production (for photons)
- Coherent (Rayleigh) scattering (for photons)

These lists are somewhat schematic and not really complete. With a much lower rate, nuclear interactions can occur also for photons (and with a further reduced, $\approx \alpha = \frac{1}{137}$, rate also for electrons and positrons). Bremsstrahlung radiation is produced as well by "heavy" charged particles, even though it is suppressed by roughly a factor $\left(\frac{m_e}{M}\right)^2$ with respect to electrons, and all charged particles, light and heavy ones, can produce $e^{\pm}$ pairs. Usually these processes can be safely neglected with some exception: for example the propagation of high energy muons, like the ones produced by cosmic rays and detected by underground experiments, is eventually dominated by bremsstrahlung and pair production.

Let us start with a particle of given energy E, and given position and direction. This particle can be the primary particle generating the shower, or a secondary one generated in a previous interaction. The first step is to "decide" how long this particle can travel before one "explicit" interaction will occur. As well known, the probability, dP, for having an interaction along an infinitesimal path length dx, is linked to the fraction of particles interacting along dx and is given by:

$$dP = -\frac{dN}{N} = \sum_{i=1}^{n} \sigma_i(E) \frac{N_A \rho_i}{P_{Ai}} dx = \Sigma(E) dx \tag{1}$$

where $\sigma_i(E)$ is the total (microscopic) cross section for interactions, ρ_i and P_{Ai} the partial density and the atomic weight of atom/nucleus of type i. N_A is the Avogadro number. The quantity, $\Sigma(E) = \sum_{i=1}^{n} \sigma_i(E) \frac{N_A \rho_i}{P_{Ai}}$, is often called the *macroscopic* cross section, and $\lambda = \frac{1}{\Sigma}$ is the mean free path of the particle. Whenever more than one reaction channel is possible (see the previous list), $\Sigma(E)$ and $\sigma_i(E)$ are expressed by a sum over all possible k interaction kinds.

$$\Sigma(E) = \sum_{i=1}^{n} \sum_{j=i}^{k} \Sigma_{ij}(E) = \sum_{i=1}^{n} \frac{N_A \rho_i}{P_{Ai}} \left[\sum_{j=i}^{k} \sigma_{ij}(E) \right] \tag{2}$$

The probability of decay along dx for unstable particles, can be rearranged in such a way to define a *macroscopic decay* cross section, Σ_d, to be simply added to the total macroscopic Σ. It can be easily checked that, for a particle having momentum $p = \gamma m v$, total energy $E = \gamma m c^2$, and mean life τ:

$$dP_d = -\frac{dN_d}{N} = \Sigma_d(E) dx = \frac{dt}{\gamma \tau} = \frac{dx}{\gamma v \tau} = \frac{m}{p \tau} dx \tag{3}$$

If all macroscopic cross sections do not depend on x (for a homogeneous medium, this implies that the particle is a neutral one, or that cross sections for charged particles do not appreciably vary along a step of the order of a few mean free paths), eq. 1 can be easily integrated to give the usual exponential attenuation law (where *tot* means that all possible processes including decay are included):

$$N(x) = N_0 e^{-\Sigma_{tot}(E) x} \tag{4}$$

which in turn implies that interaction points are also exponentially distributed, since:

$$P(x) = -\frac{1}{N_0} \frac{dN}{dx} = \Sigma_{tot} e^{-\Sigma_{tot} x} \tag{5}$$

The standard procedure would be to sample the distance to the next interaction according to the above distribution, and then to randomly decide which interaction will actually take place and on which atom/nucleus according to the relative probabilities given by $\frac{\Sigma_{ij}}{\Sigma_{tot}}$ for atomic/nuclear interactions, and by $\frac{\Sigma_d}{\Sigma_{tot}}$ for decay. This procedure is straightforward and commonly used by every simulation code for neutrons and photons. It is important to stress that neutral particles do not undergo any process in between two consecutive interactions, and their energy and direction are unaffected.

Major complications arise for charged particles: indeed the approximation that cross section are almost constant among two consecutive interactions is violated in many cases. Indeed cross sections are a function of energy, and energy and direction are changing "continuously" for charged particles in between two consecutive interactions. Nuclear interaction cross sections show significant energy variations in the low and intermediate energy range, cross sections for

δ ray production behave like $1/E_{kin}$ in the non-relativistic region etc. Furthermore the relation between track length x and energy E, $E(x) = E_0 - \int_{x_0}^{x} dx' \frac{dE}{dx'}[E(x')]$ is valid only on average, since fluctuations (see paragraph 3.3) in the energy loss rate can well modify the correspondence based on the average stopping power. Therefore any analytical approach is difficult and forcibly approximate. A possible solution, adopted in the most sophisticated models, is to sample the next interaction point for charged particles according to eq. 5, using the maximum possible value of the macroscopic cross section along the scheduled step, Σ_{max}, instead of the value corresponding at the beginning-of-step properties of the particle. Once the particle reaches the possible interaction point, its energy E_{new}, and the corresponding cross section $\Sigma_{tot}(E_{new})$, are completely defined by the processes occurred during the step. At this point the interaction is "accepted" with probability

$$P_{acc} = \frac{\Sigma_{tot}(E_{new})}{\Sigma_{max}} \tag{6}$$

while in a fraction $1 - P_{acc}$ the particle continues with no interaction. Such an algorithm (sometimes called "fictitious sigma" method), which is an example of a very powerful MonteCarlo integration method called rejection method, is able to assure *exactly* the correct distribution of interaction points, properly correlated with energy loss fluctuations etc. It is left to the reader the straightforward proof that eq. 6 and 5 with Σ_{max}, do properly reproduce the fundamental relation 1. It is important to stress that the exact value of Σ_{max} is not required at all, but whichever approximate value which fulfills $\Sigma_{max} \geq \Sigma_{tot}(E')$, $E_{new} \leq E' \leq E$ can be used.

Summarizing, the division between "discrete" and "continuous" interactions has been introduced. The former are common to all particles, while the latter are specific of charged ones. "Continuous" interactions must be modelled together with particle transport and are described in the next section. "Discrete" interactions occur at selected points, chosen according to the formulas presented in this section. Here a remark must be done about cross sections for discrete processes: while the electromagnetic ones are theoretically well known, the hadronic ones, expecially when dealing with hadron-nucleus interactions, are not so well fixed. Depending on situations, fits to experimental data, tabulations, or some modelling have to be used. A description of possible "discrete" interactions is presented after the next section.

3 Charged particle transport

The most important atomic processes (Bremsstrahlung excluded) undergone by charged particles when traversing media are related with Coulomb scattering with both atomic electrons and nuclei. Despite the basic process is always the same (Coulomb scattering), because of the very different masses of electrons and nuclei, the effect is very different: the cross section is proportional to Z^2, and when expressed as a function of the transferred 4-momentum q, is approximately independent of mass: this means that for a given projectile the energy transfer is inversely proportional to the target mass. Therefore, interactions with electrons are by far the dominant source of charged particle energy losses, while they give a contribution proportional to the atomic number Z (that is, like Z independent point unit charges) to the angular deflection. Collisions with atomic nuclei result in negligible energy losses but the angular deflection is roughly that of a single particle of charge Z, thus it is proportional to Z^2. Thus the angular deflection is associated mostly with atomic nuclei, but for the lightest elements where the two contributions become comparable.

Due to the very large number of collisions experienced by charged particles, for most applications it is impractical to reproduce in detail each elementary collision. Statistical models for both energy losses and angular deflections are therefore employed to evaluate the cumulative effect on macroscopical step lengths spanning several mean free paths. Such an approach is usually referred to as "condensed history MonteCarlo" and it is adopted by the vast majority of the codes used for simulations in the energy range of interest. The approach based on single collisions is adopted only for microdosimetry or, limited to angular deflections (see [10] for a cross section compilation), for detailed calculations of low energy electron transport [9].

3.1 "Heavy" particles dE/dx and ranges

This topic is a very well known one, and a detailed discussion is outside the aim of this lecture. Classical treatments can be found in [11, 15, 16], and a recent revue for protons in [20].

Summarizing, the formula for the average energy loss of particles much heavier than electrons and charge z, can be expressed by:

$$\frac{dE}{dx} = \frac{2\pi n_e r_e^2 m_e c^2 z^2}{\beta^2}\left[\ln\left(\frac{2m_e c^2 \beta^2 T_{max}}{I^2\left(1-\beta^2\right)}\right) - 2\beta^2 - 2\frac{C}{Z} - \delta\right] \tag{7}$$

where r_e is the classical electron radius, n_e is the number of electrons per cm^3 in the medium, $n_e = \frac{N_A Z \rho}{A}$, N_a= Avogadro's number. δ is the so called "density correction", extensively discussed in [17], and C the shell correction, which takes into account the difference between free and bound electron targets. This difference becomes important at low energies. I is the average ionization potential, and it is the main parameter characterizing the material properties [17]. The maximum energy transfer, T_{max}, to the electron is dictated by kinematics and given by:

$$T_{max} = \frac{2m_e c^2 \beta^2 \gamma^2}{1 + 2\gamma\frac{m_e}{M} + \left(\frac{m_e}{M}\right)^2} \tag{8}$$

A plot of the dE/dx and of the range of protons and pions in lead and aluminium is shown in fig. 9.

For most practical purposes , dE/dx in a given material depends only on the particle velocity β and charge z, thus particles of the same velocity and charge have roughly the same energy loss. Moreover, if one measures distances in units of ρdx, $\frac{g}{cm^2}$, the energy loss is weakly dependent on the material, as it goes like Z/A plus the logarithmic dependence on I. The proportionality to z^2 is evident.

The energy loss, when plotted as a function of $\beta\gamma = pc/M$, has a broad minimum at $\beta\gamma \approx 3-3.5$. This minimum is almost constant up to very high energies, if the restricted energy

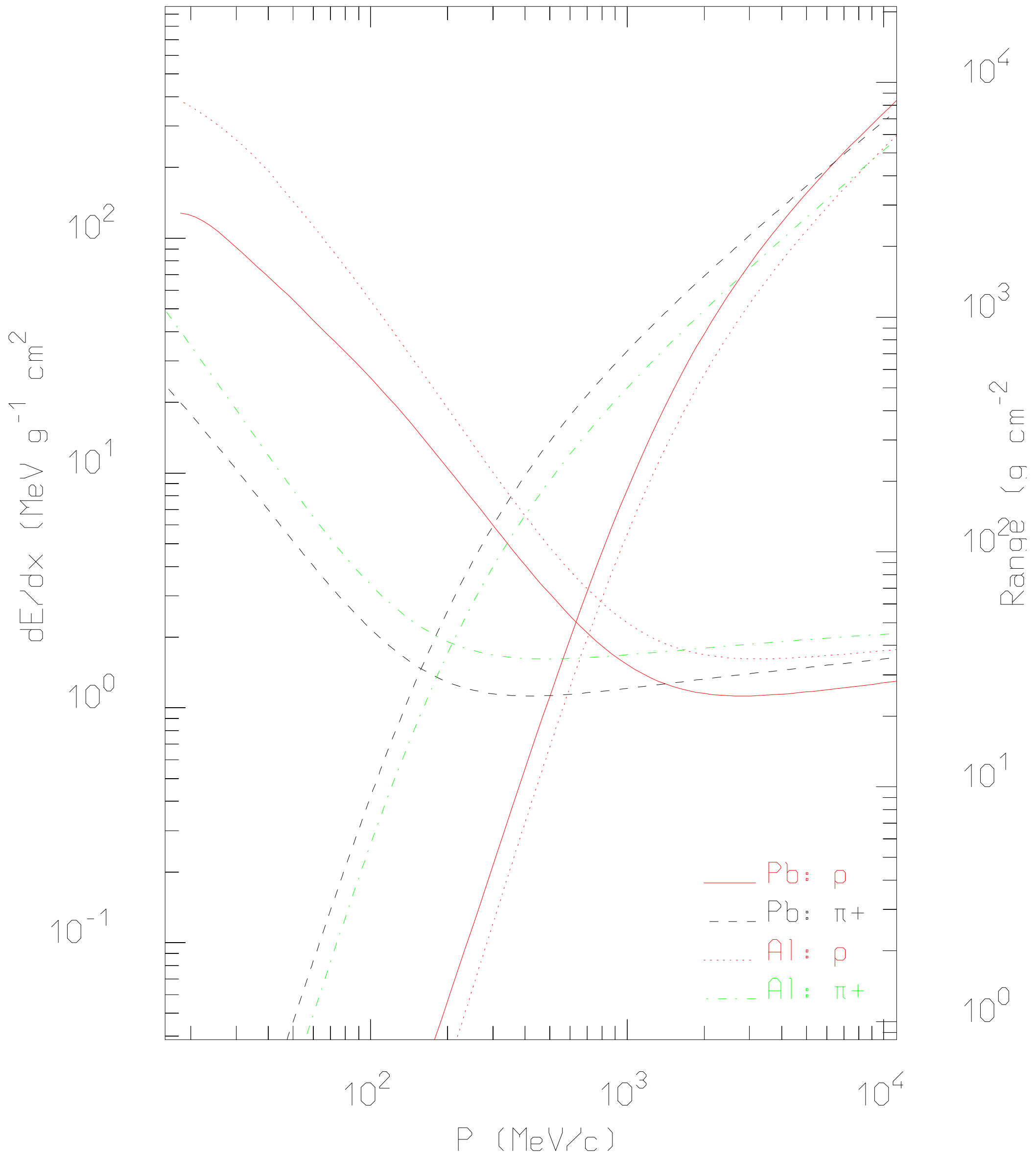

Figure 9: dE/dx and range for protons and pions in Pb and Al, as a function of particle momentum

loss (that is the energy loss due to energy transfers smaller than some suitable threshold) is considered. In practice, most relativistic particles have energy losses in active detectors close to the minimum, and are called *minimum ionizing particles*, or mip's.

The formula for the heavy particle dE/dx is customarily derived making use of the distinction between "distant" and "close" collisions, where the names refer to the magnitude of the momentum transfer and hence to the collision impact parameter (even though in a quantum mechanical sense). In distant collisions the particle interacts with the atom as a whole, while for close collisions the interaction can be considered to be with free electrons, and atomic properties are not involved. The cross section for producing an electron of energy T_e for an incident particle of kinetic energy $T_0 = (\gamma - 1)Mc^2$ is given by [11]

$$\left(\frac{d\sigma}{dT_e}\right)_0 = \frac{2\pi z^2 r_e^2}{\beta^2}\frac{m_e c^2}{T_e^2}\left[1 - \beta^2 \frac{T_e}{T_{max}}\right] \tag{9}$$

for spin 0 particles, and by:

$$\left(\frac{d\sigma}{dT_e}\right)_{\frac{1}{2}} = \frac{2\pi z^2 r_e^2}{\beta^2}\frac{m_e c^2}{T_e^2}\left[1 - \beta^2 \frac{T_e}{T_{max}} + \frac{1}{2}\left(\frac{T_e}{T_0 + Mc^2}\right)^2\right] \tag{10}$$

for spin 1/2 particles. It is important to note that, apart from the extreme tail where $T \approx T_{max}$, the dependence on the energy of the secondary electron is essentially given by the $\frac{1}{T^2}$ term. It is therefore clear from such formulae, that low energy transfers are much more likely than large ones.

3.2 e$^+$ and e$^-$ dE/dx

There is no major difference between "heavy" particle and e^+, e^- dE/dx, but the differences in "energetic" collisions with atomic electrons. The formulae for elastic Coulomb scattering for producing an electron of energy $T_e = \epsilon T_0$ on free electrons by e^- and e^+ (Møller and Bhabha scattering respectively), are given by [11]:

$$\left(\frac{d\sigma}{dT_e}\right)_{Moller} = \frac{2\pi r_e^2}{\beta^2}\frac{m_e c^2}{T_e^2}\left[1 + \left(\frac{T_e}{T_0 - T_e}\right)^2 + \left(\frac{\gamma-1}{\gamma}\right)^2\left(\frac{T_e}{T_0}\right)^2 - \frac{2\gamma-1}{\gamma^2}\left(\frac{T_e}{T_0 - T_e}\right)\right] \tag{11}$$

for Møller scattering, and

$$\begin{aligned}\left(\frac{d\sigma}{dT_e}\right)_{Bhabha} = \; & \frac{2\pi r_e^2}{\beta^2}\frac{m_e c^2}{T_e^2}\left[1 - \frac{\gamma^2-1}{\gamma^2}\frac{T_e}{T_0} + \frac{1}{2}\left(\frac{\gamma-1}{\gamma}\right)^2\left(\frac{T_e}{T_0}\right)^2\right. \\ & -\frac{\gamma-1}{\gamma+1}\frac{T_e}{T_0}\left\{\frac{\gamma+2}{\gamma} - 2\frac{\gamma^2-1}{\gamma^2}\frac{T_e}{T_0} + \left(\frac{\gamma-1}{\gamma}\right)^2\left(\frac{T_e}{T_0}\right)^2\right\} \\ & \left. + \left(\frac{\gamma-1}{\gamma+1}\right)^2\left(\frac{T_e}{T_0}\right)^2\left\{\frac{1}{2} + \frac{1}{\gamma} + \frac{3}{2\gamma^2} - \left(\frac{\gamma-1}{\gamma}\right)^2\frac{T_e}{T_0}\left(1 - \frac{T_e}{T_0}\right)\right\}\right]\end{aligned} \tag{12}$$

for Bhabha scattering. After integration on the proper kinematical limits (T_0 for positrons and $T_0/2$ for electrons), the resulting dE/dx is given by [11]:

$$\frac{dE}{dx} = \frac{2\pi r_e^2 n_e m_e c^2}{\beta^2}\left[\ln\frac{T_0^2(\gamma^2-1)}{2I^2} + (1-\beta^2) - \frac{2\gamma-1}{\gamma^2}\ln 2 + \frac{1}{8}\left(\frac{\gamma-1}{\gamma}\right)^2 - \delta\right] \tag{13}$$

for electrons,and

$$\frac{dE}{dx} = \frac{2\pi r_e^2 n_e m_e c^2}{\beta^2}\left[\ln\frac{2T_0^2(\gamma^2-1)}{I^2} - \frac{\beta^2}{12}\left\{23 + \frac{14}{\gamma+1} + \frac{10}{(\gamma+1)^2} + \frac{4}{(\gamma+1)^3}\right\} - \delta\right] \tag{14}$$

for positrons. A recent review of electron and positron ionization and radiative energy losses can be found in [21].

3.3 δ ray production and energy loss fluctuations

In 3.1,3.2 the formulae for the *average* energy loss experienced by a charged particle in traversing some stopping materials have been presented. However, a given particles loses its energy in small but finite amounts, and therefore statistical fluctuations can be observed in the amount of energy lost by particles of the same initial energy when traversing a given thickness of material.

We have seen in the previous sections that collisions with small energy transfers are more likely than those with large ones. As a consequence, the most probable energy loss is shifted to lower energies with respect to the average energy loss. Large energy tranfers are associated with the production of energetic electrons and dominate the energy loss fluctuations. It is customary to call "δ rays" knock on electrons energetic enough to produce "tracks" separated from the primary particle one. Although the energy threshold for defining a δ ray is ill-defined and problem dependent, the concept is very useful in describing the main source of straggling in charged particle energy losses. The formulae for δ ray production by heavy particles and electrons have been already presented in the previous paragraphs. Although these formulae are well known and relatively simple, the calculation of the probability distribution for having a given energy loss in a finite segment is very complicated, since it depends both on the number of collisions and the energy loss spectrum of each collision (that is given by the expression seen before).

There is an enormous amount of literature about this problem. The most popular solution is the so called Landau function, which can be derived under many simplifying assumptions. No further information will be given here, the interested reader can found suitable informations in [18, 19, 22, 23, 24, 25, 26].

3.4 (Multiple) Coulomb scattering

Coulomb scattering on (mostly) nuclei is the major source of charged particle deflections. There are two possible approaches to the modelling of charged particle multiple scattering in a condensed history MonteCarlo. The first one is based on the theory developed by **Molière** [27, 28] and slightly modified by Bethe [29], the second one relies on the theory developed by **Goudsmit and Saunderson** [30]. As usual there are advantages and disadvantages in both approaches, which are somewhat specular, that is the weak points of one approach are the strong ones of the other and viceversa.

In the following a necessarily limited summary of both models is presented with a (short) discussion of their advantages and limitations.

3.4.1 Molière model

The Molière theory makes use of the small angle approximation to derive a multiple scattering distribution which is valid provided the number of elementary scatterings along the considered step is large enough (> 20). The underlying single scattering cross section is the Rutherford one corrected for atomic screening according to an expression derived by Molière himself and essentially based on the Thomas-Fermi model of atoms. As a consequence the Molière distribution does not include spin-relativistic corrections to the Rutherford cross section. The minimum number of elementary deflections which is required by the model to be valid, sets a lower limit to the length of the allowed steps. At the same time, a higher limit on the allowed step lengths is set by the requirement that the typical deflection along a step is smaller than one radian. This limit derives of course from the small angle approximation. The two limits can easily be fulfilled for energetic particles in condensed media. Problems start to arise for gaseous media, where step lengths can be comparable with the lower limit, and mostly with low energy electrons. Indeed for high Z materials and electron energies below a few tens of keV it is impossible to match together the two constraints of the theory, which therefore is no longer valid.

Despite the underlying approximations the Molière theory has many advantages when used for simulating charged particle transport in arbitrary geometries with arbitrary step lengths since it can be expressed with universal functions using just a few material and particle dependent parameters. Furthermore this theory is in principle able to describe the distribution function of any single physical quantity of interest [28] (polar scattering angle, projected angle, position angles, lateral displacement etc.), even though it does not provide any means for computing the joint distribution of two or more of these quantities.

The multiple scattering distribution of Molière, as a function of the deflection angle θ and of the step length t, is given by:

$$F_{MOL}(\theta, t)d\Omega = 2\pi\chi d\chi \left[2e^{-\chi^2} + \frac{1}{B}f_1(\chi) + \frac{1}{B^2}f_2(\chi) + ...\right]\left[\frac{\sin\theta}{\theta}\right]^{\frac{1}{2}} \tag{15}$$

where the scaled variable χ is given by:

$$\chi = \frac{\theta}{\chi_c\sqrt{B}} \tag{16}$$

$$f_n(\chi) = \frac{1}{n!}\int_0^\infty u\ du\ J_0(\chi u)e^{-u^2/4}\left(\frac{u^2}{4}\ln\frac{u^2}{4}\right)^n \tag{17}$$

$$\begin{aligned} \chi_c &= \frac{\chi_{cc}t^{\frac{1}{2}}}{E\beta^2} \\ \chi_{cc} &= \left[\frac{4\pi n z^2 Z(Z+\xi_e)e^4}{c^4}\right]^{\frac{1}{2}} \end{aligned} \tag{18}$$

and B is solution of the trascendental equation:

$$B - \ln B = b = \ln\Omega_0 \tag{19}$$

with

$$\Omega_0 = \frac{b_c t}{\beta^2} \tag{20}$$

$$b_c = \frac{0.855^2 \chi_{cc}^2 \hbar^2}{1.167^2 m_e c^2 e^4 Z^{\frac{2}{3}} \left(1.13 + \frac{3.76\alpha^2 z^2 Z^2}{\beta^2}\right)} \tag{21}$$

3.4.2 Goudsmit-Saunderson model

The Goudsmit and Saunderson theory does not contain any of the above limitations and supplies the multiple scattering distribution as an expansion where any single scattering cross section can be inserted. The explicit expression for the probability of scattering through an angle θ after travelling a total step length t (g/cm^2) is given by:

$$P_{GS}(\theta, t) = \sum_{l=0}^{\infty} (l + \frac{1}{2}) e^{-tG_l} P_l(\cos\theta) \tag{22}$$

where $P_l(\cos\theta)$ are the Legendre polynomials and G_l is given by

$$G_l = 2\pi \frac{N_a}{P_A} \int_0^{\pi} \frac{d\sigma(\theta')}{d\Omega} (1 - P_l(\cos\theta')) \sin\theta' d\theta' \tag{23}$$

where N_a is the Avogadro's number, P_a the atomic weight and $\frac{d\sigma}{d\Omega}$ the adopted single scattering cross section.

The drawback of this model is its computational complexity. The convergence of the series in eq.22 may require up to 1000 terms, thus it is impossible to calculate the scattering probability at run time. This problem has been circumvented, for instance in [26], by offline calculation and tabulation in discrete energy and step intervals. This however severely constraints the allowed step length during transport, in order to match the values used in the tabulation, consequently causing problems at boundary crossings, where the step must be shortened.

3.4.3 Straggling

Both theories are expressed as a function of the total path length travelled by the particle. Therefore, as soon as the particle step length is not extremely short, suitable "wiggliness" corrections must be introduced to take into account the difference between the straight and the curved path length and possibly also between the actual displacement direction and the original direction of motion of the particle. Both corrections can be quite important unless severe limitations on step lengths are adopted.

The first correction algorithm to be devised was the Fermi-Eyges-Yang one [32], which is still used in GEANT and in the old version of EGS4[31]. This algorithm grossly overestimates[33] the wiggliness correction, and does not include any lateral displacement with respect to the original particle direction. As a consequence results are step-dependent, and small step lengths must be adopted. An algorithm named PRESTA[33] has been proposed afterwards and implemented in EGS, with a path correction based on the Molière theory and a correction for lateral displacement. Some approximations and limitations of this algorithm still show up in specific problems, like for instance backscattering problems. A more consistent approach, and a comprehensive discussion of the problem, can be found in [34].

4 IntraNuclear Cascade

Hadron-nucleus non-elastic interactions will be described mostly in the framework of the IntraNuclear Cascade (INC) model. This model was developed at the very beginning (the original ideas go back at the end of the 40's) of the history of energetic nuclear interaction modelling, but it is still very valid and in some energy range it is the only available choice. The model is intrinsically a MonteCarlo model, well suited for numerical applications, while no closed analytical expression can be derived without severe approximations. Therefore INC models became more and more refined and widespread with the evolution of computer codes; currently available models can reach 100,000 lines of program lines.

In the energy range going from the pion production threshold ($\approx$ 290 MeV for a free nucleon, down to 200 MeV for nucleons in nuclei because of the Fermi motion) to high energies, INC models are practically the only available tools to model hadron-nucleus interactions. At lower energies, a variety of preequilibrium models can do a very good job, with physics foundations which become surely more robust than those of INC ones as the energy is going down.

However one of the fundamental requirements for a model describing nuclear interactions to be applied in practical calculations, is **speed**. Indeed there are two possible approaches to the speed problem: the former is to develop sophisticated models, not necessarily MonteCarlo ones, possibly very accurate and maybe slow, and to produce comprehensive tabulations of energy-angle spectra of all emitted particles for a fine mesh of energies of possible projectiles. Such an approach, very similar to that adopted for neutron calculations below 20 MeV, becomes soon very impractical. Indeed, assuming 20 points per energy decade for the energy mesh (still $\approx$ 10% inaccuracy), 3 energy decades (1-1000 MeV for example), 10 deg steps for angular distributions ($\rightarrow$ 18 points), tabulated data for at least p, n, π^+, π^-, π^0, and γ, it can be easily computed that $\approx$ 5-10 Mbyte of dynamic memory will be required for each (target) isotope present in the problem setup. Even assuming possible compression schemes, such a (still rough) mesh cannot be actually used without exploding memory requirements. Furthermore this kind of tabulations, while possibly suitable for many calculations, cannot be used for problems where internal correlations among different particles emerging from the same collision are important. Indeed problems like detector efficiencies, resolutions, coincidences background studies for rare events, etc, do often require the simulation of proper correlations among many particles inside each event, and therefore cannot be studied with approaches based on precomputed data, where such correlations are forcibly lost.

The second approach (used by the vast majority of practical applications in the energy domain of interest), is to use the MonteCarlo method, simulating at run time every interaction. One of reasons of the long dating success of INC models is just their ability to model in reasonable time, almost whichever target nucleus with whichever projectile, with no or small need for external input informations or preliminary calculations. The other great advantage is that all correlation among the different quantities and particles are fully reproduced. Of course, the speed of such a model is a key feature, since a large number of interactions must be simulated within reasonable time. Actually, most INC codes do their job fast enough that they do not represent any significant limitation to the CPU required, which is instead dominated by the transport time. Until this situation will continue, the push for complex and huge pre-tabulated libraries has no serious foundation, unless the physics is much better. Furthermore, while a code can be easily updated and/or corrected, every change in the underlying physical models will require a complete recalculation of the whole library, for all isotopes, particles and energies, making "de facto" such an hypothetical library a quickly obsoleting tool.

4.1 Basic assumptions of IntraNuclear Cascade (INC) models

Classical INC codes [35, 36, 37, 38] are based on a more or less accurate treatment of hadron multiple collision processes in nuclei, the target being assumed to be a cold Fermi gas of nucleons in their potential well[39, 40]. The hadron-nucleon cross sections used in the calculations are free hadron–nucleon cross sections. Usually, the only quantum mechanical concept incorporated is the Pauli principle. Possible hadrons are often limited to pions and nucleons, pions being also produce or absorbed via isobar (mainly Δ_{33}) formation, decay, and capture. The Fermi motion is taken into account when considering elementary collisions, both for the purpose of computing the interaction cross section, and to produce the final state particles. The basic assumptions of INC models can be summarized as follow:

1. Hadrons propagate like free particles in the nuclear medium, with interaction probability per unit length given by free space cross sections, properly averaged over the Fermi motion of the target nucleons, times the local nuclear density.

2. The particle motion is formulated in a classical way. It can be subject to an average nuclear mean potential, which must be added to the free particle kinetic energy when tracking through the nucleus. The radial and energy dependence of such field are model and particle dependent.

3. The effect of the nuclear mean field on the particle motion can either be null or can produce curved trajectories in a semiclassical approach, according to energy and momentum conservation, depending on the model. The curvature effects induced by the nuclear mean field are usually referred to as refraction and reflection effects.

4. Interactions occur like in free space in the Center of Mass System of the two colliding hadrons. Of course, because of the Fermi motion, the lab frame will not coincide with the frame where the target nucleon is at rest, but suitable Lorentz boosts (see Appendix A) have to be applied to transform back the secondary particles in the lab frame.

5. Interactions occur in a completely incoherent and uncorrelated way. No coherence or diffractive effect is included. No multibody or cluster process is included, with the possible exception of pion absorption (see next sections).

6. Quantum effects are mainly limited to Pauli blocking (see section 6): only few codes contain further quantal effects (see again section 6 for a discussion).

7. Secondaries are treated exactly like primary particles, with the only difference that they start their trajectory already inside the nucleus.

An obvious requirement arising from the previous points is that the wavelength associated to hadron motion must be much shorter than the hadron mean free path inside the target nucleus, and also much shorter than the average distance among two neighboring nucleons. That is:

$$\lambda_h = \frac{2\pi\hbar}{p} \ll \frac{1}{\sigma_{hN}\rho} \tag{24}$$

$$\lambda_h = \frac{2\pi\hbar}{p} \ll \left(\frac{3}{4\pi\rho}\right)^{1/3} \tag{25}$$

The nucleon density at the center of nuclei is typically $\rho \approx 0.17$ fm^{-3}, therefore the latter condition would require a particle momentum in excess of 1 GeV/c. For a projectile nucleon, again at central density, the former condition is fulfilled only starting from 200 MeV (see fig. 10 for evaluating σ_{hN}). From these back of the envelope estimates it would appear that INC models cannot work at all, unless the projectile energy is above a few hundreds MeV. Furthermore, the transport and reinteraction inside the nucleus of secondary particles, which are at lower energies, cannot easily comply with the above requirements. Fortunately the situation is not so bad as it could appear. Pauli blocking and other effects contribute to increase particle mean free paths. In particular Pauli blocking is more effective for low energy particles, in such a way partially compensating the increase in nucleon-nucleon cross sections at low energies. Furthermore, hadronic interactions are mostly surface effects (as can be easily checked both from mean free paths and realizing that hadron-nucleus cross sections scale with the target atomic mass approximately like $A^{2/3}$). Hence the nuclear reactions mostly occur at densities significantly lower than the central one, therefore partially mitigating the requirements on particle energies. However it is clear that the physical foundations of INC are not very sound for primary or secondary particle momenta below a few hundreds of MeV/c. According to these considerations, the quality of results which can be obtained by INC codes is somewhat surprising.

4.2 The Steps of an INC simulation

A typical INC code usually follows the following logic:

- Target nucleus description, typically realized through a few concentric sphere of different density and Fermi energy

- Geometrical cross section, corresponding to the nuclear radius or to the maximum possible impact parameter
- Impact parameter selection with a constant probability over the geometrical cross section area. More than one selection can be required if the particle crosses the nucleus without interacting.
- Interaction point selection and projectile tracking through the nucleus, according to Fermi motion averaged hadron-nucleon cross sections and possibly to the nuclear mean field, including the Coulomb field
- Target nucleon selection according to σ_{hp}, σ_{hn} and local Fermi energy
- Interaction simulation according to free hN interactions, local Fermi energy and Pauli blocking
- Secondary tracking into the nucleus, until interaction, escape, or energy cut-off
- (Possible) preequilibrium stage, whenever all excited nucleons are below a given energy threshold (typically a few tens of MeV). This stage is included only in the most recent developments
- Evaporation stage whenever the preequilibrium stage is finished, or all particles are below a given threshold (usually of the order of the binding energy), and the system can be assumed to be equilibrated
- Final deexcitation stage when the excitation energy is below the threshold for particle emission and it is spent through photon emission

A description of the physics involved in all stages can be found in the next sections. It is important to remark that in principle INC codes are able to compute reaction cross sections by themselves. Indeed, the reaction cross section is given by the geometrical one times the probability of interaction. The latter information can be easily derived from the ratio of the impact parameter selections which gave rise to interactions and the total number of selected impact parameters.

4.3 Advantages and Limitations of INC models

A few of the strong points of INC codes have been already touched in the introduction to this section, however they are repeated here for completeness:

- No other model available for energies above the pion threshold
- No other model for projectiles other than nucleons
- Easily available for on-line integration into transport codes

- Every target-projectile combination, without any extra information
- Particle-to-particle correlations preserved
- Equally valid on very light as well as on very heavy nuclei (with some question mark on evaporation)
- Capability of computing reaction cross section where unknown

Before going into details about weak points of INC codes, it must be remarked that many of the historical weaknesses have been mitigated or even completely solved in some of the most recent developments [41, 42, 43]. In the following lists, points flagged with an asterisk refer to glorious but old models, typically the Bertini model [36, 44, 45], but are partially or completely solved in state-of-the-art codes.

- *Low projectile energies ($E \leq 100 - 200$ MeV) are badly described
- *Binding energy: the commonly used assumption of a constant binding energy makes the end points, shapes, and absolute intensities of emitted particle spectra increasingly meaningless for energies below 100 MeV, particularly for reactions like (p, xn) or (n, xp)
- *Backward angle emission poorly described (see [46, 47, 48, 50, 49])
- *Coulomb barrier effect: neglected when refraction/reflection are not modelled or no Coulomb potential is included
- *Cross section calculations: crazy when no potential effect is included for E <100 MeV, and anyway at low energies. This point is particularly critical for codes, like HETC, which make use of INC computed cross sections for particle transport
- *Secondary transport threshold: down to energies much lower than any safe limit for the theory
- Quasielastic peaks above 100 MeV are usually too sharp when compared with experimental data [51]
- Coherent effects as well as direct transitions to discrete states are not included
- Nuclear medium effects which can alter interaction properties are not taken into account (see [52, 53, 54] for example)
- Multibody processes, like interaction on nucleon clusters, are not included in INC approaches
- Composite particle emission (d, t, ^{3}He, α) cannot be easily accomodate into INC codes, but for the evaporation stage.

Table 1: Physical features and particles transported by various codes: X = included, – = not included, O = available via offline linking with other codes, ? = unknown to the authors

Code name	Refr. & Refl.	Preeq. stage	Qua.Eff. besides Pauli	Fermi Break Up	Frag ment ation	Max. En. (GeV)	EM part	Low en. neut.
ICM [37]	–	–	–	?	?	≈ 100	?	?
HETC [58]	–	–	–	–	–	2-3	O	O
HERMES [57]	–	–	–	–	–	2-3	O	O
FLUKA [55, 56, 42]	X	X	X	X	–	10000	X	X
LCS [59, 36],Bertini	–	X	–	X	–	2-3	O	O
LCS [59, 60],Isabel	X	X	X	X	–	1-2	O	O
CEM92 [43]	–	X	–	X	–	3	–	–
GEANT [1]	–	X	–	–	–	1000	X	X

It must be stressed that a relevant part of the improvements achieved by recent developments is due to the inclusion of a preequilibrium stage, which prevents the INC part from working in an unsafe energy range, and strongly improve the modelling of reactions at the lowest energies. Since most of the interactions occur in this energy range (see section 2), it is highly questionable the use of codes which are still based on sloppy physics in this region.

4.4 INC codes available on the market

The following table 1 is only indicative and not at all exhaustive. No judgement of merit is attached to the listed codes, the only reported informations being the energy range covered and the particle transported. Only codes of more or less general use are reported, no effort has been made to collect a complete list. We apologize in advance for any possible missing information. The quoted maximum energies are the only item where our judgement came in. They are not always those quoted in the official documentation, but rather those consistent with the physics included in the code. For example, only nucleon induced single and double pion production, and pion induced single pion production are included into the Bertini model, therefore determining the maximum reasonable energy. A scaling model is used in HETC to extend such energy, but it cannot be used with realistic results much beyond few GeVs. For the sake of completeness, there exist versions of HETC (called HETC88) and of LAHET (called SUPERHET) which make use of old versions of the FLUKA high energy model to extend the maximum energy to several hundreds GeV.

The MARS [61] and CASIM [62] codes are also extensively used for calculations at energies higher than those considered in this lecture.

5 Hadron-Nucleon interactions

The basic assumption in calculations of intranuclear cascades is that nuclear reactions involving incident particles of high energy can be described in terms of hadron-nucleon collisions within the nucleus. Models for such elementary interactions are supposed to be available possibly from phenomenology complemented by theoretical analysis. Therefore a description, mainly phenomenological, of hadron-nucleon interactions is essential in understanding the following more complex treatment of nuclear interactions and is given in this section.

5.1 Preliminary

We remind here a few concepts and formulae of general utility.

We will deal with elastic and inelastic scatterings, thus the quantities to be calculated , and sampled, will be mainly total or differential cross sections. Plenty of books exist on this subject. We re-write here well known formulae: the differential cross section as a function of scattering angle and center of mass energy can be written in terms of a *scattering amplitude* $f(s,\theta)$:

$$\frac{d\sigma}{d\Omega}(\theta) = |f(\theta)|^2 \tag{26}$$

The scattering amplitude is a complex quantity, and it is determined by the interaction matrix. A very useful theorem is the *optical theorem*, that links scattering amplitude and total (elastic scattering + reaction) cross section:

$$\sigma_T = \frac{4\pi}{k} Im f(0) \tag{27}$$

The scattering amplitude can be separated in partial amplitudes corresponding to the different values of the angular momentum l; in the case of spinless particles one has

$$f(\theta) = \frac{1}{k}\sum_l (2l+1) f_l P_l(\cos\theta) \tag{28}$$

where the P_l are the legendre Polynomials.

The experimental observation of charge invariance of nuclear forces suggested the introduction of the isotopic spin vector T. For instance, the proton and the neutron can be described as the two states of a single entity, the nucleon, having total isospin $T = \frac{1}{2}$, and possible projections $T_z = \pm\frac{1}{2}$. In the case of the nucleon, the charge is given by $q = \frac{1}{2} + T_z$. From charge independence, it follows that nuclear interactions depend only on the total isospin value, and not on its projection. Cross sections and other matrix element can be separated in isospin channels; Coulomb forces must then be treated as a correction. The isospin formalism is analogous to the spin formalism, and the Pauli principle is taken into account by (anti)-symmetrization of the wave function also with respect to isospin.

5.2 Nucleon-Nucleon elastic interactions

Below the pion production threshold, the only possible interaction between two nucleons is just elastic scattering. The cross sections for p–p (or n–n) and n–p total and elastic scattering are plotted in fig. 10. There are two basic features of these cross sections (which are the total ones up to roughly 300 MeV). The former is the rapid increase of both cross sections with decreasing energy, while the latter is the factor three at the lowest energies between the n–p and the p–p cross sections, as expected on the basis of symmetry and isospin considerations. The total cross section for the two isospin components are shown in fig. 11, according to $\sigma_T^1 = \sigma_{pp}$ and $\sigma_T^0 = 2\sigma_T^{np} - \sigma_T^{pp}$

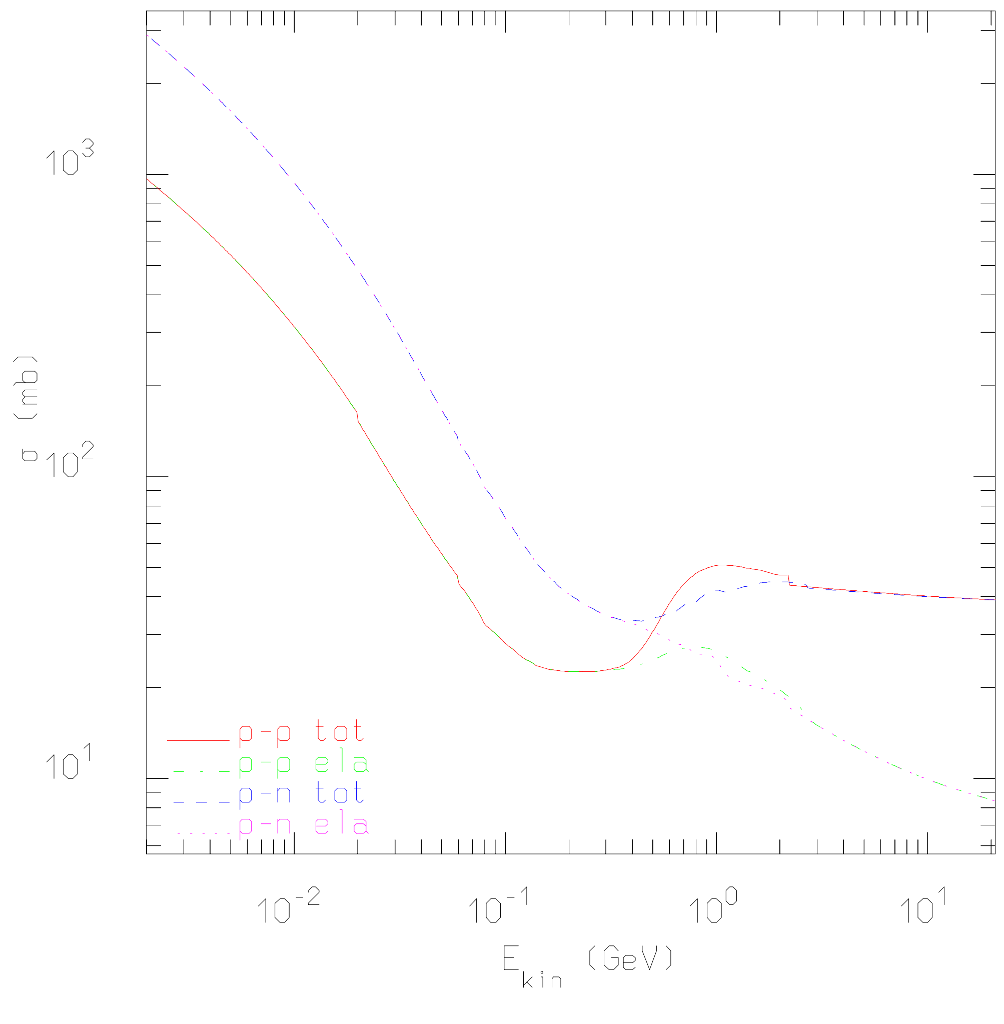

Figure 10: Total and elastic cross section for p–p and p–n scattering

The angular distributions of the p–p reaction is fairly isotropic up to ≈ 300 MeV, while the n–p one starts to exhibit a significant anisotropy at much lower energies[63].

As soon as the energy exceeds a few hundred MeV, both reactions start to develop strong

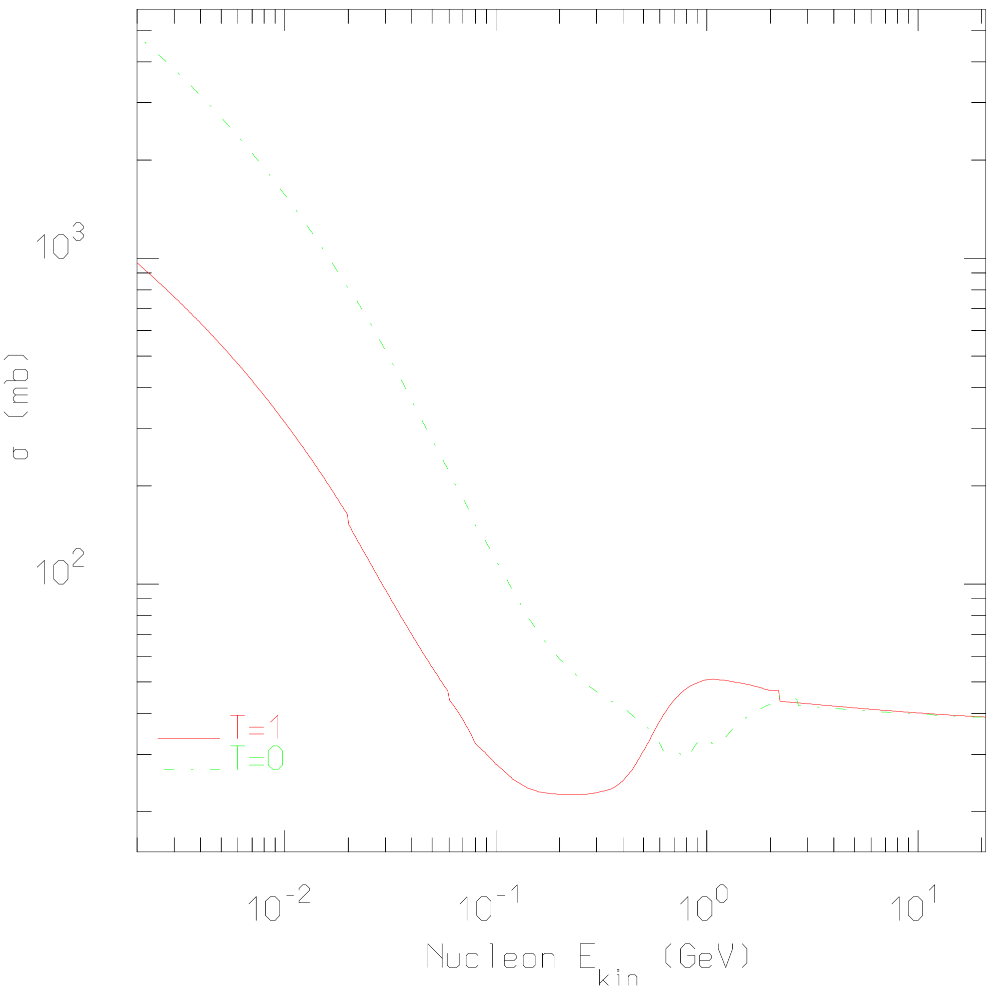

Figure 11: Total cross section for $T = 1$ and $T = 0$ isospin channels for nucleon-nucleon scattering

forward peaks, while the backward "charge exchange" peak of n–p becomes progressively smaller than the forward one, on the contrary of what can be observed at lower energies. Such a behaviour is partially reflected also in the nuclear collisions, where nucleon-nucleon elastic interactions are the dominant process for nucleon induced reactions below 1 GeV. Above 1 GeV the behaviour of the bulk of the angular distribution is well described by a standard diffraction-like expression:

$$\frac{d\sigma}{dt} = b\sigma_0 e^{bt} \tag{29}$$

where t is the four- momentum transfer, which is given in the center of mass system:

$$t = -2p_{cms}^2(1 - \cos\theta_{cms}) \tag{30}$$

5.3 Pion-Nucleon elastic and charge exchange interactions at intermediate energies

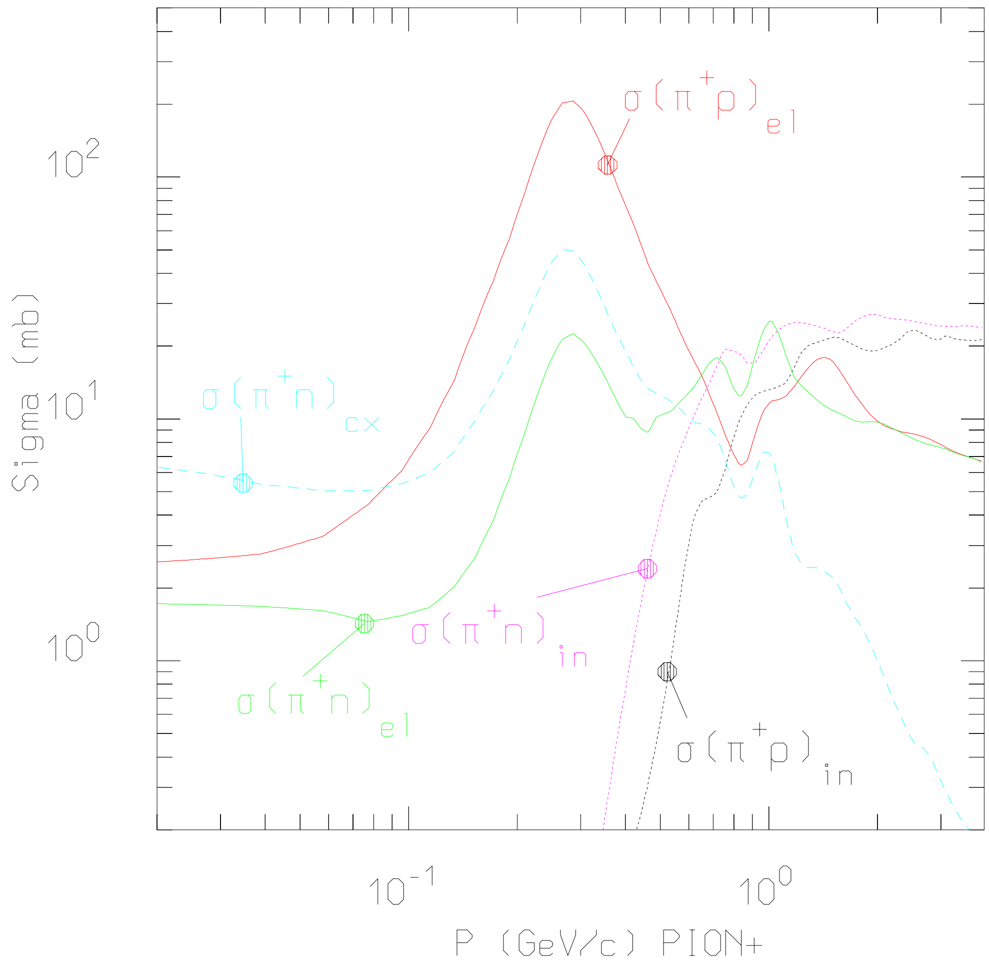

Figure 12: Cross sections for π^+ p and π^+ n reactions

Inelastic processes in Pion-Nucleon collisions remain negligible up to a pion laboratory energy of about 250 MeV, although the kinematic threshold for pion production is at 170 MeV. Up to these energies the most important processes are elastic and charge exchange scattering. Elastic, charge exchange and inelastic π^+ cross sections extracted from tabulations in [64]are shown in fig.12 All show sharp peaks, distinctive of resonances. These peaks are most conveniently examined in the Isotopic Spin formalism. The total isotopic spin for the pion is $T = 1$, and the three charge states correspond to the three values of T_z. Thus, in the pion-nucleon system two values of T are allowed : $T = \frac{1}{2}$ and $T = \frac{3}{2}$, and two independent scattering amplitudes, $A_{\frac{1}{2}}$ and $A_{\frac{3}{2}}$, enter in the cross sections. From Clebsch-Gordan coefficients one obtains the scattering amplitudes A in the different charge states:

$$A\left(\pi^+ p \to \pi^+ p\right) \quad = \quad A_{\frac{3}{2}} \tag{31}$$

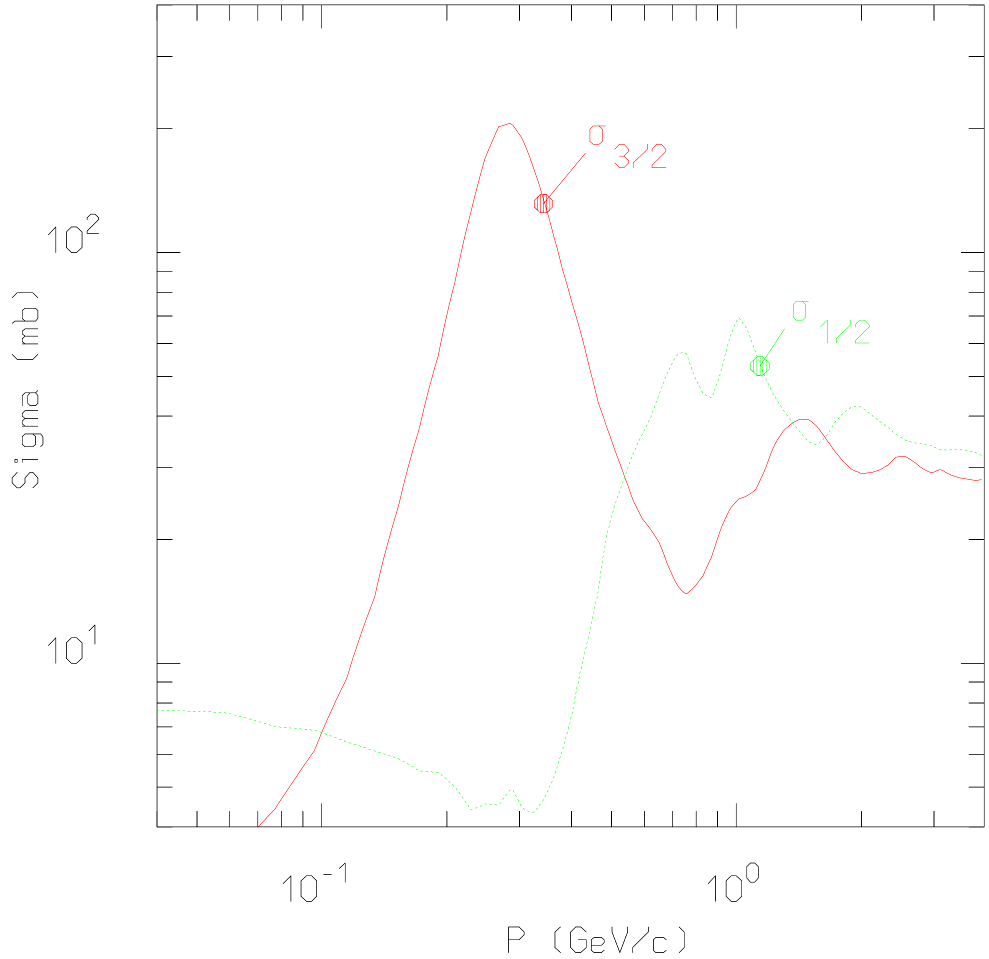

Figure 13: Total cross section for the $T = \frac{3}{2}$ and $T = \frac{1}{2}$ channels for pion-nucleon reactions

$$
\begin{aligned}
A\left(\pi^- p \to \pi^- p\right) &= \frac{1}{3}\left(2A_{\frac{1}{2}} + A_{\frac{3}{2}}\right) \\
A\left(\pi^- p \to \pi^0 n\right) &= \frac{1}{3}\left(\sqrt{2}A_{\frac{3}{2}} - \sqrt{2}A_{\frac{1}{2}}\right) \\
A\left(\pi^0 p \to \pi^0 p\right) &= \frac{1}{3}\left(2A_{\frac{3}{2}} + A_{\frac{1}{2}}\right) \\
A\left(\pi^0 p \to \pi^+ n\right) &= A\left(\pi^- p \to \pi^0 n\right) \\
A\left(\pi^- n \to \pi^- n\right) &= A\left(\pi^+ p \to \pi^+ p\right) \\
A\left(\pi^+ n \to \pi^+ n\right) &= A\left(\pi^- p \to \pi^- p\right) \\
A\left(\pi^+ n \to \pi^0 p\right) &= A\left(\pi^- p \to \pi^0 n\right) \\
A\left(\pi^0 n \to \pi^0 n\right) &= A\left(\pi^0 p \to \pi^0 p\right) \\
A\left(\pi^0 n \to \pi^- p\right) &= A\left(\pi^0 p \to \pi^+ n\right)
\end{aligned}
$$

Using these relations all differential cross sections can be derived from the three measured ones: $\sigma(\pi^+p \to \pi^+p)$, $\sigma(\pi^-p \to \pi^-p)$, $\sigma(\pi^-p \to \pi^0 n)$. Care must be taken to include the effect of the mass differences between charged and neutral pions, and between neutron and proton[65]. At low energies also Coulomb effect should be taken into account.

From 31 and from the optical theorem 27 the total cross sections for the $T = \frac{1}{2}$ and $T = \frac{3}{2}$ states can be isolated:

$$
\begin{aligned}
\sigma_T^{\frac{3}{2}} &= \sigma_T\left(\pi^+p\right) \\
\sigma_T^{\frac{1}{2}} &= \frac{3}{2}\sigma_T\left(\pi^-p\right) - \frac{1}{2}\sigma_T\left(\pi^+p\right)
\end{aligned} \tag{32}
$$

These are plotted in fig. 13 and show the dominant role of the $\Delta(1232)$ (also called Δ_{33} or simply Δ) resonance in the $T = \frac{3}{2}$ channel at 180 MeV lab. energy, and the presence of several N^* resonances in the $T = \frac{1}{2}$ at higher energies.

Detailed phase shift analysis have been performed for π^+p and π^-p scatterings up to centre of mass energies of 2.5 GeV[64]. For kinetic energies below 300 MeV the interaction is strongly dominated by s- and p-waves. The Δ resonance occurs in the $l = 1, J = \frac{3}{2}$ channel (where J is the total angular momentum). The cross sections for π^+ on p and n for the elastic, charge exchange, and inelastic (pion production) channels are shown in fig. 12.

The elastic cross section above 1 GeV has the same exponential behaviour of the nucleon-nucleon cross section.

5.4 Pion production at intermediate energies

Pion production is the first inelastic channel to be open both in pion-nucleon and nucleon-nucleon interactions, obviously because of the small pion mass. The reaction $N_1 + N_2 \to N_1' + N_2' + \pi$ has its threshold around 290 MeV, and it starts to be important around 700, while the reaction $\pi + N \to \pi' + \pi'' + N'$ opens at 170 MeV. The dominance of the Δ resonance, and of the N resonances at higher energies, in the π, N channel suggest to treat both reaction in the framework of the isobar model, that is to assume that they all proceed through an intermediate state containing at least one resonance, for instance in the case of the Δ :

$$N_1 + N_2 \to N_1' + \Delta \to N_1' + N_2' + \pi \tag{33}$$

and

$$\pi + N \to \pi' + \Delta \to \pi' + \pi'' + N' \tag{34}$$

In the intermediate state the resonance can be treated as a real particle, that is, in a Monte Carlo code it can be transported and then transformed into secondaries according to its lifetime and decay branching ratios.

The isobar model accommodates easily multiple pion production, simply allowing the presence of more than one resonance in the intermediate state[66]. Double pion production opens already at 600 MeV in nucleon-nucleon reactions, and at about 350 Mev in pion-nucleon. Again, isospin decomposition is very useful both for deriving quantities for charge states different from the experimentally known ones, and for correctly isolating the contributions of the different resonances. Analysis and parametrizations of nucleon induced pion production in terms of isospin can be found in [68, 67]

5.5 Hadron-Nucleon high energy inelastic and diffractive interactions

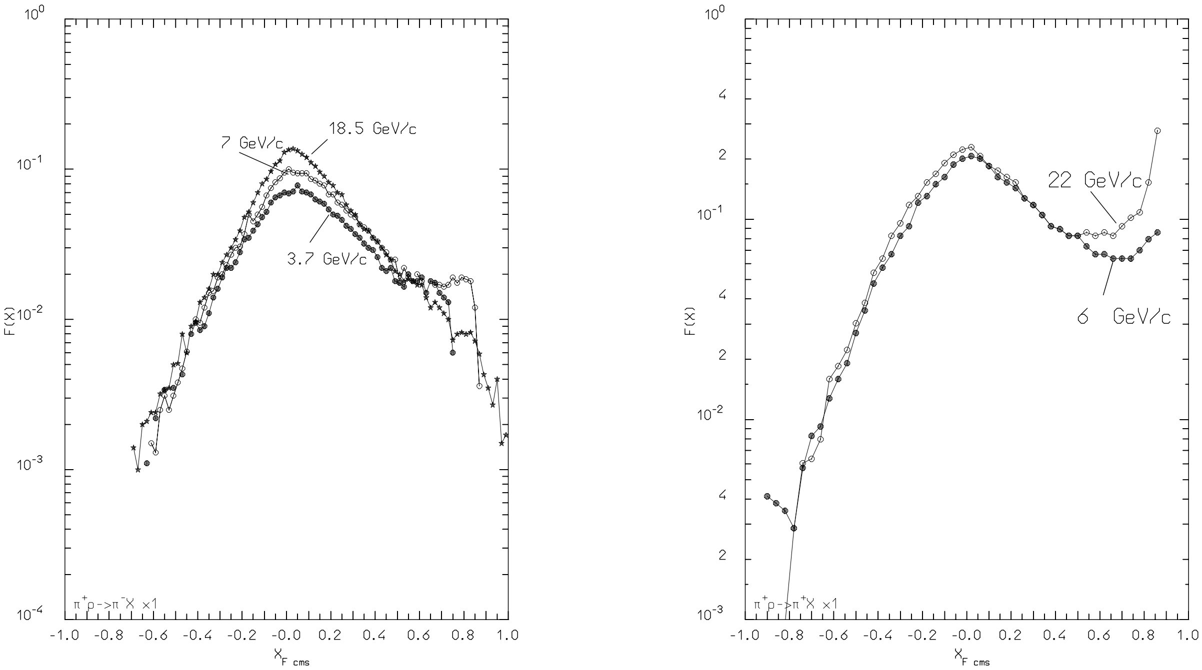

Figure 14: Invariant cross section spectra, as a function of Feynman X_F of negative (left), and positive (right) pions emitted for π^+ on protons at various momenta

As soon as the incident hadron energy exceeds 2-3 GeV, the description of nonelastic interactions via quasi two-body reactions with formation and decay of resonances starts to become difficult. The number of possible channels (and consequently of resonances) to be considered grows very rapidly, the relevant resonances are often not well established and sometimes their decay channels are unknown. More fundamentally, an inspection of experimental data clearly shows how the produced particles are no longer associated with the projectile/target fragmentation region in the centre of mass frame, but they start to preferentially populate the "central" region (see appendix A), in contrast with the naive picture of two excited objects with some transverse momentum in the CMS, decaying into particles in the forward and backward emisphere.

Hadron nucleon interactions at high energy can be described by QCD based models, only at relatively large transverse momentum. Up to fairly high energies (several tens of TeV in

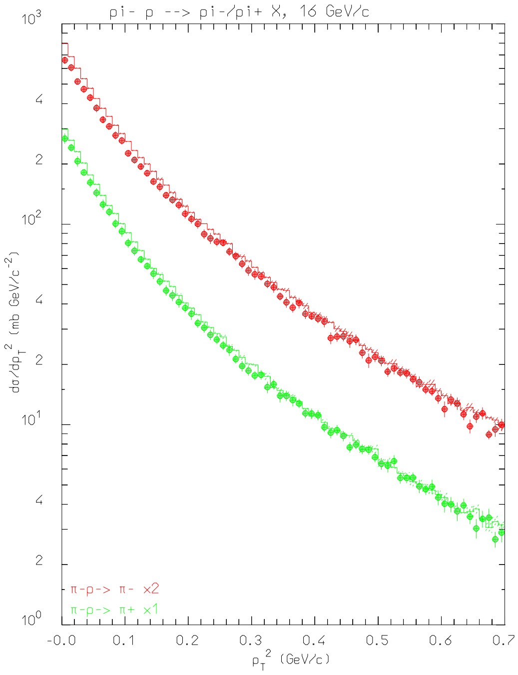

Figure 15: p_T spectra of π^+ and π^- produced by 16 GeV/c π^- incident on an hydrogen target. Symbols are exp. data, the dashed histogram is the FLUKA result

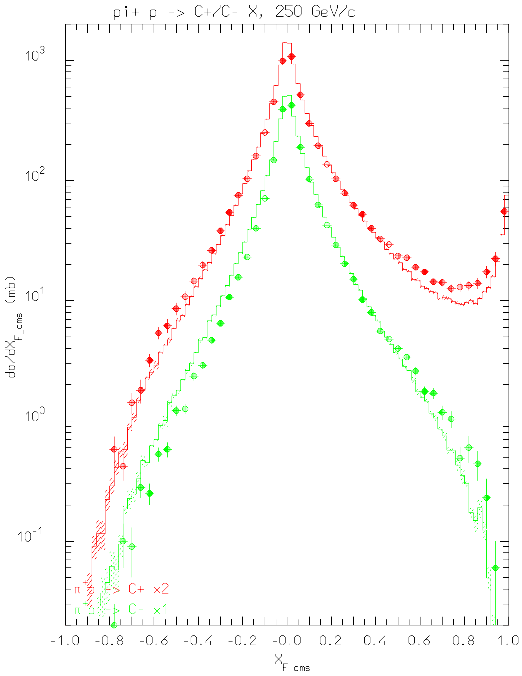

Figure 16: Feynman X_F^* spectra of positive particles and π^- produced by 250 GeV/c π^+ incident on an hydrogen target. Symbols are exp. data, the dashed histogram is the FLUKA result

the lab, where minijet production can no longer be neglected), the bulk of hadron-nucleon inelastic collisions is due to processes with small transverse momentum. In this regime QCD calculations become impractical because of the large coupling constants, which prevent the use of perturbation methods and because transverse momenta well in excess of 1 GeV are required to prevent scattered quarks to undergo multiple interactions with the spectator quarks. The produced particles essentially reflect the motion of the internal constituents, valence and sea quarks. Therefore the longitudinal distribution of produced particles is intimately linked with the longitudinal motion of the constituents, while the p_T distribution has a roughly gaussian shape, typical of multiple collisions. The scale of the p_T distribution is directly linked to the uncertainty principle, taking into account that hadrons are composite object with a rms radius $\approx$ 0.8 fm, $p_T \approx \frac{\hbar}{0.8} \approx 200 - 300$ MeV/c. The shape of the p_T distribution is fairly independent from the projectile energy up to at least several TeV in the lab, and can be well described by:

$$\sigma_{inv} = E\frac{d^3\sigma}{d^3p} \propto e^{-bM_T} \tag{35}$$

The longitudinal distribution of produced particles tend to scale with the incident energy. Such a scaling is often quoted as the hypothesis of *limiting fragmentation* [69] (see Appendix A). A consequence of this approximate scaling is that the produced particle multiplicity does not increase linearly with the system invariant mass, $\sqrt{s}$, ($\sqrt{s} \propto \sqrt{E_{beam}}$, for $E_{beam} \gg M$), but increase roughly logarithmically with s. An example of the invariant cross section distribution, $F(x) = \frac{1}{\sigma}\frac{2E_{CM}}{\pi\sqrt{s}}\frac{d\sigma}{dX_F}$, of negative pions produced in the $\pi^+ + P \rightarrow \pi^- + X$ reactions at 3.7, 7, and 18.5 GeV is presented in fig. 14. A similar plot for $\pi^+ + P \to \pi^+ + X$ is also shown in the same figure. All the experimental data have been taken from the compilation [70]. Both figures show the characteristic concentration of particles in the central region. The scaling violation occurring in that region (the scaling hypothesis originally proposed by Feynman for high energy particle production would predict that the invariant cross section when plotted as a function of the Feynman X variable does not depend on the projectile energy in the central region too) is also evident in the π^- plot. Diffractive production for π^+ at large X_F is also apparent from that figure.

More or less phenomenological models have to be used, even though motivated by physical ideas. Such models usually work at the constituent level, that is with the constituent quarks (often called *valence* quarks), and possibly also with the so called *sea* quarks which are also present inside real hadrons. The momentum or energy distribution of the constituents must be given (it is the equivalent for soft collisions of the structure functions used for hard collisions), and proper hadronization models must be provided. One of the more successful models in this field is the so called Dual Parton Model (DPM). A recent review can be found in [71]. Examples of results obtained with such a model up to very high energies can be found in [72, 73, 74], where also minijet production is taken into account. One of the few models available for high energy interactions [75], which is used in many flavors in HETC88, LAHET, HERMES, and GEANT, has been developed in the DPM framework, originally for the FLUKA code. FLUKA does now include a much more advanced version, which however is still based on the same physical basis. All examples shown here have been computed with such a version. As an example of p_T distributions, the experimental data (and the MC simulation) of the p_T spectra of pions produced by 16 GeV/c π^- on hydrogen are shown in fig. 15 (experimental data from [70]). The longitudinal distribution of positive particles and negative pions produced by 250 GeV/c π^+ on hydrogen are shown in fig. 16 (experimental data from [76]). Again the diffractive peak in the positive particle distribution is clearly visible in fig. 16. A discussion of diffraction is outside the goals of this lecture, however the interested reader can be found informations and examples of modelling of diffraction in the framework of the DPM in [77, 78, 79].

6 Nonelastic Nuclear Interactions

Hadronic nuclear interactions are by far the most complex topics of this lecture. A thorough discussion of their characteristics and of the relevant physics is outside the aims of this lecture (and perhaps of the knowledge of the lecturer). The approach followed is just to describe the basic ideas underlying the most successful models used in practice to describe such interactions. In particular the so called IntraNuclear Cascade (INC) model will be described, mainly because it is still the only one able to cover the full energy range of interest for hadron interactions, provided tools to handle the hadron-nucleon interactions are available, and the spacetime characteristics of high energy interactions are taken into account.

6.1 Nucleon Fermi motion

Some properties of nuclear matter can be explained in a very simple way by the Fermi gas model (for descriptions of this and other nuclear models see for instance[80, 81, 82]) Nucleons are described as non-interacting fermions constrained in a cubic box of linear dimension a. The confinement is somehow equivalent to the introduction of an attractive interaction among nucleons that keeps them inside the nucleus. The nucleon wave functions are that of a free-particle with the condition $\Psi(x, y, z) = 0$ at the nuclear boundary, thus with constraints on the three components of the momentum:

$$K_x a = n_x \pi \quad K_y a = n_y \pi \quad K_z a = n_z \pi \tag{36}$$

where the n's are positive integers. Each set of integers defines a solution of the Schrödinger equation energy given by:

$$E(n_x, n_y, n_z) = \frac{\hbar^2}{2M}|K|^2 \tag{37}$$

$$|K|^2 = (K_x^2 + K_y^2 + K_z^2) \tag{38}$$

Nucleons must obey the Pauli principle, thus for each set of n's, that is for a given momentum state, there can be at most four nucleons, namely two protons and two neutrons, each pair with opposite spin. The ground state of the nucleus will be that with all the lowest-lying states occupied. The number of possible states can be easily calculated in momentum space: from the above quantization it follows that each solution occupies a box in momentum space given by $\left(\frac{\pi}{a}\right)^3$; thus the number of states with momentum comprised between K and $K + dK$ is given by the volume of the spherical shell of radius K and thickness dK divided by the volume occupied by each single solution, and divided again by eight since we consider only positive values of n_x, n_y, n_z:

$$dN = \frac{|K|^2}{2\pi^2}\Omega dK \quad \Omega = a^3 \tag{39}$$

re-expressed as a function of energy :

$$dN = \frac{\Omega m}{2\pi^2\hbar^3}\sqrt{2mE}dE \tag{40}$$

Integrating eq. 39 up to a given momentum $|K_F|$, one obtains the total number of states with momentum smaller than $|K_F|$:

$$n(K_F) = \frac{4\pi}{3}\frac{K_F^3}{8(\pi/a)^3} \tag{41}$$

These n levels must be occupied by N neutrons and Z protons. If we take N=Z=A/2, and place 4 nucleons on each level, we get:

$$A = \frac{2\Omega}{3\pi^2}K_F^3 \tag{42}$$

it follows that the momentum of the highest occupied state depends only on the nuclear density $\rho = A/\Omega$:

$$\rho = \frac{2}{3\pi^2}K_F^3 \tag{43}$$

From the observed density of nuclei, $\rho = 1.7 \times 10^{38}$ nucleons/cm^3, one obtains

$$K_F = 1.36 fm^{-1} \quad E_F = 38 MeV \tag{44}$$

These are called the *Fermi momentum* and *Fermi Energy.* In nuclei with $N \neq Z$, two different values of the Fermi energy can be defined:

$$\begin{aligned} \rho_n = \frac{N}{A}\rho &= \frac{(K_F^n)^3}{3\pi^2} \\ \rho_p = \frac{Z}{A}\rho &= \frac{(K_F^p)^3}{3\pi^2} \end{aligned} \tag{45}$$

The so defined Fermi energies are obviously kinetic energies, that is energies counted from the bottom of a potential well that in this model must be input from outside. The total depth of the potential should be such to place the so-called Fermi level, i.e. the last occupied level, at a total energy corresponding to the separation energy for the nucleus considered. This gives an average potential depth of about 38+8=46 MeV. The Fermi kinetic energy distribution can be used with success in many applications. The model is also able to predict the order of magnitude of some empirical nuclear parameters, such as surface energy and asymmetry energy.

The model can be extended to account for realistic nuclear density distribution, that is not uniform, but presents a gradual decrease in what is called the nuclear skin. The Fermi energy of eq.43 can be made radius-dependent in a straightforward way, through the so called "local density approximation":

$$\rho(r) = \frac{2}{3\pi^2} K_F^3(r) \tag{46}$$

Since the density distribution is experimentally well determined, this last formulation of the Fermi energy could provide the radial behaviour and value of the nuclear potential. This is of widespread use in intranuclear cascade codes. Moreover, the same assumption, i.e. nuclear matter as a gas of noninteracting nucleons, linked with thermodynamics, leads to the definition of nuclear temperature and to a general expression for the density of nuclear excited states as a function of excitation energy. An other important quantity that can be calculated in this model is the so-called correlation function, that must be taken into account in intranuclear cascade codes, expecially when dealing with multibody processes: due to the antisymmetrization of the fermion's wave function, given a nucleon in a position $\vec{r}$ in a nucleus with density ρ_0, the probability of finding another like nucleon in a position $\vec{r}\,'$ is decreased for small values of the distance $r = |\vec{r} - \vec{r}\,'|$ by a factor

$$g(x) = 1 - \frac{1}{2}\left[\frac{3}{x^2}\left(\frac{\sin x}{x} - \cos x\right)\right]^2 \tag{47}$$

where $x = K_F \cdot r$, and the factor $\frac{1}{2}$ in front of the parenthesis accounts for the two possible spin orientations.

6.2 Nuclear Potential

The approximation of independent motion of nucleons inside a common single-particle potential is possible due to the fact that the average inter-nucleon distance is large with respect to the range of the nucleon-nucleon interaction. This is partly ensured by the Pauli principle, and partly by the presence of a repulsive core in the nucleon-nucleon interaction. The single particle potential can be thought as the mean field resulting from all the two-body interactions among nucleons. Many possible shapes of this potential have been proposed, either on the basis of self-consistency (Hartree-Fock like) or of computational usefulness linked with agreement with experimental quantities (harmonic oscillator, Nilsson anharmonic oscillator, Woods-Saxon, all with spin-orbit coupling). These potential are able to reproduce the observed level spacings and ordering, and other nuclear quantities. They are, however, less useful in scattering or reaction processes. In these application, the so called Optical Potential is introduced. It is a complex potential that enters in the Schrödinger equation for the projectile. The real part describes the scattering, the complex part describes the absorption: to illustrate this, let us suppose that the optical potential $V(\vec{r}) = -(U(\vec{r}) + iW(\vec{r}))$ has the shape of a square well. The wave functions can then be described by plane waves, and the solution of the Schrödinger equation

$$\left\{-\frac{\hbar^2}{2M}\nabla^2 + V - E\right\}\Psi_K = 0 \tag{48}$$

inside the range of the potential will be

$$\begin{aligned} \Psi_{\vec{K}} &= Ae^{i\vec{K}\cdot\vec{r}-\frac{i}{\hbar}Et} \\ E &= \frac{\hbar^2 K^2}{2M} - U - iW \end{aligned} \tag{49}$$

since E is real and equal to the energy before the collision, $\vec{K}$ must be a complex vector, thus if one looks at the dependence of the particle probability density $|\Psi|^2$ as a function of $\vec{r}$, and assuming for simplicity $K \parallel z$, one obtains

$$|\Psi|^2 \propto e^{-2ImK\cdot z} \tag{50}$$

That means that the particle can be absorbed in the nucleus with a mean free path

$$\lambda = \frac{1}{2ImK}$$

From eq. 49 one has $ImK = \frac{2M}{\hbar^2}\frac{W}{2ReK}$, and, assuming that the absorptive potential W is small with respect to $E+U$, $ReK \approx \left(\frac{2M}{\hbar^2}(E+U)\right)^{\frac{1}{2}}$, from which

$$\lambda^{-1} \approx 2\frac{W}{\hbar}\left(\frac{M}{2(E+U)}\right)^{\frac{1}{2}} \tag{51}$$

this becomes

$$\lambda^{-1} \approx 2\frac{W}{v\hbar} \tag{52}$$

where v is the particle velocity. The nucleon mean free path in a nucleus should be given, at least in first approximation, by the cross section on a single nucleon multiplied by the nuclear density: $\lambda^{-1} = \rho\sigma_{NN}$, thus a link between the absorptive nuclear potential and the nucleon nucleon cross section is immediately derived:

$$W = \frac{\hbar}{2} v \rho \sigma_{NN} \tag{53}$$

We shall see in sec. 6.5 that many effects invalidate this simple relation, which however remains a first order estimate.

The optical potential can be in derived from the convolution of the interactions between the projectile and all the nucleons in the nucleus, or can be fitted to the scattering data with preliminary assumptions about its radial dependence. The real part of the optical potential is also sometimes used to describe bound states. As life is always complicated, both the optical potential and the self consistent nuclear potential turn out to be energy dependent, but we stop here.

6.3 Pion Nuclear Potential

For pions, a standard nuclear potential exists [83]. It must be written in relativistic form, because the pion mass is small (about 139 MeV) and can be comparable with its kinetic energy. In coordinate space, and in the frame in which the nucleus is at rest, this is written as (the upper and lower signs refer to π^+ and π^-, respectively , while π°s are not sensitive to N-Z asymmetry):

$$\begin{aligned}
2\omega U_{opt}(\omega, r) &= -\beta(\omega, r) + \frac{\omega}{2M}\nabla^2\alpha(\omega, r) - \nabla \cdot \frac{\alpha}{1 + g\alpha(\omega, r)}\nabla && (54)\\
\beta &= 4\pi\left[\left(1 + \frac{\omega}{M}\right)\left(b_0(\omega) \mp b_1(\omega)\frac{N - Z}{A}\right)\rho(r) + \left(1 + \frac{\omega}{2M}\right)B_0(\omega)\rho^2(r)\right] && (55)\\
\alpha &= 4\pi\left[\frac{1}{1 + \frac{\omega}{M}}\left(c_0(\omega) \mp c_1(\omega)\frac{N - Z}{A}\right)\rho(r) + \frac{1}{1 + \frac{\omega}{2M}}C_0(\omega)\rho^2(r)\right] && (56)
\end{aligned}$$

where ω is the first component of the pion 4-momentum, M is the nucleon mass, U_{opt} is the optical potential, $b_0, b_1, c_0, c_1, B_0, C_0$ are complex parameters, g is the Lorentz-Lorenz correction parameter [83] (here and in the following the natural system of units , $\hbar c = 1$, is used). The functional form of this potential derives from that of the pion-nucleon scattering amplitude: b 's are related to s-wave pion-nucleon interaction, while c 's are related to p-wave interaction. The terms in ρ^2 account for two-nucleons mechanisms. This potential contains a divergence operator, thus it is non-local, that means that it depends on the pion velocity besides on position, or, equivalently, the potential in a given position depends on the value of the wave function at different positions. A semiclassical approximation of the particle trajectory is in principle not possible for a non-local potential. However, many localization procedures have been already devised for it [84, 86]. We do not go into details, but just give the result to understand its properties :

$$2\omega U_{opt}(\omega, K) = -\beta - K^2\frac{\alpha}{1 + g\alpha} + \frac{\omega}{2M}\nabla^2\alpha \tag{57}$$

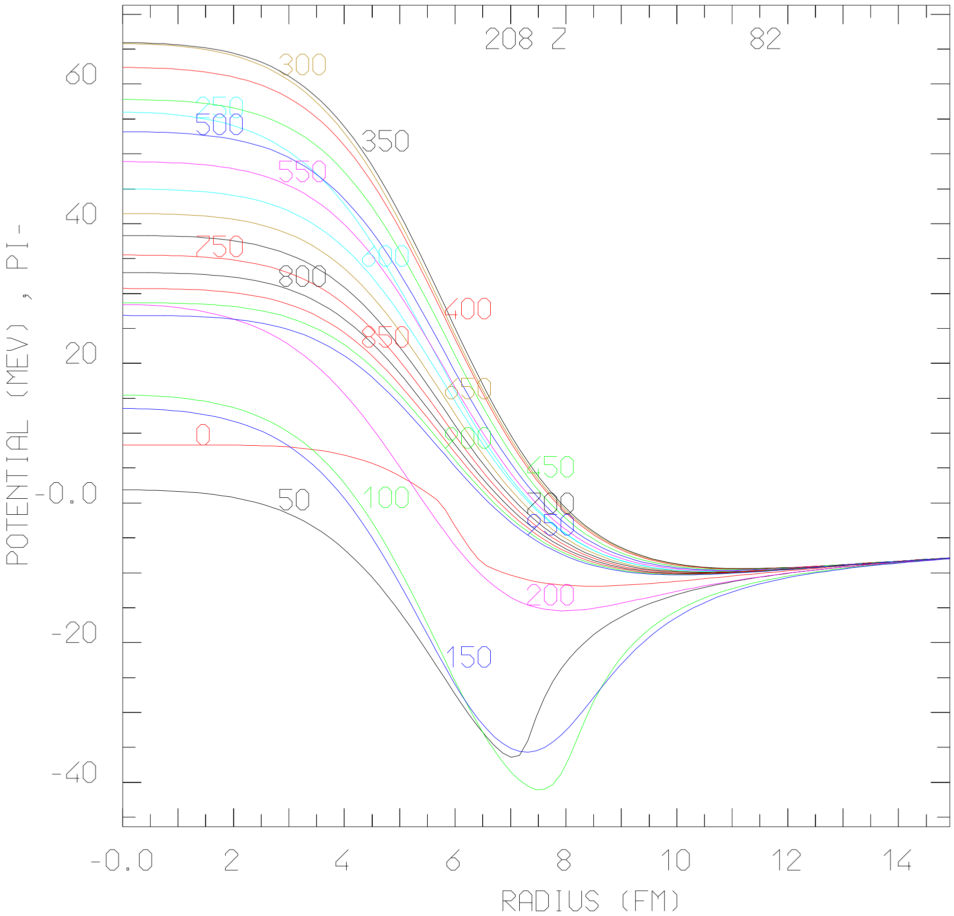

Figure 17: Nuclear potential for π^- in a Pb nucleus as a function of radius. Different curves refer to different pion kinetic energies. Coulomb potential is included

where K is the pion wave number inside the nucleus and the nuclear density that enters in α and β is the local one. It can be seen that the dependence on momentum is strong. In the literature, the Klein-Gordon equation for the pion in the nuclear optical potential is always written as:

$$\left[(\omega - V_c)^2 - 2\omega U_{opt} - K^2\right] \Psi = m_\pi^2 \Psi \tag{58}$$

From eq. 58 applying energy conservation and calling k_0 the linear momentum of the pion outside the potential range, one obtains an equation for K^2:

$$K^2 = k_0^2 + V_c^2 - 2\omega V_c^2 - 2\omega U_{opt}(\omega, K) \tag{59}$$

substituting eq. 57

$$K^2 \quad = \quad \frac{k_0^2 + V_c^2 - 2\omega V_c^2 + \beta - \frac{\omega}{2M}\nabla^2\alpha}{1 - \bar{\alpha}} \tag{60}$$

$$\bar{\alpha} = \frac{\alpha}{1 + g\alpha}$$

The real part of K^2 gives then the real part of the potential from eq. 59. As pointed out by Johnson and Bethe [87], the denominator of eq.61 approaches zero for normal nuclear densities. In ref. [87, 88] they suggested a correction which takes into account the effects of correlated scattering centers, and reduces the values of the potential as the density increases. The values of the optical potential parameters at low energies (below 50 MeV) are known [83, 89] from pionic atoms and scattering data. At higher energies, however, only an extrapolation based on pion-nucleon phase shifts is available [89]. For the dependence of the p-wave parameters on energy a resonant shape can also be assumed, following the theoretical behaviour of the pion-nucleon scattering amplitude, which is dominated by the Δ resonance channel.

The resulting potential has again a resonant shape, with strong dependences on nuclear density. Its depth reaches several tens of MeV, therefore its introduction, although complex, is essential to correctly describe the pion transport and interaction in nuclear matter. An example is shown in fig.17 for pions in Lead, as a function of pion energy and nuclear radius. In making this plot, a nuclear density of the form of eq.67 has been used.

6.4 Multibody Absorption of Pions

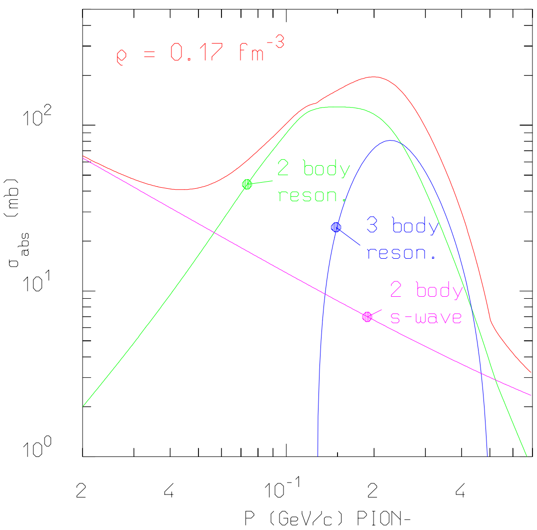

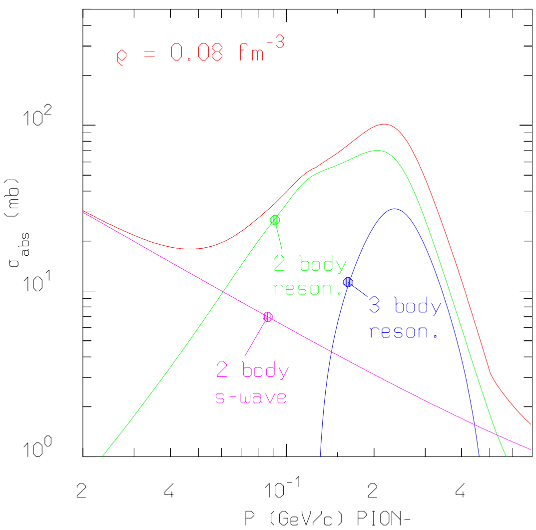

Figure 18: Charged pion absorption cross section for infinite symmetric nuclear matter at two different density values ($\lambda_{abs}^{-1} = \sigma_{abs} \cdot \frac{1}{2}\rho = \sigma_{abs} \cdot \rho_{pro} = \sigma_{abs} \cdot \rho_{neu}$)

Negative pions at rest can be captured on atomic orbits, forming pi-mesic atoms, jump on more internal orbitals with the emission of x-rays and finally be captured by the nucleus. This process is a long-studied one[84] , and led to the construction of very detailed models of low-energy pion-nucleus interactions. But this is not the only possible absorption: the in-flight one exists, and its cross section can amount to about one third of the total pion-nucleus cross section, and about one half of the reaction one. For free pions and nucleons the non-radiative absorption process does not occur since energy and momentum cannot be conserved, and the radiative absorbtion is a very weak process. Conversely, pion absorption in complex nuclei can account for a large part of the cross section: the basic process is absorption on two nucleons, thus the simplest case to be examined is the absorption on the deuteron. Both total cross sections and angular distribution of emitted nucleons have been extensively measured in the $\pi d \to pp$ reaction, and show again the dominance of the $\Delta(1232)$ resonance[85, 83]. At very low energies, the s wave non-delta interaction is important and the cross section rises as the inverse of the relative velocity. Turning to absorption on an arbitrary pair of nucleons, this dominance of non-resonant s-wave and resonant p-wave absorption is the guide to describe the process. Again, the isospin decomposition turns out to be a very useful tool. The outgoing nucleon pair can have $T = 0$ *or* 1, thus these are the two isospin channels allowed. The initial state is composed by a pion, and again an isospin $I = 0$ *or* 1 nucleon pair. If we label the amplitudes as f_{IT}, some passages of momentum combination algebra help to demonstrate that, given a pion with isospin projection λ, and a nucleon pair with isospin projection i,

$$\sigma(\lambda, t) \propto \sum_{IT} |(Ii1\lambda|Tt)|^2 \cdot |f_{IT}|^2 \ , \quad t = i + \lambda \tag{61}$$

If, now, we consider the intermediate state, in order to extract the Δ contribution, we can use the Racah coefficients to recouple the isospin and explicitate the pion-nucleon intermediate state, always in a definite total T state . In this case the amplitudes will be denoted by $g_{\frac{3}{2},T}$ and $g_{\frac{1}{2},T}$, and the link between the f and the g is given by

$$\begin{aligned} f_{01} &= \frac{1}{\sqrt{3}}\left(\sqrt{2}g_{\frac{3}{2},1} + g_{\frac{1}{2},1}\right) \\ f_{11} &= \frac{1}{\sqrt{3}}\left(-g_{\frac{3}{2},1} + \sqrt{2}g_{\frac{1}{2},1}\right) \\ f_{10} &= g_{\frac{1}{2},0} \end{aligned} \tag{62}$$

If we assume delta dominance, and put $g_{\frac{1}{2},T}$=0, from eqs 62 and 61 we obtain that for charged pions the absorption cross section on a (p,n) pair is five times that on a (p,p) (or (n,n)) pair. Moreover, the isospin 0 channel has no contribution from the delta resonance.

The formal treatment of this process inside a real nucleus is quite complex, because the pion can interact with other nucleons before being absorbed, it acquires a potential energy due to its average interaction with nucleons and to the Coulomb field, and the Δ properties, in particular the partial widths, are modified by nuclear matter: n nuclear matter, the Δ can either decay, resulting in elastic scattering or charge exchange, or interact with other nucleons, resulting in pion absorption: its width is broadened with respect to the free one[90, 6, 7, 5]. Modern calculations [6] take these effects into account by calculating energy and nuclear density dependent partial widths for the delta decay:

$$\frac{1}{2}\Gamma_T = \frac{1}{2}\Gamma_F - Im\Sigma_\Delta \tag{63}$$

$\Sigma_\Delta = \Sigma_Q + \Sigma_2 + \Sigma_3$, where Σ_Q, Σ_2 and Σ_3 are the partial widths for quasielastic scattering, two body and three body absorption. The nuclear density dependence of two and three body absorption turns out to be of the type ρ^β and ρ^γ, respectively with $\beta < 2$ and $\gamma < 3$, thus different from the simple ρ^2 (ρ^3) dependence one expects for a two-body (three-body) process. In this way pion scattering, charge exchange, two-body and even three-body absorption can be treated in a consistent way as two-step processes, the first one being the excitation of a Δ from a pion-nucleon interaction, the second is the propagation and rescattering or decay of the resonance in the nucleus. The inclusion of this process in an INC code allows to keep into account processes that are called FSI (final state interaction) and ISI (initial state interaction) that are absorption preceeded (or followed) by scattering of the projectile or of the secondaries, and the effect of the Coulomb field. These processes represent a significant complication when theoretical calculations of absorption are compared to experimental data in medium-heavy nuclei.

In addition, a two-body s-wave absorption cross section can be derived from the optical model [83] as

$$\sigma_s^A(\omega) = \frac{4\pi}{p}(1 + \frac{\omega}{2m}) Im B_0(\omega)\rho \tag{64}$$

Where ω is the pion energy in the lab frame and B_0 is a parameter of the pion optical potential.

As a result, the absorption cross section on nuclei still resembles in shape that on the deuteron, with a resonance-like behaviour, but the resonance is smoothed, and an enhancement of the π^- cross section with respect to the π^+ one arises, both due to the Coulomb field and to the neutron excess in heavy nuclei. The absorption cross section, both 2 and 3 body resonant, and 2 body non resonant, is shown in fig. 18, for two different values of the nuclear density. The figure is based on the approach outlined in [42]. The values must be taken as indicative, mainly because no difference between neutron and proton density has been included.

6.5 Hadron mean free paths in the nucleus and Pauli blocking

As already mentioned, the plain use of hadron nucleon-nucleon cross section leads to values of the mean free path of hadrons which are by far too short with respect to reality. There are many effects that influence the in-medium cross section. The first, and better known, effect, is the Pauli blocking. Any secondary nucleon created in an intranuclear interaction must obey the Pauli exclusion principle, thus it must have enough energy to jump from the Fermi sea where it lies before the interaction to an unoccupied state, above the Fermi level. The result of this is that interactions with small momentum transfer are partially inhibited. Here two points must be mentioned: the first is that the kinetic energy of the projectile inside the nucleus is changed with respect to the free one by the presence of the nuclear potential. The second is that the target nucleons possess themselves a kinetic energy, distributed accordingly to the Fermi distribution 40. The interaction kinematics must be applied in the correct frame, that of the projectile-target nucleon center of mass, to get the correct cross section and outgoing particle distribution.

Analytical calculations for the combined effect of Fermi motion and Pauli blocking on the in-nucleus nucleon-nucleon cross section can be performed under a few approximations, such as isotropy of the angular distribution and either independence of or inverse proportionality to energy of the cross section[91]. The reduction of the cross section with respect to the free one depends on the projectile energy and on the Fermi energy, for instance taking $E_F = 40$ MeV, the reduction factor is ≈ 0.3 at 20 MeV incident Energy (measured outside the nucleus) and ≈ 0.6 at 100 MeV. Even with these corrections, the mean free path of a 60 MeV nucleon results as small as 2 fm.

In a MonteCarlo cascade code, the aforementioned approximations can be avoided, by explicitly checking after each interaction that the momenta of all secondary nucleons are above the Fermi level. Pauli blocking is of course effective also in pion-nucleus interactions, both scattering and absorption.

Mechanisms other than Pauli blocking are effective in increasing the particle mean free path in nuclear medium. These mechanisms are important to prevent the well known problems [92] met by INC codes including refraction and reflection because of strong secondary absorption in the nucleus core, and to match at low energies the mean free paths obtained from optical model analysis.

- The formation zone [93] concept after pion or nucleon inelastic (pion production) interactions
- Nucleon antisymmetrization effects [82], which decrease the probability for secondary particles to reinteract on a nucleon of the same type very close to the production point (see eq.47)
- Nucleon-nucleon hard-core correlations (see for example [94]) which also prevent secondary particles to collide again too close to the production point. Typical hard-core radii used are in the range 0.5-1 fm
- "Coherence" length after elastic or charge exchange hadron-nucleon scatterings. In analogy with the formation zone concept, such interactions cannot be localized better than the position uncertainty connected with the four-momentum transfer of the collision. Reinteractions occurring at distances shorter than the coherence length would undergo interference and cannot be treated anyway as independent interactions on other nucleons. It must be stressed that this mechanism is rather selective on the outgoing direction. Forward scattered particles are preferably emitted as well as backward scattered ones if the colliding particles are identical, pp or nn for example.

6.6 Preequilibrium emission

The intranuclear cascade model [36] is the most straightforward approach when writing a MonteCarlo code, and has been successfully used for decades in the intermediate energy region. However, its physical foundation becomes approximate at low energies [4], resulting in a decrease of its accuracy. Moreover, it can be very time consuming, since many particles must be followed down to very low energies.

On the other hand, a description based simply on direct reaction plus compound nucleus evaporation is surely not sufficient. Already in 1966 Griffin [95] described the spectra following nucleon-induced reactions in terms of a "preequilibrium" model, that is, a transition between the first step of the reaction and the final thermalization.

Since then, many models have been developed (see [4] for an exhaustive review). The two leading approaches (with many different implementations) are the quantum-mechanical multistep model [96], which has a very good theoretical background, but is complex and poses some difficulties to the description of multiple nucleon emission, and the exciton model [95, 4, 97], which relies on statistical assumptions. This makes it very simple and fast, but of course leads to some limitations, especially for medium-high energy projectiles.

The approach described here is that formalized by M. Blann and coworkers [98, 99], and called Geometry Dependent Hybrid Model (GDH).

The preequilibrium process in the exciton model is described as a chain of steps, each step corresponding to a certain number of "excitons", where an exciton can be either a particle above the Fermi surface or a hole below the Fermi surface. The statistical assumption underlying the exciton model states that any partition of the excitation energy E among n excitons has the same probability to occur. The nucleus proceeds in the chain through nucleon-nucleon collisions which increase the exciton number by two units, thus assuming that the probability of having an interaction that decreases the exciton number or lets it unchanged can be neglected. The chain stops, and equilibrium is reached, when either the exciton number n is sufficiently high ($n = \sqrt{2gE}$), where g is the single particle level density, or the excitation energy is below any emission threshold.

The initial number of excitons depends on the reaction type and on the cascade history.

At each step there is a definite probability $P_{x,n}(\epsilon)$ of emitting a nucleon of type x and energy ϵ in the continuum. This probability can be factorized in two parts, one giving the fraction of n-exciton states in which one exciton is unbound and has energy ϵ in the continuum, the other giving the probability for the exciton to escape from the nucleus during its mean lifetime [98]:

$$P_{x,n}(\epsilon)d\epsilon = \sum n_{p_x} \frac{\rho_n(U,\epsilon)gd\epsilon}{\rho_n(E)} \frac{\lambda_c(\epsilon)}{\lambda_c(\epsilon)+\lambda_+(\epsilon)} \tag{65}$$

where n_{p_x} is the number of particle-like excitons which are of type x, g is the single-particle state density, U is the residual nucleus excitation energy (U=E-ϵ-Binding Energy), $\rho_n(E)$ is the density (MeV^{-1}) of exciton states, and is given by:

$$\rho_n(E) = \frac{g(gE)^{n-1}}{n!(n-1)!} \tag{66}$$

$\lambda_c(\epsilon)$ is the rate of emission in the continuum, and is related to the cross section of the inverse process (σ_{inv}) by the detailed balance principle (see par.6.7), and $\lambda_+(\epsilon)$ is the exciton reinteraction rate. The $\lambda_+(\epsilon)$ can be calculated from the nucleon mean free path in nuclear matter [91], or from the optical model. The value of the single particle density is normally taken as g=Z/14 (N/14) MeV^{-1} for protons(neutrons), although it could be a complex function of energy [100]. This formulation has been refined in the GDH [99] to account for the experimentally established importance of peripheral collisions. This has been accomplished through two mechanisms, both applied to the first step of the exciton chain. As first, the nuclear density entering the quantities in eq. 65 is no longer a constant, but depends on the impact parameter and is chosen accordingly to the experimental distribution:

$$\rho = \frac{\rho_0}{1 + \exp \frac{r - R_0}{a}} \tag{67}$$

The Fermi energy has then the density-dependent form of eq. 46. Secondly, the exciton state density is modified from eq. 66 by the assumption that any hole-like exciton cannot carry an excitation energy larger than the (local) Fermi energy. Explicit formulae for the constrained exciton state densities can be found in [99]. Both mechanisms contribute to the enhancement of the hardest part of the emitted particle spectra.

In the exciton model the angular dependence has to be somehow added, since it is not intrinsic in the formulation. Many different approaches have been recently developed, most of which rely on the fast particle approximation. We describe here the formulation of Mantzouranis et al. [101], as implemented by Akkermans et al. [102]. In this model the angular orientation of the nucleus at each step is defined by the direction of the fast particle, which changes gradually in a series of two-body collisions. The transition rate between different exciton states is supposed to be factorizable in an energy-dependent and an angle-dependent factor. The same factorization holds then for the resulting emission probability :

$$\frac{dP_{x,n,\theta}(\epsilon)d\epsilon}{d\Omega} = P_{x,n}(\epsilon)d\epsilon \cdot \sum_l a_l P_l(cos(\theta)) \tag{68}$$

Besides the fast particle one, other approximations are introduced in the calculations leading to eq. 68: in the binary collisions the Fermi motion of target nucleons and the Pauli exclusion principle are neglected, as are reflection/refractions at the nuclear boundary.

6.7 Evaporation/Fragmentation

At the end of the exciton chain, or of the INC part whenever no preequilibrium stage is included in the calculation, the nucleus is supposed to be left in an equilibrium state, in which the excitation energy U is shared by a large number of nucleons. The excitation energy can be higher than the separation energy, thus nucleons and light fragments (α,d,^{3}H, ^{3}He) can still be emitted: they constitute the low-energy (and most abundant) part of the emitted particles, having an average energy of few MeV. The emission process can be well described as an evaporation from a hot system. The treatment starts from the formula of Weisskopf [103], that is an application of the detailed balance principle, linking the probabilities $P_{i \to f}$ to go from a condition i to a condition f and viceversa through the density ρ of states in the two systems:

$$P_{i \to f}\rho(i) = P_{f \to i}\rho(f) \tag{69}$$

$P_{f \to i}$ is the probability of capturing a particle and form a composite nucleus, and is given by the product of the compound nucleus cross section σ_{inv} times the particle flux. Restricting to a volume Ω, the particle flux is $\frac{v}{\Omega}$, and

$$P_{f \to i} = \sigma_{inv} \frac{v}{\Omega}$$

The evaporation probability for a particle of type j , mass m_j and kinetic energy E is thus

$$P_j(E)dE = \frac{(2S_j+1)m_j}{\pi^2 \hbar^3} \sigma_{inv} \frac{\rho(f)}{\rho(i)} E dE \qquad (70)$$

where the ρ's are the nuclear level densities, and the non-relativistic phase space density for a free particle of spin S in a volume Ω has been used (eq 40 with a spin term) and entered in the final state density.

Eqn. 70 must be implemented with a suitable form for the nuclear level density and the inverse cross sections. Many recipes have been suggested for both. In the original work of Dostrovski [106], where the evaporation process has been translated into a MonteCarlo code for the first time, the Fermi gas expression for the nuclear level density $\rho(U) \approx C e^{2\sqrt{aU}}$, with $a = \frac{A}{8}$ and C a normalization constant, has been used. This has led to a simple form for the evaporation probability:

$$P_j(E)dE = \frac{(2S_j+1)m_j}{\pi^2 \hbar^3} \sigma_{inv} \frac{e^{2\sqrt{a(U-E-Q_j)}}}{e^{2\sqrt{aU}}} E dE \qquad (71)$$

In the same work, the inverse cross sections have been parametrized in a very simple way, so that expression 71 can be analytically integrated and used for MonteCarlo sampling.

To get a first idea of the spectrum of emitted nucleons, one can isolate the dominant dependence on the outgoing particle energy, in the case of neutrons, where one can assume an almost constant σ_{inv}:

$$\begin{aligned} P_j(E)dE &\propto E \frac{e^{2\sqrt{a(U-E-Q_j)}}}{e^{2\sqrt{aU}}} dE \\ &\approx E \frac{e^{2\sqrt{aU}\left(1-\frac{1}{2}\frac{E+Q_j}{U}\right)}}{e^{2\sqrt{aU}}} dE \\ &\approx E e^{-\frac{E}{T}} dE \qquad (72) \end{aligned}$$

from which the evaporative Maxwellian shape of the spectrum is evident, once the nuclear temperature $T \approx \sqrt{\frac{U}{a}}$ is introduced (this definition of the temperature comes from thermodynamical considerations). Taking for instance $U = 20$ MeV in an A=80 nucleus ($a = 10$), the emitted neutron spectrum is peaked at about 2.8 MeV, that is quite a low energy. The emission of protons is reduced and the spectrum is shifted toward higher energies due to the Coulomb barrier.

The total width for neutron emission can be found by integrating 71 between zero and the maximum possible ejectile energy $(U - Q_j)$

$$\Gamma_j = \hbar \int_0^{(U-Q_j)} P_j(E)dE \tag{73}$$

The Fermi expression for the nuclear density must however be refined, essentially allowing the value of a to depend both on nuclear species and on excitation energy. As a first step the so-called backshifted level density should be used, where $\rho(U) = Ce^{2\sqrt{aU}}$ is substituted by $\rho(U) = Ce^{2\sqrt{a(U-\Delta)}}$, Δ being the pairing gap in the nucleus considered.

The a dependence on A and Z accounts for shell and deformation effects, and has been extensively studied and calculated: careful tabulations exist in literature. The energy dependence is an experimentally observed effect, and both phenomenological and statistical model approaches have been followed, ending in a few different formulations. For detailed discussions of these topics see [107, 105, 104].

The evaporative process is in competition with another equilibrium process, that is fission [108]. A fraction of the excitation energy may be spent to induce a collective deformation. As the nucleus shape departs from sphericity the surface energy increases but the Coulomb energy decreases. The potential energy reaches a maximum at a deformation stage that is called "saddle point". The height of the potential energy over the ground state is the fission barrier B_f. Once a nucleus reaches the saddle point, the fission occurs, and the nucleus separates, most of the times into two heavy fragments. The height of the fission barrier can be in first order calculated with the liquid drop model, although shell effects have to be incorporated. For the fission probability, a statistical method can be used[103, 109]: it will be equal to the probability of reaching the saddle point, because this is a no-way-back point. Given the excitation energy U, this will be divided between a relative kinetic energy of the two fragments E and a residual excitation. All the procedure is like the one for evaporation, where now the spectrum is that of the kinetic energy at the saddle point, the $P_{f\to i}$ is simply one times the flux of "ingoing " fragments, but the system is confined to one dimension because of the path to saddle point. One has for the total fission width:

$$\Gamma_f = \frac{1}{2\pi}\frac{1}{\rho(U)}\int_0^{U-B_f} \rho_f(U - B_f - E)dE \tag{74}$$

Fission barrier vary roughly with the fissility parameter $\frac{Z^2}{A}$: measured values range from about 25-30 MeV at $\frac{Z^2}{A} \approx 30$ to 6 MeV for $\frac{Z^2}{A} > 34$. Fission for nuclei with $Z < 70$ can be neglected in any practical calculation.

In other nuclei, the fission width has to be compared with the evaporation widths to determine the relative importance of the two processes [110]. The level density at the saddle point ρ_f is different from that of the nucleus in its ground state, because of the high deformation. From comparison to experimental data, it turns out that a_f is greater than the a used for evaporation of about 10% at low excitation energies, and the two a's become equal at high energies.

After scission, the fragment acquire kinetic energy from the Coulomb repulsion between them. Their mass distribution depends on Z and on the excitation energy of the fissioning nucleus: for low Z fissioning system the mass distribution is centered around the half mass, while for high Z nuclei, the mass distribution has a symmetric component and an asymmetric one in which one of the fragment has always a mass around 140. The relative importance of the symmetric component grows with growing excitation energy.

For light nuclei, the statistical assumptions and the sequential emission scheme underlying the classical evaporation models become less and less sound, because:

- Already moderate excitation energies can represent a substantial fraction of the (total) binding energy of such nuclei
- The level structure of such nuclei is usually highly specific and anyway level spacings can be comparable with the excitation energy
- The "evaporation" of light fragments other than p or n becomes meaningless, since the mass of the "evaporated" fragment can be comparable or even larger than the mass of the residual nucleus

Therefore other deexcitation mechanisms are more suitable for these light (typically A≤16) nuclei. Probably the most popular one, is the so called Fermi Break-up model[111, 112], where the excited nucleus is supposed to disassemble just in one step into two or more fragments, with branching given by plain phase space considerations. In particular, the probability for disassembling a nucleus of N neutrons, Z protons, and E^* excitation energy (total mass $M^* = E^* + M_{A,Z}$) into n fragments ($n \geq 2$) of the same total charge and baryon number, is given by:

$$W = \frac{g}{G}\left[\frac{V_{br}}{(2\pi\hbar)^3}\right]^{n-1}\left(\frac{1}{M^*}\prod_{i=1}^{n} m_i\right)^{3/2}\frac{(2\pi)^{3(n-1)/2}}{\Gamma(\frac{3}{2}(n-1))}E_{kin}^{3n/2-5/2} \tag{75}$$

where the spin factor g, and the permutation factor G are given by (n_j is the number of identical particles of jth kind)

$$g = \prod_{i=1}^{n}(2S_i+1), \;\; G = \prod_{j=1}^{k} n_j! \tag{76}$$

and E_{kin} is the total kinetic energy of all fragments at the moment of break-up. V_{br} is a volume of the order of the initial residual nucleus volume. Therefore, the final state can be conveniently selected by means of a MonteCarlo procedure, by evaluating such an expression for all possible combinations of fragments energetically allowed (including all excited states with their spin treated as independent particles), and making a random selection. Once the final state configuration has been selected, the kinematical quantities of each fragment can be chosen according to n-body phase space distribution. Such a selection must be performed having care to subtract from the available energy the Coulomb repulsion of all charged particles: the Coulomb energy must then be added back to the charged particles alone, to simulate properly the effect of the Coulomb repulsion. In practice E_{kin} at disassembling will be given by:

$$E_{kin} = E^* - \left(\sum_{i=1}^{n} m_i c^2 - M_{A,Z}c^2\right) - B_{Coul} \tag{77}$$

where it must be recalled that the emitted fragments can well be in an excited state. The total Coulomb barrier B_{Coul} of the selected configuration has to be distributed to charged particles after disassembling.

A similar process occurs also in medium-heavy nuclei, although it becomes important only at multi-GeV proton induced reactions or in heavy ion induced reactions. This is called *nuclear fragmentation* and is characterized by the emission of low energy complex fragments with $A \geq 5$ from a thermalized nucleus. Reviews of this topic can be found in [114, 117, 115]. Fragmentation is expected to occur when the excitation energy per nucleon exceeds about 3 MeV[112], that in A=100 mass nucleus correspond to 300 MeV of excitation energy *after* all direct and preequilibrium emissions. As an example, the cross sections for emitting Sodium or Magnesium isotopes in proton induced reaction on gold are or the order of 0.03 mb at 0.5 GeV, 0.5 mb at 1 GeV and saturate at values between 3 and 10 mb for incident energies larger than 10 GeV. This is not a process that will influence the development of a shower or the average energy deposition, but it is the only one that can produce residual nuclei very far both from the target mass and from the fission product distribution, thus it must be taken into account for a detailed analysis of residual nuclei.

Theoretical descriptions of fragmentation model it as a two-stage process, the first being the production of a sufficiently hot compound nucleus, the second being the fragmentation itself. For the first stage, both intranuclear cascade[116, 112], and Fluidodynamical[113] models have been employed. The second stage can be described in terms of statistical methods or in terms of the fluctuations of the nuclear mean field. The statistical approach of [112] and that of [118] are among the few examples of implementation in a Monte Carlo code.

6.8 Residual nucleus deexcitation

The evaporation process continues till it is energetically possible, and leaves generally the residual nucleus in an excited state. The residual excitation energy is then dissipated by emission of γ rays. Actually γ emission occurs even during evaporation, as a competing process, but with a small branching ratio. The statistical approach can be applied also in this case, starting again from the detailed balance principle. The inverse cross section can either be taken from photon absorption cross sections or theoretically estimated . To give some qualitative features, it suffices to remind that the emission probability is higher for low multipolarities of the photon (just like in atomic physics), and that electric-type transitions are favoured over magnetic ones; the γ width for a given multipole l is proportional to $E_\gamma^{(2l+1)}$, to be convoluted with the nuclear level densities (and possibly other effects, such as the influence of the giant resonance). Thus, the statistical deexcitation proceeds mainly trough E1 (Electric dipole) transitions down to the point where nuclear levels can no longer be treated as a continuum, since the distance between levels is much larger than the level width. Here discrete transitions take place, with energy and multipolarities constrained by level spins, parities, and intrinsic configurations. Some general hint about this part of the spectrum can be made by assuming that the nuclear levels are organized in collective rotational or vibrational bands, and that deexcitation proceeds through these bands with the aforementioned dependence on multipolarity and energy joined to parity and angular momentum conservation. This results in E2 (electric quadrupole) or E2/M1 (elec. quad. plus magnetic dipole) cascades.

6.9 High energy interactions: Glauber cascade and formation zone

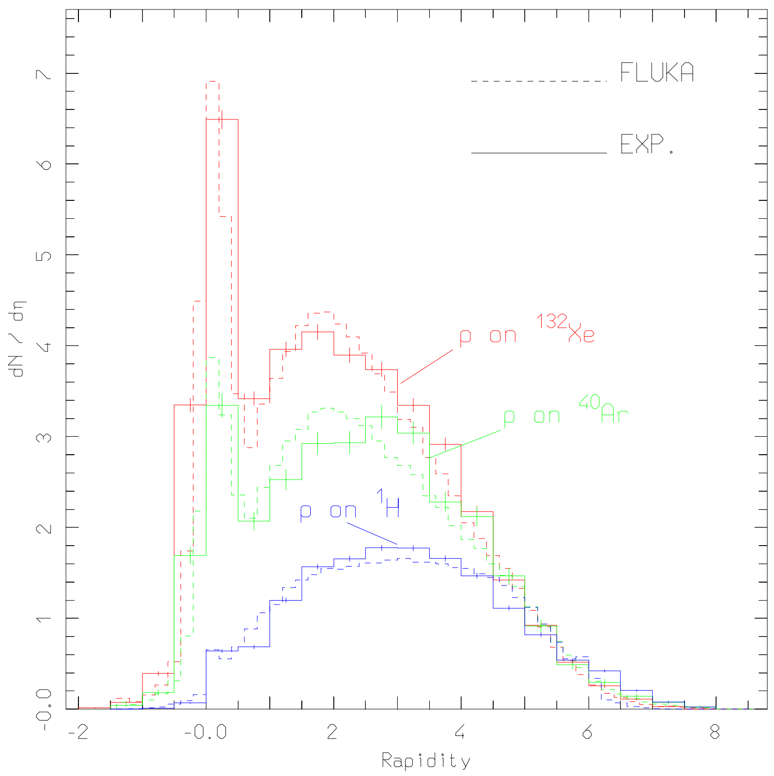

Figure 19: Rapidity distribution of charged particles produced in 200 GeV proton collisions on hydrogen, Argon, and Xenon targets

Once suitable models are available for the description of hadron-nucleon (hN from now) interactions (see paragraph 5.5), there are still two basic ingredients to be added for a sensible description of hadron-nucleus (hA from now) interactions at high energies. Both stem from experiments which show some distinct features of these interactions when compared with hN interactions at the same energy, or with hA interactions at lower energies. The former is the increasing number of shower particles produced with increasing mass number of the target. The latter is the apparently reduced cascading into the nucleus when compared with naive expectations based on hN cross sections and hN multiplicities.

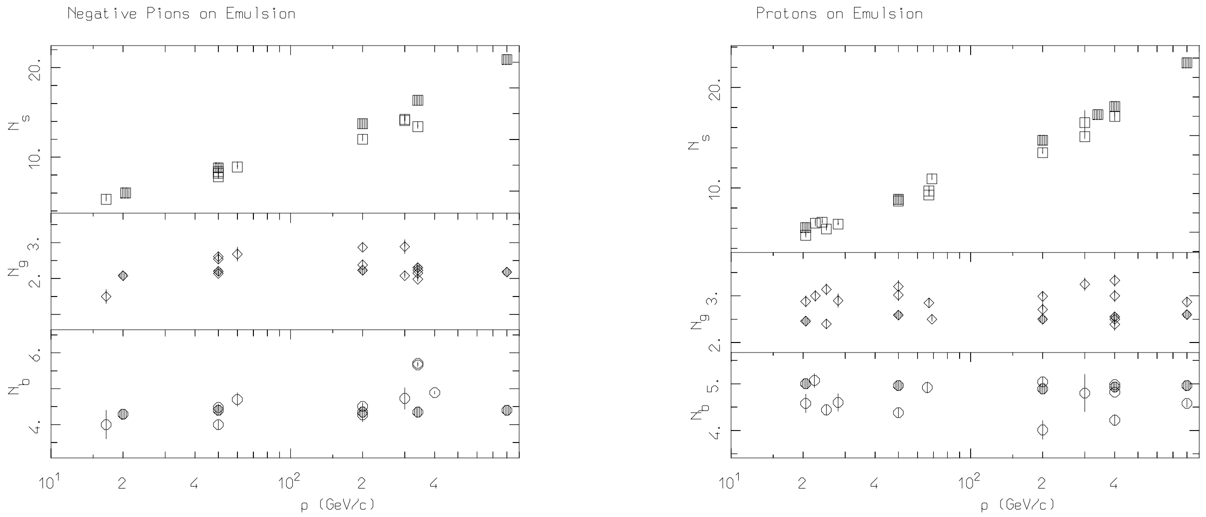

Figure 20: Shower, grey, and black tracks multiplicities for π^- (left) and protons (right) incident on emulsion, as a function of the projectile momentum. Open symbols are experimental data, full symbols are FLUKA results

6.9.1 Glauber Cascade and Multiple Primary Collisions

To better appreciate the increase of shower particle multiplicity as a function of the target mass number, fig. 19 shows the experimental rapidity distributions of charged particles produced in interactions of 200 GeV protons with hydrogen, Argon, and Xenon. Both experimental data, taken from [122] (which are actually pseudorapidity spectra above about 1 GeV) and FLUKA results are presented. The peak at low rapidity in the Ar and Xe data is due to grey particles emitted following cascading of secondaries produced in primary interaction. The standard interpretation of these results is that the primary particle undergoes multiple interactions with target nucleons, and that the number of such interactions is increasing with the target mass. According to such a picture, a simple estimate of the average number of "primary" collisions is given by:

$$< \nu > = \frac{A \cdot \sigma_{hN}}{\sigma_{hA}} \tag{78}$$

where σs are to be intended as inelastic cross sections. Since high energy hA inelastic cross sections scale well with the mass number:

$$\sigma_{hA} = \sigma_0 \cdot A^{\alpha} \tag{79}$$

with σ_0 usually some 20-30% higher than σ_{hN} and α very close to 2/3, it is easy to verify that the average number of primary collisions scales roughly like $< \nu > \propto A^{1/3}$, with the proportionality constant slightly smaller than unity. Therefore $< \nu >$ can be significantly larger than unity for heavy nuclei, giving rise to a substantial increase of shower particle multiplicity with respect to the hN case. The theoretical explanation of this multiple collision approach is the so called

Glauber-Gribov cascade [123, 124, 126, 125, 127]. It is not our aim to go further, but it suffices to say that within such an approach multiple collisions of primary particles are naturally accounted for, and their distribution as a function of the impact parameter can be computed once σ_{hN} is known. It is only important to stress that the term "multiple collisions" must not be interpreted as several successive interactions of the primary particle, or maybe of the leading particle coming from the previous interaction (which are surely impossible, see the next paragraph), but rather as an expansion of the interaction cross section into several diagrams, the first one representing the exchange of "something" in between the primary particle and one target nucleon, the second one with two nucleons etc.

6.9.2 Formation Zone

It has been known for many years that a plain treatment of INC at high energies, on the basis of elementary hadron-nucleon cross sections, overestimates measured particle yields, if the incident energy exceeds a few GeV [37, 36]. In particular, experiments support the effect of some mechanism in limiting the reinteractions of energetic particles. In emulsion experiments for example, while shower particle multiplicities increase steadily with the energy of the primary particle, the multiplicities of grey and black tracks rapidly saturate at few tens of GeV, and stay constant (see fig. 20, the exp. data are taken from [128, 129]). The physical mechanism which is believed to be at work in limiting high energy secondary reinteractions in nuclei, is the so called "formation zone" [93, 130, 131]. This concept has a strong analogy with the Landau-Pomeranchuk-Migdal [132] (LPM) effect which reduces electron bremsstrahlung and photon pair production at very high energies.

Naively, it can be understood considering that hadrons are composite objects and that the typical time of strong interactions is of the order of 1 fm (please note that space units are used for time in all this paragraph, $x = ct$). If one thinks about the hadrons emerging from an inelastic interaction, it requires some time to them to "materialize" and be able to undergo further interactions. The amount of time can be qualitatively estimated considering a secondary particle of mass M and of momentum components $p_{||}$ and p_T with respect to the original projectile direction. Making a Lorentz transformation to the frame where the longitudinal momentum is null (remember that p_T is invariant under Lorentz transformations), the uncertainty principle tell us:

$$\bar{t} = \Delta t \approx \frac{\hbar}{E_T} = \frac{\hbar}{\sqrt{p_T^2 + M^2}} \tag{80}$$

This time interval can be translated into the particle proper time, τ, and the lab frame time, t, taking care of the Lorentz dilation among the various frames:

$$\tau = \frac{M}{E_T}\bar{t} = \frac{\hbar M}{p_T^2 + M^2} \tag{81}$$

$$t_{lab} = \frac{E_{lab}}{E_T}\bar{t} = \frac{E_{lab}}{M}\tau = \frac{\hbar E_{lab}}{p_T^2 + M^2} \tag{82}$$

The time interval in the lab frame can be also expressed as a function of the particle rapidity, y, by:

$$t_{lab} = \bar{t}\cosh y = \frac{\hbar}{\sqrt{p_T^2 + M^2}}\cosh y \tag{83}$$

If such an interaction takes place inside a nucleus, the condition for having (possible) reinteractions of our secondary particle is expressed by :

$$v \cdot t \leq R_A \approx r_0 A^{\frac{1}{3}} \tag{84}$$

Such an equation can be used to define a critical rapidity, above which particles have no chance to reinteract and will "materialize" already outside the nucleus. Inserting typical values for pions inside eq. 83, $E_T \approx 0.3$ GeV, $E \approx 10$ GeV, it can be easily checked that the formation time can easily exceed heavy nuclei radii. All this derivation must be taken with a lot of care: among all other uncertainties, it is not clear whether the particle entering the formulae must be the final one, or rather the "mother" resonance. Nevertheless the concept is very powerful, and using a scale factor for the formation time as a free parameter, very nice agreement for hadron-nucleus and nucleus-nucleus interactions have been obtained [131, 133]. Examples of complete models including all effects described above can be found in [134, 135].

7 Elastic Nuclear Interactions

The elastic scattering of nucleons on nuclei is normally described in terms of the optical model. An optical potential as described in sec. 6.2 is used to model the nucleus as a scattering centre. The potential is most frequently chosen as a sum of a central and a spin-orbit part, with a Woods-Saxon radial dependence for the real part, and a more periphery-peaked shaped imaginary part. The parameters of the optical potential are determined by fitting the existing data, after corrections for the Coulomb effect on proton scattering: they are found to vary both with A and with projectile energy.

The behaviour of the differential elastic cross section exhibits a shape similar to a diffraction pattern, and becomes more strongly forward peaked as the projectile energy increases. In first approximation, this pattern can be reproduced with the expression of the scattering from a black disk:

$$\frac{d\sigma}{d\Omega} = (1-a)^2 R^2 \left[\frac{J_1(2kR\sin\theta/2)}{2\sin\theta/2}\right]^2 \tag{85}$$

where R is the scattering sphere radius, and a gives the opacity of the sphere[63]:

$$\begin{aligned} \sigma_{EL} &= \pi R^2 (1-a)^2 \\ \sigma_R &= \pi R^2 (1-a^2) \\ \sigma_T &= 2\pi R^2 (1-a) \end{aligned} \tag{86}$$

for complete absorption $a = 0$, and the reaction cross section becomes equal to the geometrical one.

The same diffractive pattern is found in pion-nucleus scattering. At resonance, the diffraction minima and the total cross section can be very well described by the black disk formulation with $a = 0$, due to the strong pion-nucleus interaction.

At higher energies (> 1 GeV), the pion and nucleon elastic scattering on nuclei is more and more forward peaked: the first minimum of eq.85 is at $\theta \approx 0.61\frac{h}{pR}$, that means that for a 1 GeV nucleon on Carbon it is situated at about 12°. Eventually, the usual exponential form becomes appropriate. One remark to be made is that these forward-peaked scatterings involve very small energy losses, thus the importance of elastic scattering on particle propagation becomes small at high energies. Examples of high energy hadron-nucleus cross sections can be found in[119, 120, 121].

8 Practical Examples of INC calculations

In the previous sections, a brief description of the processes occurring during hadronic inelastic interactions in the energy range of interest has been given. In the present section, a few representative comparisons between model results and experimental data on particle production in the energy range of interest are presented. All the presented results have been obtained with the last version of the FLUKA [55, 56] code, and more precisely with the model used for the intermediate energy range [42] and called PEANUT (PreEquilibrium-Approach-to-NUclear-Thermalization). Such a model combines both an INC part, and a preequilibrium part, with a smooth transition around 50 MeV for secondary nucleons, and 30 MeV for primary ones. Nuclear potential effects (refraction and reflection) are modeled into the code, as well as quantal effects, like Pauli blocking, nucleon-nucleon correlations, fermion antisymmetrization, coherence length and formation zone. The results obtained with such a code are not at all representative of the majority of the INC models, usually based on some flavour of the Bertini INC code [36, 44, 45], or similar approaches. Among the available INC codes, possibly only CEM92 [43] and the LAHET version with the preequilibrium model included[41] can be compared with this model for nucleon induced interactions. For pion induced interactions, the approach of PEANUT is very different from all other mentioned codes, none of which includes a complex optical potential or absorption effects computed according to modern approaches [6, 7, 5] including three body absorption (for example, CEM92 [136] derives 2-body absorption cross sections just multiplying the deuteron one by a tunable factor, and uses a square well potential of fixed depth for pions).

8.1 From plain INC to more complex models

In paragraph 4.3 a list of known weaknesses of INC codes have been presented. Here some examples are given, trying to illustrate the sources of such deficiencies. Examples of the problems met by classical INC codes based on the plain Bertini model or similar approaches can be

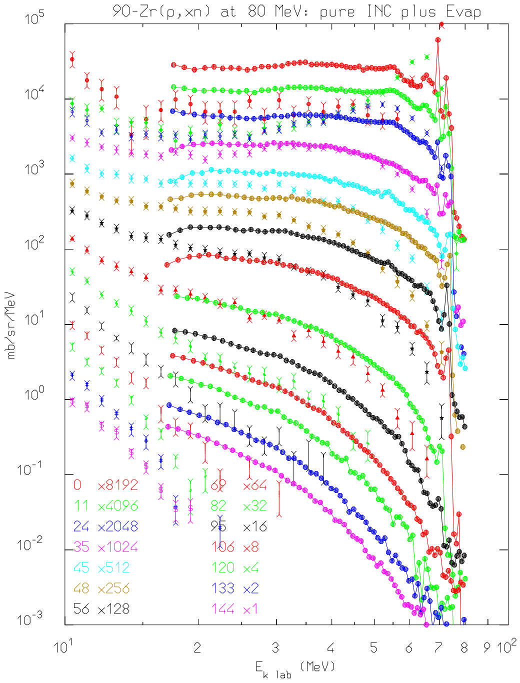

Figure 21: ^{90}Zr(p,xn) at 80.5 MeV, plain INC (see text) calculation

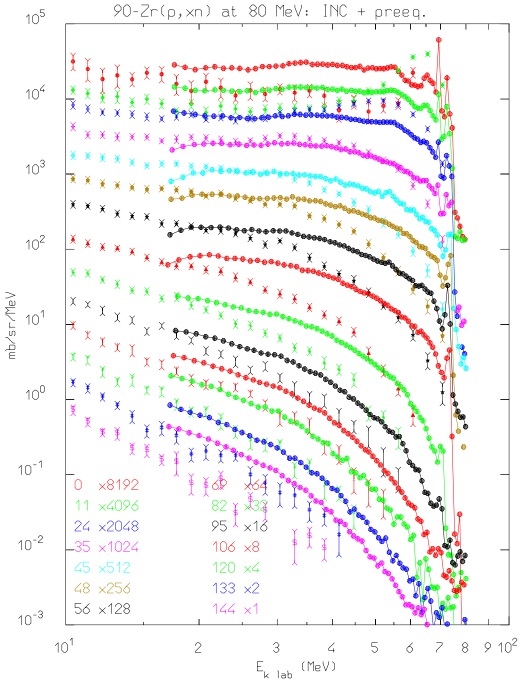

Figure 22: ^{90}Zr(p,xn) at 80.5 MeV, plain INC plus preequilibrium (see text) calculation

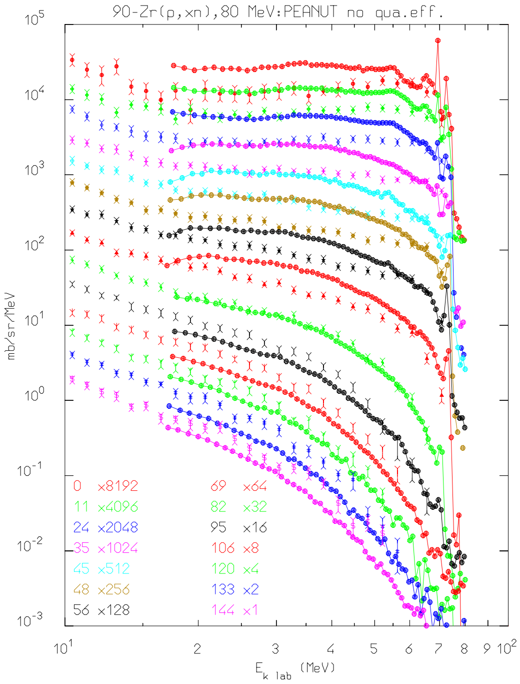

Figure 23: ^{90}Zr(p,xn) at 80.5 MeV, PEANUT (see text) calculation with no quantal effect, but Pauli blocking

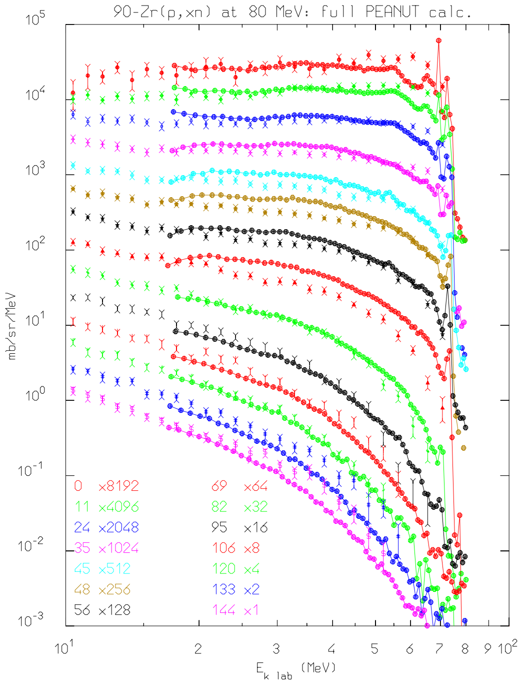

Figure 24: ^{90}Zr(p,xn) at 80.5 MeV, full PEANUT (see text) calculation

found in [51], PSI and Julich contributions, where the results of an intercomparison carried by the Nuclear Energy Agency are reported. Results on ^{208}Pb(p,xn), and ^{90}Zr(p,xn), ^{90}Zr(p,xp)

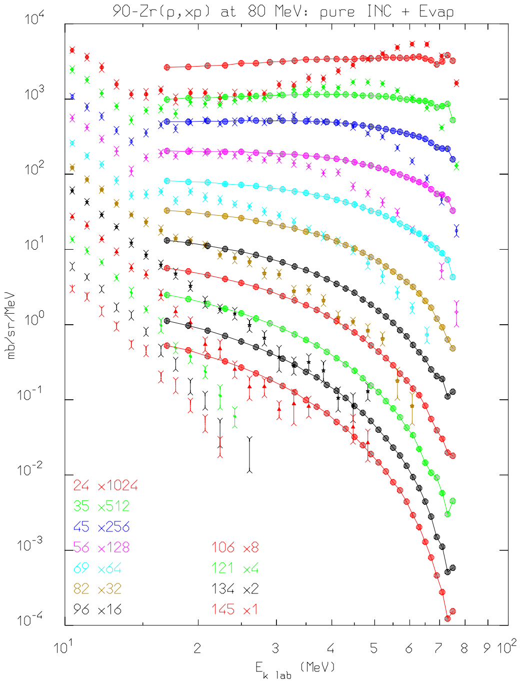

Figure 25: ^{90}Zr(p,xp) at 80.5 MeV, plain INC (see text) calculation

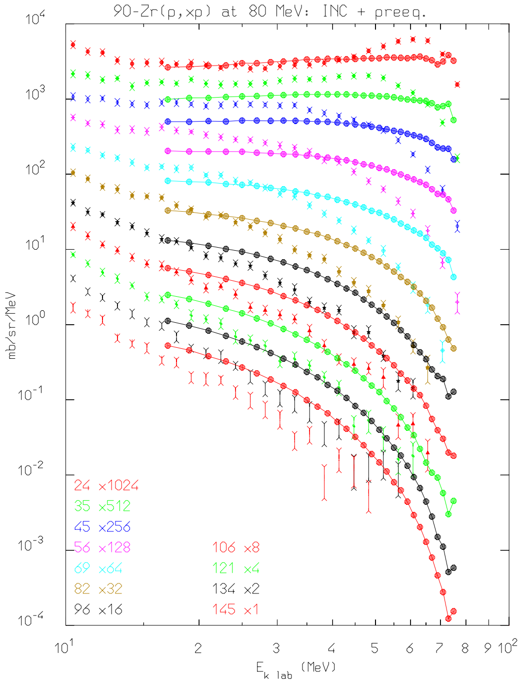

Figure 26: ^{90}Zr(p,xp) at 80.5 MeV, plain INC plus preequilibrium (see text) calculation

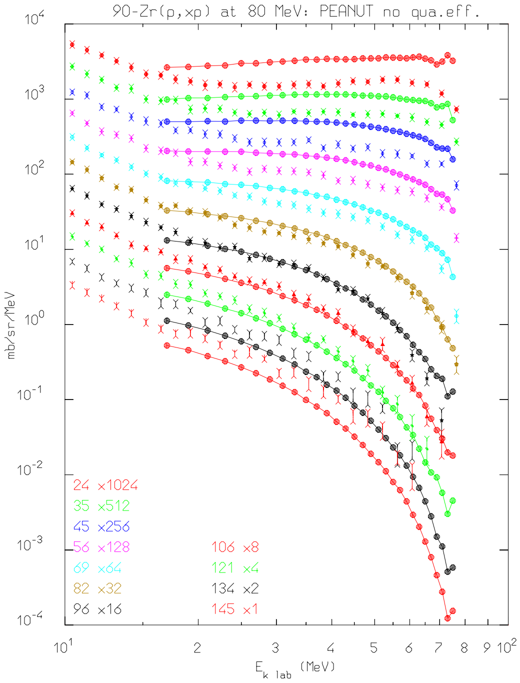

Figure 27: ^{90}Zr(p,xp) at 80.5 MeV, PEANUT (see text) calculation with no quantal effect, but Pauli blocking

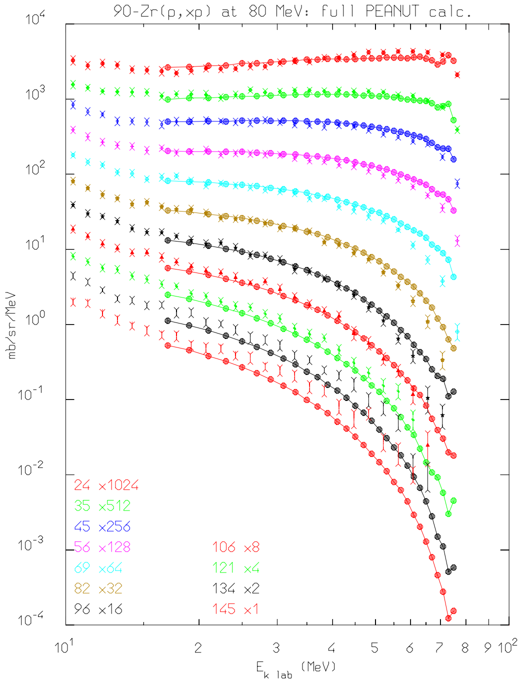

Figure 28: ^{90}Zr(p,xp) at 80.5 MeV, full PEANUT (see text) calculation

reactions where the topic of the intercomparison. The equivalent set of data computed with PEANUT, 1994 status, can be found in [137]. It is important to remind that the Bertini model

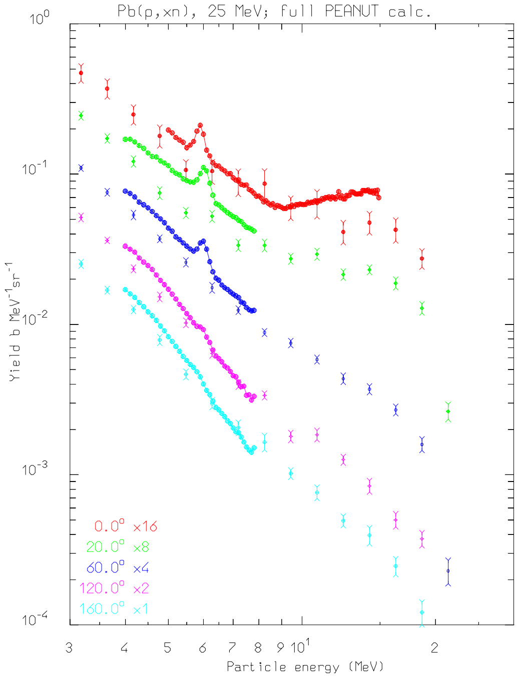

Figure 29: ^{208}Pb(p,xn) at 25 MeV, PEANUT calculation

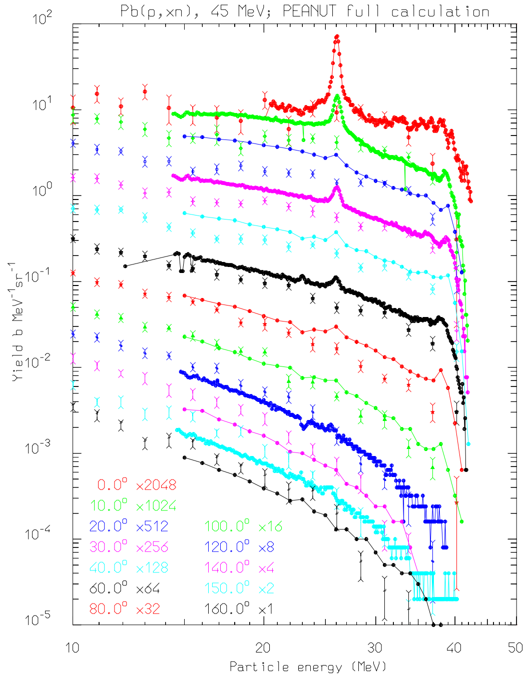

Figure 30: ^{208}Pb(p,xn) at 45 MeV, at several emission angles

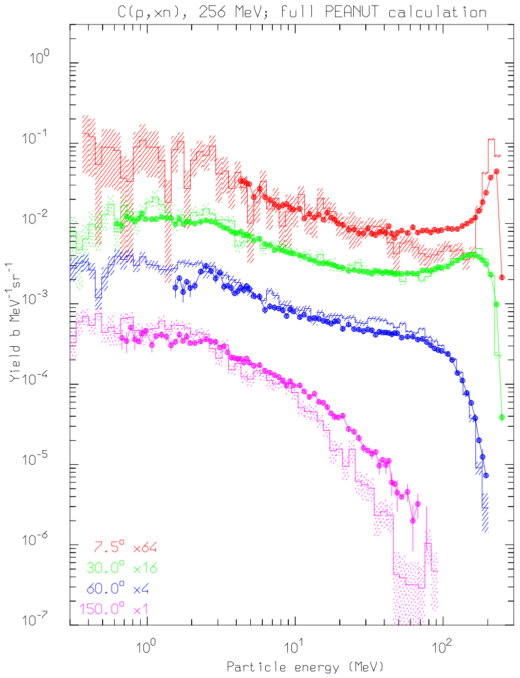

Figure 31: ^{12}C(p,xn) at 256 MeV, at several emission angles

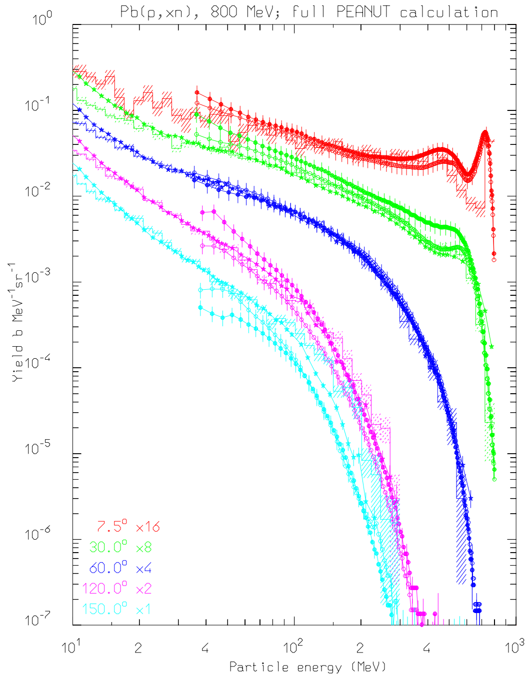

Figure 32: Pb(p,xn) at 800 MeV, at several emission angles

does not include reflection or refraction, neither includes any preequilibrium stage. Furthermore an average binding energy is used throughout all cascading process without account for actual Q values of the different reaction channels.

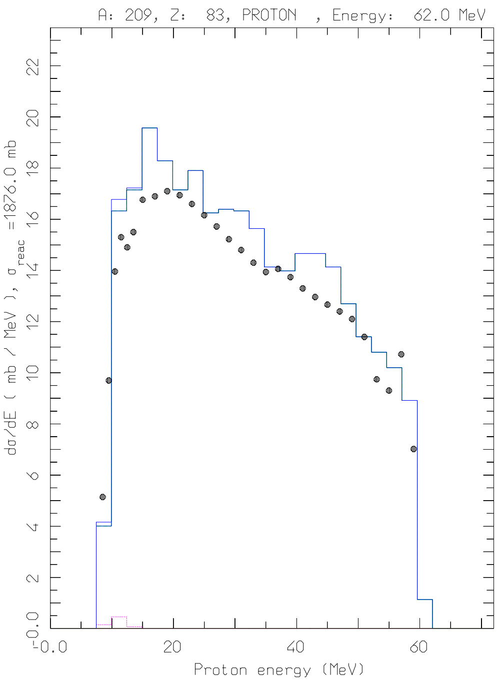

Figure 33: ^{209}Bi(p,xp) at 62 MeV, angle integrated spectrum preequilibrium only.

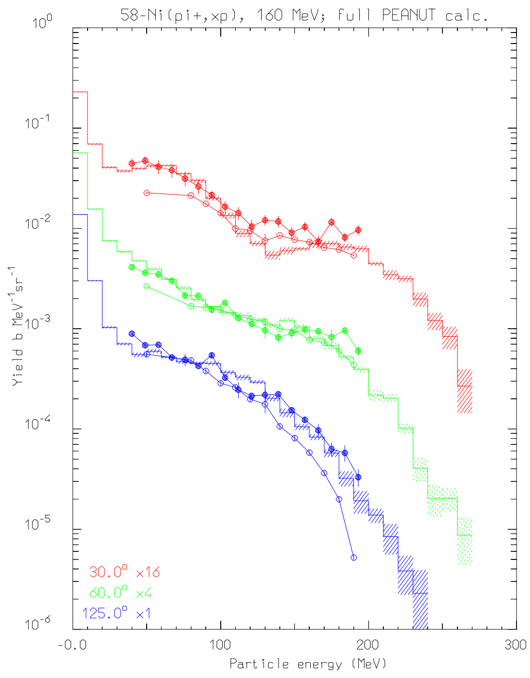

Figure 34: ^{58}Ni(π^+,xp) at 160 MeV, at several emission angles

In order to illustrate the effect of the various ingredients, the same projectile-target combination, 80.5 MeV protons on ^{90}Zr, has been computed under different assumptions and the results compared with experimental data [138, 139]. Four different trials have been performed, always using PEANUT with all or only a few of the ingredients at work. The results of the exercise are presented in figs. 21,22,23,24, for (p,xn), and in figs. 25,26,27,28, for (p,xp). In all these figures as well as in following ones, experimental data are plotted as full symbols joined by a line, while model results are given or by symbols with error bars, or by histograms with shaded areas representing the statistical error.

The first attempt (figs. 21,25) has been performed using a plain INC approach with no preequilibrium stage, no refraction and reflection, and only Pauli blocking activated among the quantal effects. The transport threshold for secondary nucleons was set equal to the average binding energy. As can be easily seen results are very poor, with an overestimation of the forward peak and a strong underestimation of backward angle emission. These results have been obtained with assumptions which are quite consistent with those used by the Bertini model, but the binding energy which, as usual in PEANUT, has been correctly set at each emission stage to match the actual reaction Q-value. This is the explanation, maybe paradoxically, of the slightly worse results of this trial at medium/large angles with respect for example to the PSI contribution in [51],. The use of a constant binding energy value in [51] overestimates the available ejectile energy of about 6.9 MeV, shifting the spectra of the same amount towards larger energies.

The second trial does not yet use refraction and reflection, but the preequilibrium stage is there. There is a clear improvement in the results, particularly at backward angles, but still

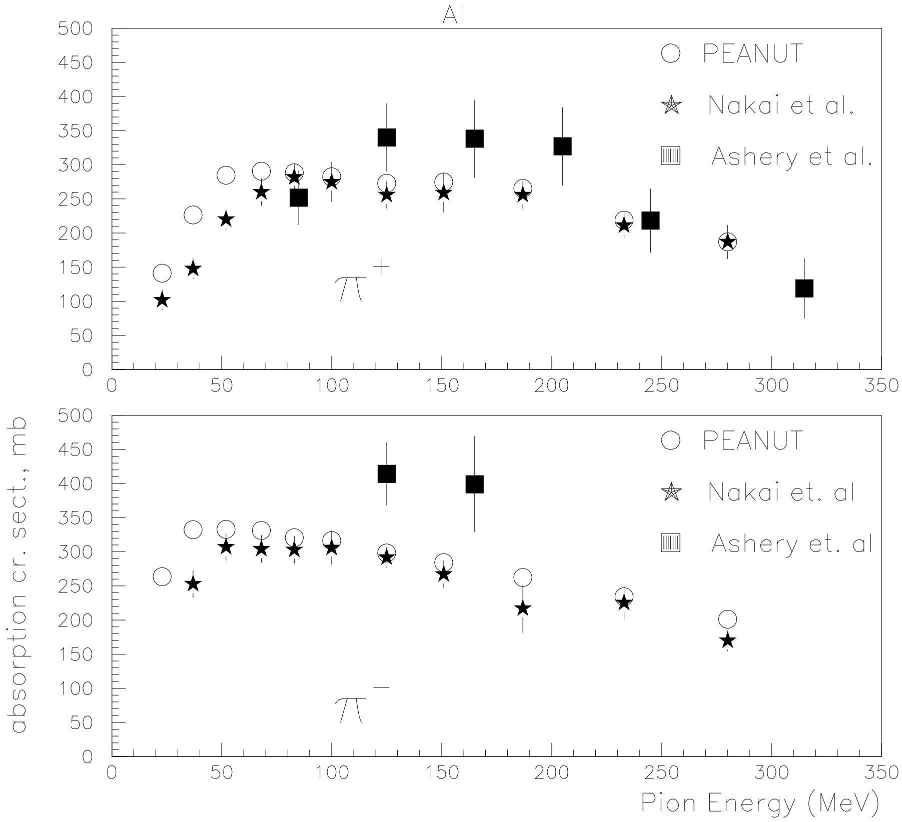

Figure 35: Pion absorption cross section on Aluminum as a function of energy

there are large discrepancies.

The third trial has been performed switching on all the refraction and reflection business, but still limiting the quantal effects to Pauli blocking alone. There is a great improvement, with still discrepancies at the forward angles, but a reasonable description of backward ones. The reason for these last deficiencies is related to the effect of particle curvature in the nucleus which both increase the particle track length and hence the reinteraction probability, and at the same time "pushes" particles towards the nucleus centre, again increasing the interaction probability.

The fourth and last trial has been performed with all quantal effects on, that is with coherence length, nucleon correlation, and fermion antisymmetrization effects on. Clearly these are effective in increasing particle mean free paths in the nuclear medium resulting in a quite reasonable description of the whole spectrum at all angles (see also [94] for the effect of nucleon correlations).

The effect of particle curvature on interaction rates are typical of INC codes which include refraction and reflection [38]. The reason for the good results, at least for angle integrated spectra, of INC models based on straight trajectories (like the Bertini INC) probably lies in

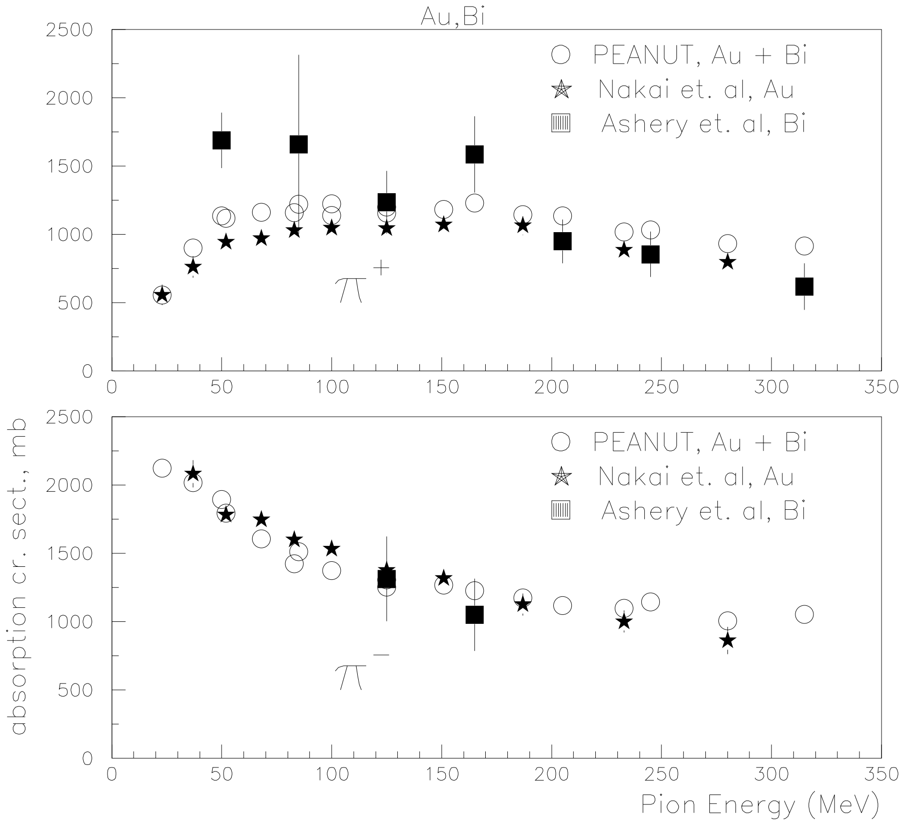

Figure 36: Pion absorption cross section on Gold or Bismuth as a function of energy

the compensating effect of the lack both of mechanisms able to lengthen particle mean free paths, and of the curvature effect which operate in the opposite direction. The price is the poor description of angular distributions, at least for energies not much larger than typical potential energies. Such a picture is consistent with what has been already reported in the literature [50, 49, 46, 48].

Other examples of complete calculations of neutron double differential spectra are reported in fig. 29,30,31, and 32. The experimental data have been taken from ref. [50, 48, 140, 142]. It is particularly interesting to note that in the PEANUT model at 25 MeV incident energy no INC stage is performed and all the emission is due to preequilibrium. At 45 MeV the INC stage starts to contribute (compare fig. 30 with ref. [50] to appreciate the improvement over plain INC models), while at higher energies it dominates the most energetic part of the spectra. Neutron double differential spectra following C(p,xn) at 256 MeV (exp. data from [48]), and Pb(p,xn) at 800 MeV (exp. data from [140, 142]) are presented in figs. 31,32. In the latter figure three experimental curves are drawn, two come from [142] and correspond to two possible choices for the efficiencies of the scintillators used in the experiment, the third one comes from [140]. The relative disagreement among these curve can give an idea of the experimental uncertainties in this energy range. An inspection of the literature data for 113, 256, 597, and 800 MeV proton energies [46, 48, 140, 141], shows how "classical" INC are more and more reliable with increasing energy. However, it must be taken into account that the onset of the effects discussed in paragraph 6.9, and the need for physical models other than those based on isobar production and decay (see paragraph 5.4,5.5), limit the validity range to a maximum of 1.5–3 GeV.

An example of angle integrated spectra computed with the preequilibrium model alone (no INC) is reported in fig. 33, for ^{209}Bi(p,xp) (exp. data from ref. [49]). Again a comparison with the Bertini results reported in the original reference shows the superior capabilities of preequilibrium models in this energy range.

A few results about pions are finally presented in fig. 34,35,36 The first figure presents the double differential emission spectrum of protons, following π^+ interactions on ^{58}Ni at 160 MeV (exp. data from [143, 144]). The contribution of absorption in the energetic part of the spectra is evident. The last two figures show the experimental [146, 145] and calculated absorption cross section for incident π^+ and π^- on Aluminium, and on Bismuth and Gold. The comparison is made on an absolute scale, since the calculated results have been obtained making use of the capability of PEANUT (as of all other INC models) of computing reaction cross sections.

8.2 Residual Nuclei

The problem of a reliable description of individual isotopes produced in spallation reactions is still an open one. While the general features of the residual nuclei distributions are usually well reproduced by INC with the possible exception of fragmentation products, see paragraph 6.7), predictions on individual isotopes can be out of large factors. Many reasons contribute to this uncertainty:

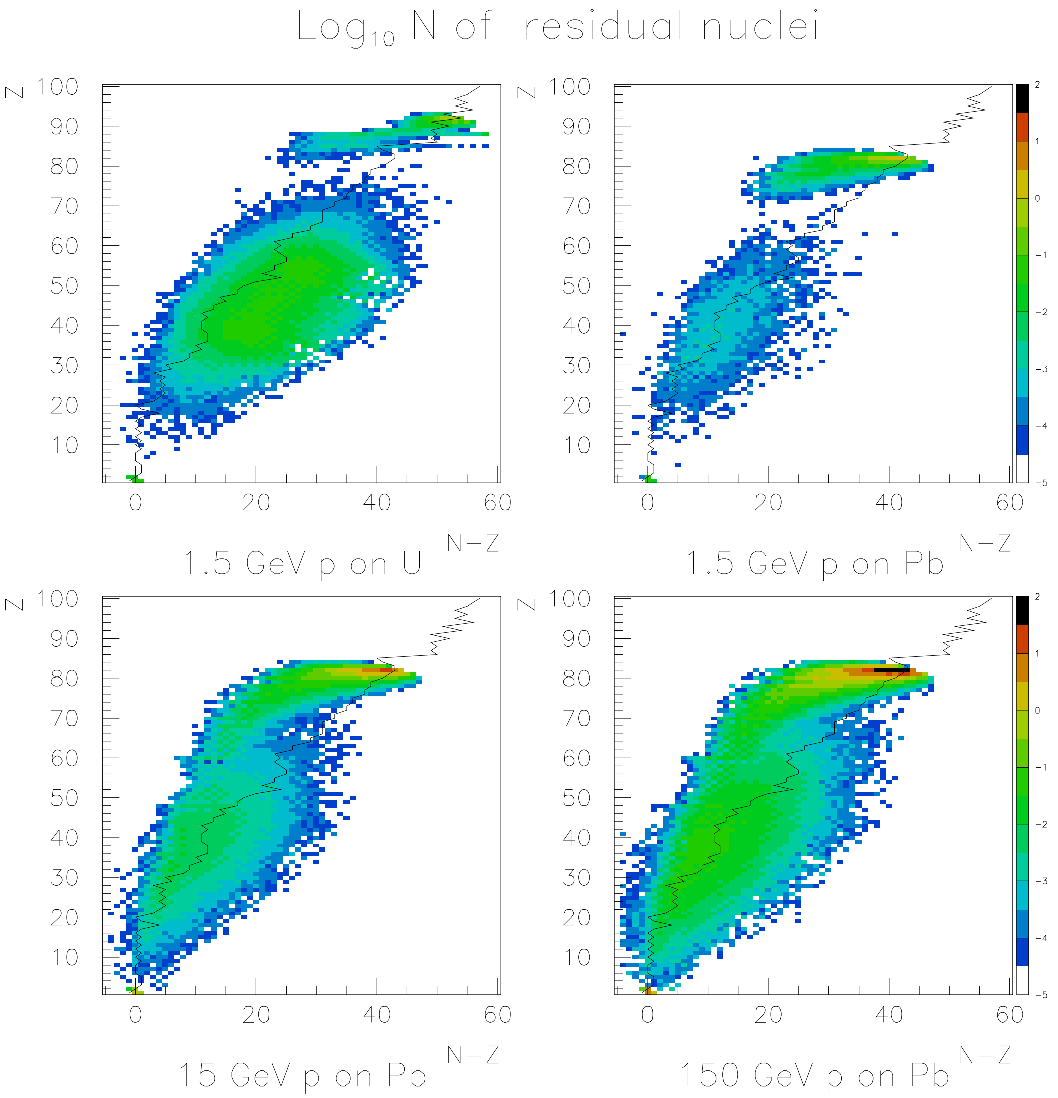

Figure 37: Residual nuclei distribution for protons on Pb and U at different energies. Only residuals produced by all particles but neutrons below 20 MeV are presented. The abscissa is the neutron excess, N-Z, and the ordinate the atomic number Z. The stability line is also shown.

- Slight inaccuracies in excitation energy spectra reaching the evaporation stage can results in small shifts in particle multiplicities, but in substantial shifts among close isotopes
- The lack of spin and parity dependent (Hauser-Feshbach) calculations in the last stage can also bias the very last steps and hence the final residual nucleus
- Charged particle emission channels of low probability can be badly reproduced because of sub-barrier effects etc
- No prediction about metastable states is possible
- Fragmentation is usually not included

Besides these physical reasons, there are also "technical" ones. What is often required when looking for residual nuclei production, is the production cross section of some specific isotopes, for example because of its toxicity or long life time etc, which however can be a very small fraction of the total reaction cross section. Therefore a good agreement over the gross part of emission spectra is not at all a proof of a similar agreement on some specific and relatively unlikely isotope production channel.

Sticking however at our previous statement, that is that the general features of isotope production are reasonably reproduced, in fig. 37 the residual nuclei distribution produced by protons of 1.5 GeV on a depleted Uranium target, and of 1.5, 15, and 150 GeV on a natural Lead target are presented. The isotope shown, are only those produced by particles other than neutrons below 20 MeV.

A few important features can be seen in these plots, taking into account that neutron-rich isotope sit to the right of the stability line, and proton-rich one to the left:

- The fission zone in the U plot, and to a lesser extent also in the Pb, 1.5 GeV one
- The spallation zone, with the characteristic peak close to the original target A and Z, populated mainly by proton-rich isotopes
- The increasing extension of the spallation zone with increasing energy

The production of proton-rich isotopes is one of the distinct features of spallation induced by energetic particle. It is mainly due to the reduced emission probability of charged particles in the evaporation stage, due to the Coulomb barrier. A last word must be spent about the life times of these impressive inventories of nuclides: a good fraction of them are very short half-life ones, created relatively far from the stability line. Codes able to model the evolution with time of such inventories are therefore required for a proper evaluation of incineration rates or other effects of interest. However a bit of caution must always be taken when considering INC code results on residual nuclei, particularly for isotope far from the original target. An international intercomparison on residual nuclei production, organized by the Nuclear Energy Agency, is currently in progress with the goal to fix the present status of model predictions in this field.

9 ElectroMagnetic Showers

ElectroMagnetic showers are not of great interest for applications of accelerators beams to energy production, waste transmutation, tritium production, and similar problems. However as soon as the primary beam energy exceeds the pion production threshold, an increasing fraction of the beam energy is dissipated through electromagnetic cascades. In first approximation and for high energy cascades, the fraction of the initial energy that goes into the electromagnetic sector is[148]

$$f_{EM} = 1 - \left(\frac{E}{E_0}\right)^{(\alpha-1)} \qquad \alpha \approx 0.8 \quad E_0 \approx 1 \text{ GeV} \tag{87}$$

Therefore a simple introduction to EM cascades will be also given, assuming that the basic interactions of electrons and photons with matter are already known.

9.1 EM Shower Development

Let us consider an electron, or positron, of quite high energy, say a few hundreds of MeV, traversing a slab of material. It will lose energy mainly by bremsstrahlung, thus producing photons. For photons with energy higher than several MeV, the dominant interaction is pair production, thus most bremsstrahlung photons will produce an electron and a positron, and so on, building up what is called the EM shower[149, 150]. The shower will continue until the energy of its charged particles becomes low and they start to dissipate most of the energy in ionization. The distance traversed by the shower is most conveniently measured in *radiation lengths* X_0. The radiation length is the distance over which an electron energy is reduced to e^{-1} of the initial one by bremsstrahlung emission. The radiation length is given by

$$\frac{1}{X_0} = 4\alpha r_e^2 \frac{N_A}{A}\left[Z^2(\ln(184.15Z^{\frac{-1}{3}}) - f_c(Z)) + Z\ln(1194Z^{\frac{-2}{3}})\right] \tag{88}$$

where $f_c(Z)$ is the Coulomb correction[151, 152]. An easy-to-use expression for X_0 is :

$$X_0 = \frac{716.4A}{Z(Z+1)\ln(287/\sqrt{Z})} \quad \frac{g}{cm^2} \tag{89}$$

Another characteristic quantity is the critical energy E_c, defined as the energy at which the collision energy loss becomes equal to the radiation energy loss. It can be approximated by

$$E_c = \frac{1600}{Z}mc^2 \tag{90}$$

The longitudinal development of the shower cannot be calculated analytically, but a simple toy model can help in understanding its gross features: let us assume that each particle , electron or positron or photons, travels a length X_0 before interacting, and that $e^{\pm}$ loose one half of their energy at each interaction, and each created lepton in pair production carries one half of the photon energy. Moreover, let us neglect collision energy loss above E_c, and conversely neglect radiation energy losses below E_c. This means that at each radiation length the number of particle in the shower is multiplied by two. After n radiation lengths there will be $N(t) = 2^t$ particles, each carrying an average energy $E_t = \frac{E_0}{2^t}$. At a certain depth t_c, the shower stops its development because the average particle energy equals the critical one: $\frac{E_0}{2^t_c} = E_c$. This happens at $t_c = \frac{\ln(E_0/E_c)}{\ln 2}$, that is, the maximum shower depth decreases logarithmically with energy. This simple model is in qualitative agreement with more refined ones; obviously the shower does not stop abruptly at t_c, but decreases gradually.

The lateral development of the shower scales with what is called the *Molière radius* R_M. This can be derived from a gaussian approximation to the Molière multiple scattering distribution: the width of this gaussian distribution for unit charge particles is

$$\theta_0 \approx \frac{\sqrt{\frac{4\pi}{\alpha}} m_e c^2}{\beta c p} \sqrt{\frac{x}{X_0}} \tag{91}$$

where βc and p are the projectile velocity and momentum. The lateral size of the shower at the shower maximum, ($E = E_c$) can be estimated by assuming that the particles will travel one interaction length before interacting or stopping. The width of the angular deflection will be given by

$$\theta_c = \frac{E_s}{E_c} \; ; \; E_s = \sqrt{\frac{4\pi}{\alpha}} m_e c^2 \tag{92}$$

and the radial width after a path X_0, that is the Molière radius becomes:

$$R_M = \frac{E_s}{E_c} X_0 = 21.2 \frac{X_0}{E_c} \tag{93}$$

From measurements of the shower cascades, it turns out that only 10% of the energy lies outside the radius R_M.

Acknowledgments

The authors are greatly indebted to A. Fassò and J. Ranft for the many stimulating discussions and the continuous support, and to prof. M. Salvatores for the invitation to give this lecture.

Appendix A: useful kinematical quantities

It is customary in high energy physics to make use of a few “strange” kinematical variables to describe particle kinematical properties. Let us assume to deal with a particle, c, of mass M, total energy E, and momentum $\vec{p} = (p \sin\theta \cos\phi, p \sin\theta \sin\phi, p \cos\theta)$, possibly emerging from an interaction of the kind $a + b \to c + X$. From, now variable with an asterisk (e.g. E^*, p^*) are supposed to be evaluated in the Centre of Mass System (CMS) of the collision, variables labelled with $_L$ are suppose to be computed in the lab frame (that is the frame where particle b is at rest), and variables with no particular labelling can be in whichever frame. The invariant mass squared of the system, s, ($\sqrt{s} \equiv$ the total energy of the system in the CMS frame) is given by:

$$s = (E_a^* + E_b^*)^2 = (E_a + E_b)^2 - (\vec{p}_a + \vec{p}_b)^2 = M_a^2 + M_b^2 + 2 M_b E_{aL} \tag{94}$$

The Lorentz transformation required to go from the original frame to another one moving with velocity $\vec{v}$ with respect to the first one, are given by:

$$\vec{\beta} \;\; = \;\; \frac{\vec{v}}{c} \tag{95}$$

$$\begin{aligned}
\gamma &= \frac{1}{\sqrt{1-\vec{\beta}^2}} && (96)\\
\vec{\eta} &= \vec{\beta}\gamma,\ (\gamma^2 - \vec{\eta}^{\,2} = 1) && (97)\\
\vec{p}^{\,\prime} &= \vec{p} - \vec{\eta}\left(E - \frac{\vec{\eta}\cdot\vec{p}}{\gamma+1}\right) && (98)\\
E' &= \gamma E - \vec{\eta}\cdot\vec{p} && (99)
\end{aligned}$$

The inverse transformation is readily obtained exchanging non-primed variables with primed ones, and $\vec{\eta} \to -\vec{\eta}$. In particular, for a system of particles with total energy E_{tot}, and total momentum $\vec{p}_{tot}$, the transformation to the Center of Mass System can be accomplished using:

$$\begin{aligned}
\gamma_{CM} &= \frac{E_{tot}}{\sqrt{s}} && (100)\\
\vec{\eta}_{CM} &= \frac{\vec{p}_{tot}}{\sqrt{s}}, (s = E_{tot}^2 - \vec{p}_{tot}^{\,2}) && (101)
\end{aligned}$$

The single particle inclusive cross section for particle c is defined as:

$$\sigma_{inv} = E_c \frac{d^3\sigma_{ab}}{d^3 p_c}\left(\sqrt{s}, p_{||}^*, p_T\right) \equiv f_{ab}^c\left(\sqrt{s}, p_{||}^*, p_T\right) \quad (102)$$

where the labels a, b, c are there just to remind that this is the inclusive distribution of particle c after an interaction with particle a impinging on particle b. Such a distribution is often called the *invariant cross section*, since $\frac{d^3p}{E}$ can be shown to be Lorentz invariant, and therefore:

$$E_c^* \frac{d^3\sigma}{d^3p_c^*} = E_c \frac{d^3\sigma}{d^3p_c} \quad (103)$$

The transverse momentum p_T and the transverse mass E_T or M_T (which are all invariant under Lorentz transformation), are defined by:

$$\begin{aligned}
p_T &= p\sin\theta = \sqrt{E^2 - M^2}\sin\theta && (104)\\
M_T &= E_T = \sqrt{p_T^2 + M^2} && (105)
\end{aligned}$$

The longitudinal momentum, $p_{||}$ is instead frame dependent. A very useful quantity connected with longitudinal momentum is the so called X Feynman variable, defined as the ratio of the particle longitudinal momentum and the maximum possible longitudinal momentum, in a given frame, usually assumed to be the CMS (but sometimes also the lab frame is used):

$$X_F^* = \frac{p_{||}^*}{p_{||}^*(Max)} \approx \frac{2p_{||}^*}{\sqrt{s}} \quad (106)$$

Please note that $-1 \leq X_F^* \leq 1$. The regions $X_F^* > 0$ and $X_F^* < 0$ are usually called the *projectile fragmentation region*, and the *target fragmentation region*, the region $X_F^* \sim 0$ is called the *central region*. The *hypothesis of limiting fragmentation* [69] just supposes that in the projectile and target fragmentation regions the following scaling holds (see eq. 102):

$$f_{ab}^c\left(\sqrt{s}, p_{||}^*, p_T\right) \overset{\sqrt{s}\to\infty}{\to} \bar{f}_{ab}^c\left(X_F^*, p_T\right) \quad (107)$$

A stronger version of the scaling hypothesis, due to Feynman, assumes that such a scaling holds also in the central region. As a consequence $\bar{f}^c_{ab}(0, p_T))$ should be a constant, and the produced particle multiplicity should scale like, $< n_{ab} > \propto n_0 + n_1 \ln s$. Both predictions are violated, but they can be used as order of magnitude guesses without too much danger. Other variables very frequently used are the *rapidity*, y (dy is again Lorentz invariant, that is ys differ in different frames only of a constant factor), and the *pseudorapidity*, η, whose major (and unique) advantages are that it can be easily measured and it coincides with rapidity for $p_T \gg M$

$$y = \text{acosh}(\frac{E}{M_T}) = \text{atanh}(\frac{p_{\|}}{E}) = \frac{1}{2} \ln \left(\frac{E + p_{\|}}{E - p_{\|}} \right) \tag{108}$$

$$\eta = -\ln \left(\tan \frac{\theta}{2} \right) = \frac{1}{2} \ln \left(\frac{p + p_{\|}}{p - p_{\|}} \right) \tag{109}$$

References

[1] R. Brun et al., CERN DD/EE/84-1 (1987).

[2] O.G. Ryazhskaya, report **LNGS 94/110** 1994

[3] R. Bonetti et al., Phys. Rep. **247** (1994) 1

[4] E. Gadioli and P. E. Hodgson, *Pre-equilibrium Nuclear Reactions* (Clarendon Press, Oxford, 1992).

[5] M.J. Vicente Vacas and E. Oset, Nucl. Phys. **A568** (1994), 855.

[6] E. Oset and L.L. Salcedo, Nucl. Phys. **A468** (1987) 631.

[7] L.L. Salcedo et al., Nucl. Phys. **A484** (1988) 557.

[8] A. Ferrari and P. R. Sala, **Improvements to the Electromagnetic part of the FLUKA code**, to be published; P. A. Aarnio, A. Fassò, A. Ferrari, J. -H. Moehring, J. Ranft, P.R. Sala, G.R. Stevenson and J.M. Zazula, "Electron-photon transport: always so good as we think? Experience with FLUKA", *Proc. of the MC93 Int. Conf. on Monte Carlo Simulation in High-Energy and Nuclear Physics*, Feb. 22-26, 1993. Ed. P. Dragovitsch, S.L. Linn, M. Burbank, World Scientific, Singapore, 1994 (p. 100).

[9] C.T. Ballinger et al, Nucl. Instr. Meth. **B72** (1992) 19.

[10] M.E. Riley, C.J MacCallum, and F. Biggs, ADNDT **15**, 443 (1975)

[11] E.A. Uehling, Ann. Rev. Nucl. Sci., **4** (1954), 315

[12] M. B. Emmett, *The MORSE Monte Carlo radiation transport code system*, Report ORNL–4972 (1975).

[13] J.F. Briesmeister, editor *MCNP - A general Monte Carlo code for neutron and photon transport*, Los Alamos report **LA–7396–M** Rev.2 (1986)

[14] J.P. Both et al. Proc. of the *8th International Conference on Radiation Shielding*, Arlington, April 24-28 1994, American Nuclear Society ed., Vol. 1 373 (1994).

[15] H. Bethe, and J. Ashkin, *Passage of radiation though matter*, in E. Segre (ed.) *Experimental Nuclear Physics*, Vol. 1, Part 2, Wiley New York (1959)

[16] U. Fano, Ann. Rev. Nucl. Sci., **13** (1963), 1

[17] R.M. Sternheimer, Phys. Rev.**88** (1952), 851; R.M. Sternhiemer, S.M. Seltzer, and M.J. Berger, Phys. Rev. **B26** (1982), 6067, see also the erratum, **B27** (1983), 6971

[18] L. Landau, J. Phys. USSR, **8** (1944), 201

[19] O. Blunck, and K. Westphal, Z Phys. **130** (1951), 641

[20] Int. Commission on Rad. Units and Measurements, *Stopping Powers and Ranges of Protons and Alpha Particles*, ICRU Report **49** (1993)

[21] Int. Commission on Rad. Units and Measurements, *Stopping Powers for Electrons and Positrons*, ICRU Report **39** (1984)

[22] P.V. Vavilov, JETP **5** (1957), 749

[23] H. Bichsel, and R.P. Saxon, Phys. Rev. **A11** (1975), 1286

[24] H. Bichsel, Rev. Mod. Phys. **60** (1988) 663

[25] V.A. Chechin, and V.C. Ermilova, Nucl. Instr. Meth. **136** (1976), 551

[26] M.J. Berger, and R. Wang, in *MonteCarlo Transport of Electrons and Photons*, T.M. Jenkins and W.R. Nelson eds, Plenum press New York (1988), 21

[27] G.Z. Molière, Z. Naturforsch. **3a** (1948), 78

[28] G.Z. Molière, Z. Naturforsch. **10a** (1955), 177

[29] H.A. Bethe, Phys. Rev. **89** (1953), 1256

[30] S. Goudsmit, and J.L. Saunderson, Phys. Rev. **57** (1940), 24; S. Goudsmit and J.L. Saunderson, Phys. Rev. **58** (1940), 36

[31] W. R. Nelson, H. Hirayama and D.W.O. Rogers, Report SLAC–265 (1985).

[32] L. Eyges, Phys. Rev. **74**, 1534 (1948); C.M.Yang, Phys. Rev. **84** (1951), 599; see also B.Rossi and K.Greisen, Rev. Mod. Phys. **13** (1941), 267

[33] D.W.O. Rogers, Nucl. Instr. Meth. **227** (1984) 535

[34] A. Ferrari, P. R. Sala, G. Guaraldi and F. Padoani, Nucl. Instr. Meth. **B71** (1992) 412.

[35] N. Metropolis et al., Phys. Rev., **100(1)** (1958), 185; N. Metropolis et al., Phys. Rev., **100(1)** (1958), 204

[36] H.W. Bertini, Phys. Rev., **131(4)** (1963), 1801

[37] V.S. Barashenkov et al., Sov. Phys. Usp. **16(1)** (1973) 31; V.S. Barashenkov et al.,Nucl. Phys **A222** (1974) 204;

[38] K. Chen et al., Phys. Rev., **166** (1968), 949; K. Chen et al., Phys. Rev., **176** (1968), 1208;

[39] R. Serber, Phys. Rev., **72** (1947), 1114.

[40] M.L. Goldberger, Phys. Rev., **74** (1948), 1269.

[41] R.E. Prael and M. Bozoian, Los Alamos report **LA-UR-88-3238** 1988

[42] A. Ferrari, and P. R. Sala, Proc. of the MC93 Int. Conf. on Monte-Carlo Simulation in High-Energy and Nuclear Physics, Tallahassee, Florida, 22-26 february (1993), World Scientific ed. (1994), 277; A. Fassò, A. Ferrari, J. Ranft, and P. R. Sala, Proc. of the *Specialists' Meeting on Shielding Aspects of Accelerators, Targets & Irradiation Facilities*, Arlington, April 28-29 1994, published by OECD/NEA (1995), 287; A. Fassò, A. Ferrari, J. Ranft, and P. R. Sala, in *Intermediate Energy Nuclear Data: Models and codes*, Proc. of a specialist' meeting, Issy-les-Moulineaux, May 30th - June 1st 1994, published by OECD/NEA (1994), 271.

[43] S.G Mashnik and S.A. Smolyansky, JINR preprint E2-94-353 , Dubna (1994)

[44] H.W. Bertini, Phys. Rev., **C1(2)** (1970), 1801

[45] H.W. Bertini, Phys. Rev., **6(2)** (1972), 631

[46] M.M. Meier, D.A. Clark, C.A. Goulding, J.B. McClelland, G.L. Morgan and C.E. Moss, Nucl. Sci. and Eng., **102** (1989), 310

[47] M.M. Meier et al, Nucl. Sci. and Eng., **104** (1990), 339

[48] M.M. Meier, W.B. Amian, C.A. Goulding, G.L. Morgan and C.E. Moss, Nucl. Sci. and Eng., **110** (1992), 289

[49] F.E. Bertrand, and R.W. Peelle, Phys. Rev., **C8** (1973), 1045

[50] A. Galonsky et al., Phys. Rev., **C14** (1976), 748

[51] *International Code Comparison for Intermediate Energy Nuclear Data*, M. Blann, H. Gruppelaar, P. Nagel and J. Rodens eds., OECD/NEA (1994).

[52] G.Q. Li, R. Machleidt, and Y.Z. Zhuo, Phys. Rev., **C48(3)** (1993), 1062.

[53] G.Q. Li, and R. Machleidt, Phys. Rev., **C48(4)** (1993), 1702

[54] G.Q. Li, and R. Machleidt, Phys. Rev., **C49(1)** (1993), 566.

[55] A. Fassò, A. Ferrari, J. Ranft, P. R. Sala, G. R. Stevenson, and J. M. Zazula, Proc. of the workshop on *Simulating Accelerator Radiation Environment*, SARE, Santa Fè, 11-15 january (1993), A. Palounek ed., Los Alamos LA-12835-C (1994), 134.

[56] A. Fassò, A. Ferrari, J. Ranft and P. R. Sala, Proc. of the IV International Conference on Calorimetry in High Energy Physics, La Biodola (Elba), September 19-25 1993, A. Menzione and A. Scribano eds., World Scientific (1994), 493.

[57] P. Cloth et al., *HERMES, a Monte Carlo program system for beam-materials interaction studies*, Report KFA/Jül–2203 (1988).

[58] K.C. Chandler, and T.W. Amstrong, *Operating instructions for the high-energy nucleon-meson transport code HETC*, ORNL–4744 (1972); K.C. Chandler, and T.W. Amstrong, Nucl. Sci. and Eng., **49** (1972), 110; R.G. Alsmiller, F.S. Alsmiller and O.W. Hermann, Nucl. Instr. Meth., **A295** (1990), 337.

[59] R. E. Prael and H. Lichtenstein, LA-UR-89-3014 Los Alamos (1989).

[60] Y. Yariv, and Z. Fraenkel, Phys. Rev., **C24** (1981), 488.

[61] N. V. Mokhov, *The MARS10 code system: inclusive simulation of hadronic and electromagnetic cascades and muon transport*, Fermilab report FN–509 (1989)

[62] A. Van Ginneken, *CASIM: program to simulate hadronic cascades in bulk matter*, Fermilab report FN–272 (1975)

[63] W. O. Lock and D. F. Measday, *Intermediate Energy Nuclear Physics* Methuen & co, London, 1970.

[64] Phase shift solutions KH78, KH80, in *Landolt-Börnstein , new series* , **Vol. 9, part II**, 1983.

[65] C.J. Joachain, *Quantum Collision Theory* North-Holland, Amsterdam, 1975

[66] K. Hänssgen, and J. Ranft, Nucl. Sci. Eng., **88** (1984), 537

[67] J.Bystricky et al., *Energy dependence of nucleon-nucleon inelastic total cross sections*, **DPhPE 87-03** 1987

[68] B.J. VerWest, and R.A. Arndt, Phys. Rev., **C25(4)** (1982), 1979

[69] J. Benecke, T.T. Chou, C.N. Yang, and E. Yen, Phys. Rev., **188(5)** (1969), 2159

[70] M.E Law et al., *A Compilation of Data on Inclusive Reactions*, Internal Report LBL-80 (1972)

[71] A. Capella et al., Phys. rep., **236** (1994), 225

[72] K. Hahn, and J. Ranft, Phys. Rev., **D41(5)** (1990), 1463

[73] R. Engel, F.W. Bopp, D. Petermann, and J. Ranft, Phys. Rev., **D46(11)** (1992), 5192

[74] P. Aurenche et al., Phys. Rev., **D45(1)** (1992), 92

[75] J. Ranft and S. Ritter, Z. Phys. **C27** (1985) 413

[76] M. Adamus, Z. Phys., **C39** (1988), 311

[77] K. Goulianos, Phys. Rep., **101** (1983), 169

[78] S. Roesler, R. Engel, and J. Ranft, Z. Phys., **59** (1993), 481

[79] J. Ranft, and S. Roesler, Z. Phys., **C62** (1994), 329

[80] A. deShalit and H. Feshbach *Theoretical Nuclear Physics, vol 1: Nuclear Structure*, Wiley 1974

[81] A.G. Sitenko and V.K. Tartakovskij,*lektsii po teorii iadra*, Atomizdat, Moskow 1972

[82] A. Bohr, B.R. Mottelson, *Nuclear Structure* **Vol. 1**, W.A. Benjamin, Inc. (1969).

[83] T. Ericson and W. Weise *Pions and Nuclei* (Clarendon Press, Oxford, 1988).

[84] M. Krell and T.E.O. Ericson Nucl. Phys. **B11** (1969) 521.

[85] H. J. Weyer, *Phys. Rep.* **195** (1990) 295.

[86] J.N. Ginocchio and M.B. Johnson, *Phys. Rev.* **C21** (1980) 1056.

[87] M.B. Johnson and H.A. Bethe, Nucl. Phys. **A305** (1978) 418.

[88] M.B. Johnson and B.D. Keister Nucl. Phys. **A305** (1978) 461.

[89] K. Stricker, H. McManus, and J.A. Carr Phys. Rev. **C19** (1979) 929.

[90] J.N. Ginocchio, Phys. Rev. **C17** (1978) 195.

[91] K. Kikuchi and M. Kawai, it Nuclear Matter and Nuclear Interactions (North-Holland, Amsterdam, 1968)

[92] K. Chen *et al.*, *Phys. Rev.* **166, 4** (1968) 949

[93] L. Stodolski, Proc. Vth Intern. Coll. on Multiparticle React., Oxford, 1975, 577

[94] K. Chen et al., Phys. Rev. **C4, 6** (1971) 2234

[95] J. J. Griffin, Phys. Rev. Lett., **17** (1966) 438

[96] H. Feshbach, A. M. Kerman, S. Koonin, Ann. Phys., **125** (1975) 429

[97] M. Blann, Ann. Rev. Nucl. Sci., **25** (1963) 123

[98] M. Blann, Phys. Rev. Lett., **27** (1971) 337.

[99] M. Blann, Phys. Rev. Lett., **28** (1972) 757.

[100] S. Shlomo, Nucl. Phys **A539** (1992) 17

[101] G. Mantzouranis, D. Agassi, and H. A. Weidenmüller, Phys. Lett., **57B** (1975) 220

[102] J. M. Akkermans, H. Gruppelaar and G. Reffo, Phys. Rev., **C22** (1980) 73

[103] V.F. Weisskopf, Phys. ReV **52** (1937) 295

[104] A.S. Iljinov and M.V. Mebel, Nucl. Phys. **A543** (1992) 517

[105] S.G. Mashnik, acta phys. slov. **43** (1993) 86

[106] I. Dostrowsky, Z. Fraenkel and G. Friedlander, Phys. Rev., **116** (1959) 683

[107] A.V. Ignatyuk, G.N. Smirenkin and A.S. Tishin, Sov. J. Nucl. Phys., **21** (1975), 255

[108] R. Vandenbosh and J. R. Huizenga, *Nuclear Fission*, Academic Press, NeW York, 1973

[109] N Bohr and J.A. Wheeler, Phys. Rev. **56** (1939) 426

[110] F. Atchison, *Meeting on Targets for neutron beam spallation sources*, ed. G. Bauer, KFA Jülich Germany, **Jül-conf-34** 1980.

[111] E. Fermi, Prog. Theor. Phys., **5** (1950) 1570

[112] A.S. Botvina et al. Nucl. Phys. **A475** (1987) 663

[113] S. Leray et al., Nucl. Phys. **A511** (1990) 414

[114] W. G. Lynch, Ann. Rev. Nucl. Part. Sci. **37** (1987) 493

[115] J. Richert, report CRN **93-11**

[116] X. Campi et al., Pyus. Lett **142** (1984) 8

[117] L. G. Moretto and G. J. Wozniak, Ann. Rev. Nucl. Part. Sci. **43** (1993) 379

[118] P.A. AArnio and M. Huhtinen, *Proc. of the MC93 Int. Conf. on Monte Carlo Simulation in High-Energy and Nuclear Physics*, Feb. 22-26, 1993. Ed. P. Dragovitsch, S.L. Linn, M. Burbank, World Scientific, Singapore, 1994 (p. 1).

[119] G.D. Alkhazov et al., Nucl. Phys., bf A381 (1982), 430.

[120] A. Schiz et al., Phys. Rev., **D21(11)** (1980), 3010.

[121] G. Bellettini et al. Nucl. Phys. **79** (1966) 609

[122] C. De Marzo et al., *Phys. Rev.* **D26** (1982) 1019.

[123] R.J. Glauber, Phys. Rev., **100** (1955), 242

[124] V.N. Gribov, Sov. Phys. JETP, **29(3)** (1969), 483; L. Bertocchi, Nuovo Cimento, **11A** (1972), 45

[125] K. Zalewski, Ann. Rev. Nucl. Part. Sci., **35** (1985), 55

[126] A. Capella, and A. Krzywicki, Phys. Rev., **D18(9)** (1978), 3357

[127] A. Capella, Nucl. Phys., **A25** (1991), 133c

[128] A. Tufail et al., Phys Rev., **D42** (1990), 2187

[129] S. Fredriksson et al., Phys. Rep., **144** (1987), 187

[130] Z. Pengfei, and C. Weiqin, Nucl. Phys. **A552** (1993), 620

[131] J. Ranft, Z. Phys., **C43** (1988), 439

[132] L. Landau, I. Pomeranchuk, Dokl. Akad. Nauk SSSR **92** (1953) 535; A.B. Migdal, Phys. Rev. ,**103** (1956) 1811

[133] H.-J. Möring, J. Ranft, Z. Phys., **C52** (1991), 643

[134] J. Ranft, Phys. Rev., **D51(1)** (1995), 64

[135] G. Battistoni, C. Forti, and J. Ranft, Astroparticle Physics, **3** (1995), 157

[136] S.G Mashnik, JINR preprint E2-93-470 (1993)

[137] *Intermediate Energy Nuclear Data: Models and codes*, Proc. of a specialits' meeting, Issy-les-Moulineaux, May 30th - June 1st 1994, published by OECD/NEA (1994).

[138] M. Trabandt et al., Phys. Rev., **C39** (1989), 452.

[139] A.A. Cowley et al., Phys. Rev., **C43** (1991), 678.

[140] W.B. Amian et al., Nucl. Sci. Eng., **112** (1992), 78.

[141] W.B. Amian et al., Nucl. Sci. Eng., **115** (1993), 1.

[142] S. Stamer et al., Phys. Rev., **C47(3)** (1993), 1647.

[143] W.J. Burger et al., Pys. Rev., **C41** (1990), 2215.

[144] R.D. McKeown et al., Phys. Rev., **C24** (1981), 211.

[145] K.Nakai et. al. Phys. Rev. Lett. **44** (1979) 1446

[146] D. Ashery et al., Phys. Rev. **C23** (1981) 2173.

[147] W. Heitler, *The Quantum Theory of Radiation*, Oxford University Press, (1935).

[148] T.A. Gabriel et al., Nucl. Inst. Meth. **A338** (1994) 336

[149] R. Fernow, *Introduction to experimental particle physics* Cambridge University Press, 1986

[150] Particle Data Group, *review of particle Properties*, Phys. Rev. **D50** part 1, 1994

[151] Y.S. Tsai, Rev. of Mod. Phys., **46** (1975) 815.

[152] H.A. Bethe and L.C. Maximon, Phys. Rev. **93** (1954) 768; H. Davies, H.A. Bethe, and L.C. Maximon, Phys. Rev. **93** (1954) 788.